MUTATIONS IN TWO DISTINCT GENETIC PATHWAYS RESULT IN CEREBRAL CAVERNOUS MALFORMATIONS

by

Aubrey C. Chan

A dissertation submitted to the faculty of
The University of Utah
in partial fulfillment of the requirements for the degree of

Doctor of Philosophy

Department of Oncological Sciences

The University of Utah

August 2011

The University of Utah Graduate School

STATEMENT OF DISSERTATION APPROVAL

The dissertation of **Aubrey C. Chan**

has been approved by the following supervisory committee members:

Dean Y. Li	, Chair	**2011-05-26** Date Approved
Stephen L. Lessnick	, Member	**2011-05-26** Date Approved
Anne M. Moon	, Member	**2011-05-26** Date Approved
L. Charles Murtaugh	, Member	**2011-05-26** Date Approved
Jody Rosenblatt	, Member	**2011-05-26** Date Approved

and by **Donald E. Ayer** , Chair of the Department of **Oncological Sciences**

and by Charles A. Wight, Dean of The Graduate School.

ABSTRACT

Cerebral cavernous malformation (CCM), or cavernous angioma, is a common disease that can occur sporadically or familially with autosomal dominant inheritance. CCMs are vascular malformations, predominantly in the brain, consisting of dilated, thin-walled, blood-filled caverns. These lesions can lead to headaches, seizures, focal neurological deficits, and hemorrhagic stroke, but the only available treatment is surgical resection. Familial CCM has been linked to three genes: *KRIT1*, *CCM2*, or *PDCD10*. These genes encode structurally unrelated proteins of poorly understood function, but the three are hypothesized to work as a complex[1].

Generation of an animal model that faithfully recapitulates CCM disease would greatly benefit the study of the natural history and pathophysiology of CCM and the search for therapeutics. In this dissertation, I demonstrate that *Pdcd10* and *CCM2* signal through distinct pathways, but that loss of heterozygosity is a common genetic mechanism by which both genes lead to CCM disease. I show that Ccm2 acts to suppress the activity of the small GTPase RhoA, whereas Pdcd10 acts through the GCKIII family of kinases. Studies of knockout mice demonstrate that Ccm2 and Pdcd10 serve essential, but different, functions in the endothelium during development. I also examined Pdcd10 function using the fruitfly *Drosophila melanogaster*, which has a homolog for *PDCD10* but not *KRIT1* and *CCM2*. These studies revealed that Pdcd10 regulates lumen formation in the *Drosophila* tracheal system and genetically interacts with GCKIII, distinguishing it

from Ccm2 and indicating that Pdcd10 can function independently of the other CCM genes. Despite these differences in function, loss of heterozygosity at either locus results in the highly penetrant formation of dilated, vascular caverns in mice that phenocopy human CCM histologically and radiologically.

My studies led to the surprising conclusion that the CCM proteins do not share a common signaling mechanism. The distinct pathways, however, lead to a common pathology by the genetic mechanism of loss of heterozygosity. My work has also begun to elucidate the underlying biochemistry behind CCM, which may suggest potential therapies. The establishment of an animal model with highly penetrant disease, similar to human disease, is a powerful first step in developing these therapies.

TABLE OF CONTENTS

ACKNOWLEDGEMENTS

I wish to thank the many people who contributed to this work. These include: members of the Li Lab, especially Dean Li, Kevin Whitehead, Jing Ling, Stavros Drakos, Kirk Thomas, Lise Sorensen, Nyall London, Matthew Smith, Amy Lim, Christopher Gibson, and Tara Mleynek; Alexandra Smith, Oscar Ruiz, and Mark Metzstein; George Davis and members of his lab; Edward Hsu and Osama Abdullah at the Small Animal Imaging Core Facility; Chris Rodesch and the staff at the Cell Imaging/Fluorescence Core Facility; Nancy Chandler and the staff at the Electron Microscopy Core Facility; David Stillman and the NIH T32-GM007464 Genetics Training Grant.

CHAPTER 1

RECENT INSIGHTS INTO CEREBRAL CAVERNOUS MALFORMATIONS: ANIMAL MODELS OF CCM AND THE HUMAN PHENOTYPE

The following chapter was reprinted with permission from Blackwell Publishing. In addition to myself, the other authors were Dean Li, Michel Berg, and Kevin Whitehead. It was originally published in FEBS Journal, 2010 Mar;277(5):1076-83, Epub 2010 Jan 22. This manuscript was one of a three-part review series and focuses on the human phenotype of cerebral cavernous malformation disease and animal models.

the FEBS Journal

MINIREVIEW

Recent insights into cerebral cavernous malformations: animal models of CCM and the human phenotype

Aubrey C. Chan[1], Dean Y. Li[1,2], Michel J. Berg[3] and Kevin J. Whitehead[1,2]

1 Molecular Medicine Program, University of Utah, Salt Lake City, UT, USA
2 Division of Cardiology, University of Utah, Salt Lake City, UT, USA
3 Department of Neurology, University of Rochester Medical Center, NY, USA

Keywords
animal model; cavernous angioma; CCM; CCM2; cerebral cavernous malformation; Krit1; mouse model; OSM; PDCD10; zebrafish

Correspondence
K. J. Whitehead, Molecular Medicine Program, University of Utah, 15 N. 2030 East, Salt Lake City, UT 84112, USA
Fax: +1 801 585 0701
Tel: +1 801 585 1694
E-mail: kevin.whitehead@hsc.utah.edu

(Received 8 September 2009, revised 5 November 2009, accepted 6 November 2009)

doi:10.1111/j.1742-4658.2009.07536.x

Cerebral cavernous malformations are common vascular lesions of the central nervous system that predispose to seizures, focal neurologic deficits and potentially fatal hemorrhagic stroke. Human genetic studies have identified three genes associated with the disease and biochemical studies of these proteins have identified interaction partners and possible signaling pathways. A variety of animal models of CCM have been described to help translate the cellular and biochemical insights into a better understanding of disease mechanism. In this minireview, we discuss the contributions of animal models to our growing understanding of the biology of cavernous malformations, including the elucidation of the cellular context of CCM protein actions and the *in vivo* confirmation of abnormal endothelial cell–cell interactions. Challenges and progress towards developing a faithful model of CCM biology are reviewed.

Introduction

Cerebral cavernous malformation (CCM) is a common vascular disease consisting of clusters of dilated, thin-walled vessels lacking smooth muscle support and prone to hemorrhage. They are found in 1 in 200–250 individuals in the general population [1,2]. Although named for their predilection for the central nervous system (CNS), CCMs are also found in the retina, skin and other organs [3]. CCMs can be sporadic or familial, with the familial form manifesting with earlier onset and a higher number of malformations. The familial form is linked to three genes, *KRIT1* (*KREV1/RAP1A interaction trapped-1* also known as *CCM1*) [4,5], *CCM2* (also known as *OSM* or *Osmosensing scaffold for MEKK3*) [6–8] and *PDCD10* (*Programmed cell death 10*, also known as *CCM3*) [9]. The genetics of cavernous malformations is reviewed by Riant *et al.* [10].

The proteins encoded by these three genes are structurally unrelated and lack catalytic domains. Considerable progress has been made characterizing the interaction partners and the signaling pathways of the CCM proteins. The biochemistry of these pathways is reviewed by Faurobert & Albiges-Rizo [11]. Although such basic mechanistic studies are necessary to come to a more complete understanding of the underlying cellular processes that lead to disease, these studies are difficult to interpret without the context of *in vivo* correlation. Furthermore, these studies have been performed in a variety of cell types, both primary cultures and established laboratory cell lines. An understanding

Abbreviations
CCM, cerebral cavernous malformations; CNS, central nervous system; MEKK3, mitogen-activated protein kinase kinase kinase.

of the relevant cell types in the formation of vascular malformations in CCM is needed to put these studies into a physiological context. Ultimately, the goal of all research into CCM is to understand the basic processes that have been disrupted, resulting in the vascular malformation. Between observational and genetic studies in humans and biochemical and cellular studies at the bench lies a gap. This minireview explores the contributions of animal models to bridge this gap and add to our growing understanding of CCM pathophysiology.

Conservation of CCM genes

The genes responsible for CCM are very well conserved among different organisms (Fig. 1). These genes are found not only in mammals, fish and other vertebrates, but are also found in much more simple and primitive organisms that lack a closed circulatory system, such as *Caenorhabditis elegans*. The presence of these genes in genetically tractable organisms has allowed the development of numerous experimental animal models, as discussed below.

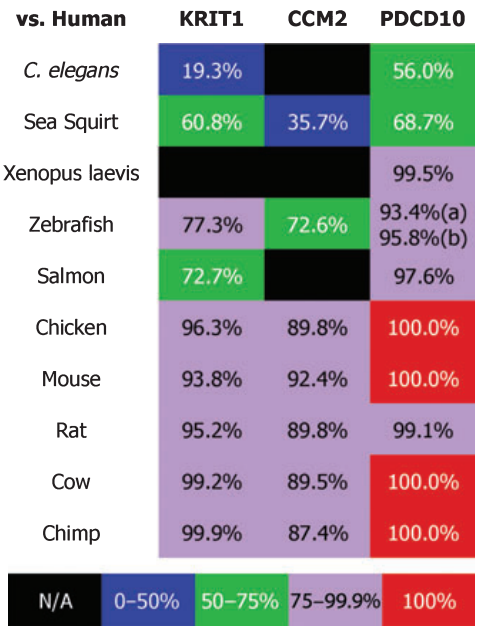

Fig. 1. Conservation of CCM proteins across species. Similarity scores were generated for the three CCM proteins in comparison with human protein sequences (KRIT1, accession number AAH98442; CCM2, accession number AAH16832; PDCD10, accession number NP_665859). Protein sequences or predicted protein sequences for a variety of vertebrate and nonvertebrate species were included if similarity was detected by BLASTp algorithm across a full-length protein sequence. Blank fields represent species for which an orthologous gene has yet to be identified in available databases. All three proteins are well conserved across species, and are found in nonvertebrate species. Conservation is particularly strong for PDCD10, the smallest of the three proteins. Note that *Pdcd10* has been duplicated in the zebrafish genome; the two proteins are denoted (a) and (b). *C. elegans*, *Caenorhabditis elegans*.

Human phenotype

Although humans are generally not considered in the category of animal models of disease, one can view the field of human genetics as probing a vast natural mutagenesis screen involving billions of individual organisms. As in any mutagenesis screen, the important information on genotype must be coupled with a detailed characterization of phenotype. All other animal models are relevant to disease to the degree that they help us further understand the human phenotype. Recent investigations have further refined our understanding of this phenotype, and bear reviewing in this manuscript.

In human CCM disease, the lesions exhibit a number of characteristic features; these features will serve as guideposts on the road to developing animal models of CCM disease. Classically, a CCM consists of a cluster of dilated blood vessels [12,13]. Each vessel in the cluster is grossly dilated, earning the name of a cavern; each vessel is lined only with a single layer of endothelium, with the absence of normal vascular support cells, such as smooth muscle cells. To be histologically classified as a CCM, the lesion must contain multiple such vessels adjacent to each other (Fig. 2). Grossly, this cluster gives the lesion an appearance likened to a raspberry. In addition, no brain parenchyma occurs in between the vessels. Single dilated vessels, called capillary telangiectasias, are not CCMs, although it has been hypothesized that the disease progresses from a single capillary telangiectasia that blossoms into a multivessel CCM [13]. Functionally, the lesion vessels are subject to subclinical bleeding, because hemosiderin, a breakdown product of blood, is found in the brain tissues surrounding CCM lesions [14]. Although CCMs have been clinically associated as occurring with developmental venous malformations [15], it has been shown that these two types of malformations are not linked genetically [16], and familial cases of CCM are not generally associated with venous malformations. Although these clinical features define CCMs for physicians, little is known about the cellular mechanisms that underlie and result in such characteristics. These mechanisms are what must be discovered, using either animal models or by deeper study of human CCM patients.

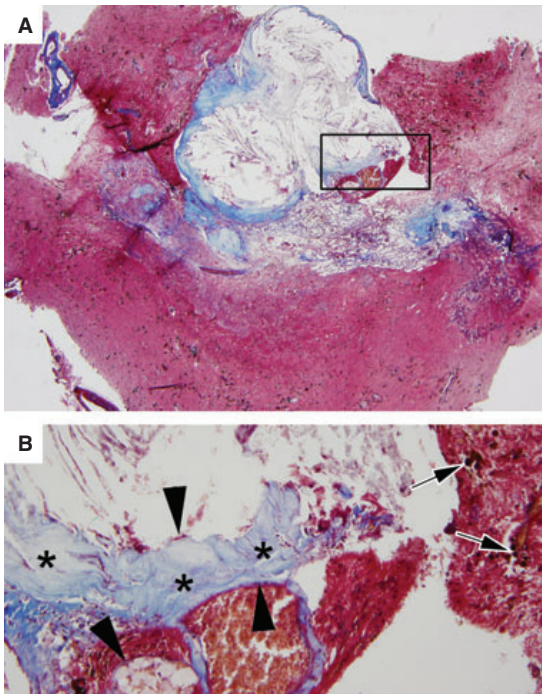

Fig. 2. Histology of CCM. Masson trichrome stain of surgically excised cavernous malformation. (A) Low-magnification view of CCM and surrounding brain. Hyalinized caverns of varying size are observed, surrounded by a rim of collagen deposits (blue). The adjacent brain shows evidence of gliosis (red). (B) Higher magnification view of boxed area. The caverns are lined by a single layer of endothelium (arrowheads) without smooth muscle support. Rather than smooth muscle cells or pericytes, a hyalinized rim of collagen surrounds the caverns (asterisks). Brown hemosiderin deposits are observed in the surrounding gliotic brain tissue (arrows).

One aspect of disease discovered in humans is that CCMs are associated with an inflammatory response. CCM lesions harbor a variety of immune cells [17], and oligoclonal banding of IgG has been observed in the CCM tissue [18]. What is still not known, however, is whether this inflammatory response is a secondary reaction to antigens exposed by the defective blood–brain barrier of a CCM [19] or if inflammatory action is part of the mechanism of pathogenesis leading to formation of aberrant blood vessels. It is intriguing that the mitogen-activated protein kinase kinase kinase MEKK3 plays a key role in immune signaling [20], and CCM2 protein has been shown to function as a scaffold for MEKK3 in response to stress [6]. The finding of immune involvement in CCM illustrates the complexity of the disease; CCM is a vascular disease localized mainly to neural tissues with an additional immune component. The involvement of multiple cell and tissue types raise the question of where the CCM genes primarily function, and in which cell type their loss leads to pathogenesis of disease.

Aside from the question of tissue specificity of CCM gene function, another important question of disease pathogenesis is that of a triggering event – what events on a molecular, cellular or physiological level lead to the formation of these isolated malformations? A clue comes from studying patients with sporadic CCM and those with familial CCM. People with an inherited form of CCM have a larger number of lesions and more frequent sequellae, such as seizure and hemorrhage. These features are reminiscent of the cancer retinoblastoma, which led to the Knudson 'two-hit' hypothesis. Similarly, a two-hit hypothesis has been proposed for the pathogenesis of CCM, in which an inherited mutant allele is a silent, but predisposing hit, and a second mutation acquired during life leads to a disease phenotype. The data supporting this hypothesis have been reviewed by Riant *et al.* [10] in an accompanying minireview. In addition to genetic and epigenetic events leading to CCM, these studies do not explore physiologic stressors as potential disease triggers in the heterozygous patient. For example, serum levels of the angiogenic vascular endothelial growth factor have been correlated with disease progression in case reports [21,22].

Recent cell biology observations, supported by data from mice, call to mind an important observational study [19]. Using detailed ultrastructural examination of surgically excised CCM specimens, the investigators observed abnormal endothelial cell junctions from the cavernous malformation. An important component of the normal blood–brain barrier, tight junctions form between endothelial cells and can be observed by electron microscopy. Although the cavernous malformation was found in the CNS where such tight junctions are the rule, the investigators observed numerous regions with impaired or deficient tight junctions between adjacent endothelial cells. These areas of junctional breakdown were associated with hemosiderin pigment as functional evidence that junction breakdown was associated with pathologic vascular leak, one of the defining features of CCMs.

Zebrafish

Hailed for its transparency and genetic tractability, a significant body of work has been carried out in zebrafish to determine the functions of the CCM genes. Initial results were described for *santa* (*san*, the zebrafish orthologue of *KRIT1*) and *valentine* (*vtn*, the zebrafish

orthologue of *CCM2*). Zebrafish with loss-of-function mutations in *san* or *vtn* share a common phenotype with fish lacking *heart of glass* (*heg*). Although mutations in the human orthologue of heart of glass (*HEG1*) have not been identified in patients with CCM, this gene has been shown to be functionally and genetically related to *santa* and *valentine*.

Heg is a single-pass transmembrane protein. Zebrafish with a nonsense *heg* mutation exhibit a dilated heart phenotype. The myocardium proliferates to a normal number of cells, but instead of building into concentric layers to form the walls of the heart, the myocardial cells form into a single layer, resulting in a dilated, thin-walled heart whose structure is reminiscent of a CCM vessel. *Heg* has two soluble splice variants in addition to the transmembrane isoform, but it is the transmembrane isoform that is essential in cardiac patterning. Although the defect is one of myocardial patterning, *heg* is expressed in the endocardial cells, indicating that this cell layer signals to the myocardium via Heg [23].

Interestingly, fish with nonsense mutations in *san* and *vtn* were later shown to exhibit the same phenotype as the *heg* mutant fish – that of the dilated heart covered by a single layer of myocardium. The similarity of the phenotype in these nonsense alleles suggested that these three proteins share a common developmental function. In addition, co-morpholino experiments demonstrated synergy among the three genes, putting them into a common genetic pathway [24]. Another group refined the characterization of the *santa* and *valentine* phenotypes using different mutant alleles. Focusing on the vasculature instead of the heart, they found that these fish developed dilated, thin-walled vessels that failed to form lumens. The dilated, thin-walled, closed vessels, like the dilated, thin-walled heart of these fish, are very reminiscent of human CCM vessels and the closed vessels seen in CCM knockout mice (see below). This dilation was attributed to abnormal endothelial cell spreading, a potential mechanistic insight into CCM pathogenesis. Of note, these abnormal vessels were able to be rescued by the transplantation of endothelial cells from wild-type fish, again hinting that the endothelial cell is the cell type that most needs the function of the CCM proteins [25]. Later work also showed that loss of *heg* or *vtn* via morpholino knockdown resulted in non-patent vessels that patterned normally, similar to the phenotypes seen in the *Krit1* and *Ccm2* knockout mice (see below) [26]. Most recently, it has been shown that a deletion mutation of *pdcd10* (*ccm3*), which is duplicated in the zebrafish genome, results in the same developmental defects as mutations in *santa* and *valentine* [27], making the zebrafish the first non-human model organism to link all three CCM genes phenotypically. Specifically, these defects are caused by the loss of Ccm3 interaction with the kinases serine/threonine kinase 25 (STK25) and mammalian sterile twenty-like 4 (MST4), giving a hint to the signaling pathway in which Ccm3 belongs, as both STK25 and MST4 belong to a family of kinases that are thought to act upstream of the mitogen-activated protein kinases (see the accompanying minireview [11] on the biochemical interactions of the CCM proteins).

Furthering the pursuit of genetic interactions, co-morpholino experiments were performed to examine the interactions between the CCM genes and *rap1b*, a Ras family small GTPase known to regulate cell junctions [28] and notable as being closely related to RAP1A, the binding partner bait originally used to identify KRIT1 [29]. Knockdown of *rap1b* via morpholino resulted in defective endothelial cell junctions and intracerebral hemorrhage in the fish, reminiscent of both the slow, unpredictable blood leak and the frank hemorrhage associated with CCMs [30]. The dose of *rap1b* morpholino was then titrated down so that the hemorrhage phenotype was seen in only a small percentage of fish. Combining this low dose of *rap1b* morpholino with a similarly low dose of *san* morpholino resulted in a synergistic increase in both the intracerebral hemorrhage phenotype of *rap1b* and the cardiac developmental phenotype of *san*.

The zebrafish experiments demonstrate the role of the CCM genes in cardiac and vascular development; the genetic tractability of the fish also provided a powerful way to discover genetic interactions between the CCM proteins and other proteins such as *rap1b* and the previously unknown *heg*. A mystery remains as to why *HEG1* mutations are not found in humans with CCMs. The synergistic effects of low-dose knockdown of the CCM genes and their partners imply that a similar mechanism may be responsible for pathogenesis in humans; however, as previously stated, such polygenic effects have yet to be identified in human tissue samples.

Mouse

Mice have long been favored as a model organism for laboratory studies and are the closest relative to humans commonly used in genetic studies. Knockout mice lacking *Krit1* [31] and *Ccm2* [26,32–34] have been generated and described. Although an experimental model of CCM lesions in the CNS was desired, neither mice with heterozygous knockout of *Krit1* nor *Ccm2* develop CNS vascular lesions with any useful fre-

quency [26,31–34]. Although disappointing, this lack of faithful disease modeling has generally been the case for most mouse genotype equivalents of human disease [35–38].

An important role for mouse models of genetic disease is to identify essential roles for protein function *in vivo*, especially in development where the proof of essential function is often embryonic lethality in complete knockouts. Indeed, mice lacking either *Krit1* or *Ccm2* die in mid-gestation with vascular defects at the same developmental stage, and with a similar phenotype [26,31,33,34]. The complete loss of *Krit1* or *Ccm2* results in vascular defects with a failure to connect the developing heart to the developing aorta with a functioning, patent first branchial arch artery. The associated rostral portions of the aorta are similarly narrowed (Fig. 3). As a result, circulation is not established as expected at E8.5 [33], and developmental arrest and death ensue. Prior to developmental arrest, cardiac and neural development proceeds normally.

Cavernous malformations are vascular lesions that form predominantly in the CNS. The basis for this anatomic predisposition is uncertain, but one possibility suggested by the abundant neuronal expression of the CCM genes [32,39–42] is a mechanism by which there is impaired signaling from neuronal cells to the endothelium, with a primary defect in the neuronal cell. Alternatively, the defect may lie primarily in endothelial cells, and the CNS selectivity of the disease could be a result of a unique sensitivity of the CNS vasculature to CCM gene function. To address these possibilities, mice with tissue-specific deletions of *Ccm2* using the Cre–Lox inducible recombination system have been generated and described. Two separate floxed *Ccm2* alleles were generated by different research groups [33,34]. Using Cre recombinase driven by the Tie2 promoter to direct recombination in endothelial cells, both groups found an absolute requirement for *Ccm2* in the endothelium during development. The neuronal expression of *Ccm2* was not required for development (as shown by deletion using the Nestin promoter-driven Cre recombinase).

Whereas *Krit1*, *Ccm2* and *Pdcd10* have similar widespread expression patterns in the mouse [32,39–42], the expression of the mouse orthologue of *heart of glass* (*Heg1*) is restricted to the endothelium and endocardium. Unlike zebrafish, *Heg1* knockout mice do not phenocopy *Krit1* or *Ccm2* knockouts [26]. Rather, *Heg1* knockout mice die later in gestation or in early postnatal stages with a variety of cardiac, vascular and lymphatic defects. Although pulmonary hemorrhage, cardiac rupture or chylous effusions may variably be the mechanism of death, a common theme throughout was disruption of the cell–cell junctions within the endothelial or endocardial cells. *Heg1* and *Ccm2* were also shown to genetically interact in the mouse as previously seen in fish [26]. Mice with both homozygous knockout of *Heg1* and heterozygous for *Ccm2* were found to have a much more severe phenotype than either mutant in isolation. These dual knockouts phenocopy mice with homozygous knockout of *Ccm2* or *Krit1*.

Multiple lines of investigation implicate a role for impaired cell-to-cell communication and endothelial cell junction integrity in states of CCM protein deficiency. Endothelial cell tight junctions are required to retain cells and macromolecules within the vasculature and to prevent vascular leak. Although mice heterozygous for *Ccm2* do not frequently develop CCM lesions like their human counterparts, these mice were shown to have abnormal vascular leak in the dermis when stressed with vascular endothelial growth factor [33]. Tight junctions are significantly regulated by the Rho family of GTPases. Endothelial cell culture experiments had implicated abnormally increased activity of RhoA *in vitro*. A role for increased RhoA activity *in vivo* was suggested by the ability of statins – known inhibitors of Rho GTPases [43] – to rescue the

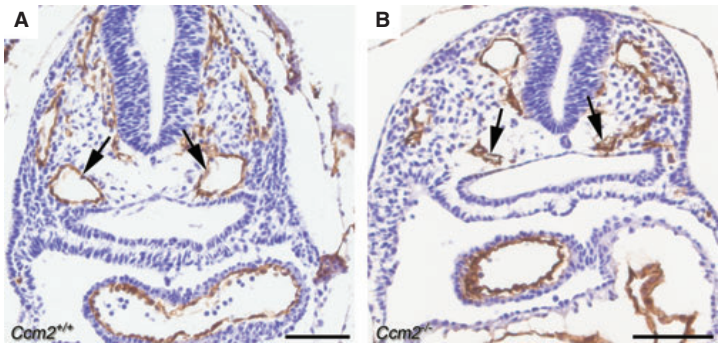

Fig. 3. Narrowed arteries associated with circulation failure in mice lacking *Ccm2*. The connections of the heart to the aorta, and the associated cranial portions of the dorsal aorta are narrowed in mice lacking Ccm2. The paired dorsal aortae in a wild-type embryo at E9.0 are shown in (A) (arrows), stained for the endothelial marker CD31. Although endothelial cells are present in the correct location in a *Ccm2* gene trap mutant littermate (arrows in B), little to no lumen is formed to support circulation.

abnormal vascular leak of *Ccm2* heterozygous knockout mice [33].

It is not clear what is responsible for the difference in susceptibility between mice and humans for the cerebral vascular lesions. Although differences in lifespan and brain mass may contribute to the lack of vascular lesions in *Krit1* or *Ccm2* heterozygous knockout mice, modifying factors are being sought which increase the risk of CCM lesion formation. As discussed above, observational studies in CCM patients suggest that a 'two-hit hypothesis' may underlie some lesions. Taking advantage of the high rate of spontaneous mutations in mice lacking the tumor suppressor p53, Krit1 heterozygous knockouts have been mated onto a p53 knockout background [44]. It was hoped that this model would reproduce both the human genotype (two genetic hits) and phenotype (cavernous malformations). Cerebral vascular lesions were observed in a high proportion of animals on this background with characteristics varying from capillary telangiectasias to more complex cavernous malformations, but the potential second hit mutation was not found. Unfortunately, mice lacking p53 have a shortened lifespan because of a high frequency of spontaneous tumors, including occasional brain tumors [13,45], It is unfeasible to study the natural history of CCM disease in these mice as they die from tumor burden shortly after developing CCM lesions. Great caution must be taken when interpreting the genetic contribution to vascular lesions on this background with potential for cancer-related vascular dysregulation and other physiologic stressors that may contribute to CCM lesion development. These results suggest, however, that a two-hit model may produce malformations useful for study; this second hit could come from recombination mediated by an inducible promoter driving Cre recombinase, thereby eliminating the confounding effects of the p53 null background.

Discussion

Vascular malformations result in considerable morbidity and mortality, especially with respect to lesions of the central nervous system. The ability to prevent or treat such lesions requires a greater understanding of the underlying biology of lesion formation. In this regard, cerebral cavernous malformation as a genetic disorder offers unique opportunities to understand the biology of vascular malformations. Initial insights regarding the biochemistry of the CCM genes left a considerable gap in understanding between protein function and lesion biology. By exploring the function of the CCM genes in animal models this gap is being bridged. Animal models have demonstrated the central importance of endothelial cell–cell interactions in the pathogenesis of CCM vascular disease. Endothelial cells need to be coordinated to organize into proper sized lumens and to maintain vascular barrier function. As a result of research into CCM, it becomes apparent that vascular malformations may result from the loss of genes crucial to vascular stability.

In addition to providing the important *in vivo* context for insights gained from biochemistry, animal models can allow an acceleration of translational research to ultimately impact the patients and families with CCM. Recent work in mice shows the promise of this approach, in that testable phenotypes can be identified and potential therapies can be evaluated in mice genetically similar to CCM patients. Manipulations of the current animal models to more closely mimic human disease also appear promising. Ultimately, we hope that a complete model of CCM lesion biology can be developed to act as a vital link between bench and bedside.

Acknowledgements

This work was funded by the US National Institutes of Health (K.J.W. and D.Y.L.), including training grant T32-GM007464 (A.C.C.), the American Heart Association (K.J.W. and D.Y.L.), the H.A. and Edna Benning Foundation, the Juvenile Diabetes Research Foundation, the Burroughs Wellcome Fund and the Flight Attendants Medical Research Institute (D.Y.L.).

References

1 Otten P, Pizzolato GP, Rilliet B & Berney J (1989) A propos de 131 cas d'angiomes caverneux (cavernomes) du S.N.C. repérés par l'analyse rétrospective de 24 535 autopsies. *Neuro-Chirurgie* **35**, 82–83, 128–131.

2 Robinson JR, Awad IA & Little JR (1991) Natural history of the cavernous angioma. *J neurosurg* **75**, 709–714.

3 Toldo I, Drigo P, Mammi I, Marini V & Carollo C (2009) Vertebral and spinal cavernous angiomas associated with familial cerebral cavernous malformation. *Surg neurol* **71**, 167–171.

4 Laberge-le Couteulx S, Jung HH, Labauge P, Houtteville JP, Lescoat C, Cecillon M, Marechal E, Joutel A, Bach JF & Tournier-Lasserve E (1999) Truncating mutations in CCM1, encoding KRIT1, cause hereditary cavernous angiomas. *Nature genetics* **23**, 189–193.

5 Sahoo T, Johnson EW, Thomas JW, Kuehl PM, Jones TL, Dokken CG, Touchman JW, Gallione CJ, Lee-Lin

SQ, Kosofsky B *et al.* (1999) Mutations in the gene encoding KRIT1, a Krev-1/rap1a binding protein, cause cerebral cavernous malformations (CCM1). *Hum mol genet* **8**, 2325–2333.

6 Uhlik MT, Abell AN, Johnson NL, Sun W, Cuevas BD, Lobel-Rice KE, Horne EA, Dell'Acqua ML & Johnson GL (2003) Rac-MEKK3-MKK3 scaffolding for p38 MAPK activation during hyperosmotic shock. *Nat Cell Biol* **5**, 1104–1110.

7 Liquori CL, Berg MJ, Siegel AM, Huang E, Zawistowski JS, Stoffer T, Verlaan D, Balogun F, Hughes L, Leedom TP *et al.* (2003) Mutations in a gene encoding a novel protein containing a phosphotyrosine-binding domain cause type 2 cerebral cavernous malformations. *Am J hum genet* **73**, 1459–1464.

8 Denier C, Goutagny S, Labauge P, Krivosic V, Arnoult M, Cousin A, Benabid AL, Comoy J, Frerebeau P, Gilbert B *et al.* (2004) Mutations within the MGC4607 gene cause cerebral cavernous malformations. *Am J hum genet* **74**, 326–337.

9 Bergametti F, Denier C, Labauge P, Arnoult M, Boetto S, Clanet M, Coubes P, Echenne B, Ibrahim R, Irthum B *et al.* (2005) Mutations within the programmed cell death 10 gene cause cerebral cavernous malformations. *Am J hum genet* **76**, 42–51.

10 Riant F, Bergametti F, Ayrignac X, Boulday G & Tournier-Lasserve E (2010) Recent insights into cerebral cavernous malformations: the molecular genetics of CCM. *FEBS J* **277**, 1070–1075.

11 Faurobert E & Albiges-Rizo C (2010) Recent insights into cerebral cavernous malformations: a complex jigsaw puzzle under construction. *FEBS J* **277**, 1084–1096.

12 Shenkar R, Venkatasubramanian PN, Zhao JC, Batjer HH, Wyrwicz AM & Awad IA (2008) Advanced magnetic resonance imaging of cerebral cavernous malformations: part I. High-field imaging of excised human lesions. *Neurosurgery* **63**, 782–789; discussion 789.

13 Shenkar R, Venkatasubramanian PN, Wyrwicz AM, Zhao JC, Shi C, Akers A, Marchuk DA & Awad IA (2008) Advanced magnetic resonance imaging of cerebral cavernous malformations: part II. Imaging of lesions in murine models. *Neurosurgery* **63**, 790–797; discussion 797-798.

14 Zhang J, Clatterbuck RE, Rigamonti D, Chang DD & Dietz HC (2001) Interaction between krit1 and icap1-alpha infers perturbation of integrin beta1-mediated angiogenesis in the pathogenesis of cerebral cavernous malformation. *Hum Mol Genet* **10**, 2953–2960.

15 Abe T, Singer RJ, Marks MP, Norbash AM, Crowley RS & Steinberg GK (1998) Coexistence of occult vascular malformations and developmental venous anomalies in the central nervous system: MR evaluation. *Ajnr* **19**, 51–57.

16 Guclu B, Ozturk AK, Pricola KL, Seker A, Ozek M & Gunel M (2005) Cerebral venous malformations have distinct genetic origin from cerebral cavernous malformations. *Stroke* **36**, 2479–2480.

17 Shi C, Shenkar R, Du H, Duckworth E, Raja H, Batjer HH & Awad IA (2009) Immune response in human cerebral cavernous malformations. *Stroke* **40**, 1659–1665.

18 Shi C, Shenkar R, Batjer HH, Check IJ & Awad IA (2007) Oligoclonal immune response in cerebral cavernous malformations. Laboratory investigation. *J Neurosurg* **107**, 1023–1026.

19 Clatterbuck RE, Eberhart CG, Crain BJ & Rigamonti D (2001) Ultrastructural and immunocytochemical evidence that an incompetent blood-brain barrier is related to the pathophysiology of cavernous malformations. *J Neurol Neurosurg Psychiatry* **71**, 188–192.

20 Konno H, Yamamoto T, Yamazaki K, Gohda J, Akiyama T, Semba K, Goto H, Kato A, Yujiri T, Imai T *et al.* (2009) TRAF6 establishes innate immune responses by activating NF-kappaB and IRF7 upon sensing cytosolic viral RNA and DNA. *PloS one* **4**, e5674.

21 Jung KH, Chu K, Jeong SW, Park HK, Bae HJ & Yoon BW (2003) Cerebral cavernous malformations with dynamic and progressive course: correlation study with vascular endothelial growth factor. *Arch neurol - Chicago* **60**, 1613–1618.

22 Abe T, Morishige M, Ooba H, Kamida T, Fujiki M, Kobayashi H, Sakoda T & Kimba Y (2009) The association between high VEGF levels and multiple probable punctuate cavernous malformations. *Acta neurochirurgica* **151**, 855–859.

23 Mably JD, Mohideen MA, Burns CG, Chen JN & Fishman MC (2003) Heart of glass regulates the concentric growth of the heart in zebrafish. *Curr Biol* **13**, 2138–2147.

24 Mably JD, Chuang LP, Serluca FC, Mohideen MA, Chen JN & Fishman MC (2006) Santa and valentine pattern concentric growth of cardiac myocardium in the zebrafish. *Development* **133**, 3139–3146.

25 Hogan BM, Bussmann J, Wolburg H & Schulte-Merker S (2008) Ccm1 cell autonomously regulates endothelial cellular morphogenesis and vascular tubulogenesis in zebrafish. *Hum Mol Genet* **17**, 2424–2432.

26 Kleaveland B, Zheng X, Liu JJ, Blum Y, Tung JJ, Zou Z, Sweeney SM, Chen M, Guo L, Lu MM *et al.* (2009) Regulation of cardiovascular development and integrity by the heart of glass-cerebral cavernous malformation protein pathway. *Nature medicine* **15**, 169–176.

27 Voss K, Stahl S, Hogan BM, Reinders J, Schleider E, Schulte-Merker S & Felbor U (2009) Functional analyses of human and zebrafish 18-amino acid in-frame deletion pave the way for domain mapping of the cerebral cavernous malformation 3 protein. *Hum mutat* **30**, 1003–1011.

28 Cullere X, Shaw SK, Andersson L, Hirahashi J, Luscinskas FW & Mayadas TN (2005) Regulation of vascular endothelial barrier function by Epac, a cAMP-activated exchange factor for Rap GTPase. *Blood* **105**, 1950–1955.

29 Serebriiskii I, Estojak J, Sonoda G, Testa JR & Golemis EA (1997) Association of Krev-1/rap1a with Krit1, a novel ankyrin repeat-containing protein encoded by a gene mapping to 7q21-22. *Oncogene* **15**, 1043–1049.

30 Gore AV, Lampugnani MG, Dye L, Dejana E & Weinstein BM (2008) Combinatorial interaction between CCM pathway genes precipitates hemorrhagic stroke. *Disease models & mechanisms* **1**, 275–281.

31 Whitehead KJ, Plummer NW, Adams JA, Marchuk DA & Li DY (2004) Ccm1 is required for arterial morphogenesis: implications for the etiology of human cavernous malformations. *Development (Cambridge, England)* **131**, 1437–1448.

32 Plummer NW, Squire TL, Srinivasan S, Huang E, Zawistowski JS, Matsunami H, Hale LP & Marchuk DA (2006) Neuronal expression of the Ccm2 gene in a new mouse model of cerebral cavernous malformations. *Mamm Genome* **17**, 119–128.

33 Whitehead KJ, Chan AC, Navankasattusas S, Koh W, London NR, Ling J, Mayo AH, Drakos SG, Jones CA, Zhu W *et al.* (2009) The cerebral cavernous malformation signaling pathway promotes vascular integrity via Rho GTPases. *Nature medicine* **15**, 177–184.

34 Boulday G, Blecon A, Petit N, Chareyre F, Garcia LA, Niwa-Kawakita M, Giovannini M & Tournier-Lasserve E (2009) Tissue-specific conditional CCM2 knockout mice establish the essential role of endothelial CCM2 in angiogenesis: implications for human cerebral cavernous malformations. *Disease models & mechanisms* **2**, 168–177.

35 Ishibashi S, Brown MS, Goldstein JL, Gerard RD, Hammer RE & Herz J (1993) Hypercholesterolemia in low density lipoprotein receptor knockout mice and its reversal by adenovirus-mediated gene delivery. *J Clin Invest* **92**, 883–893.

36 Pereira L, Andrikopoulos K, Tian J, Lee SY, Keene DR, Ono R, Reinhardt DP, Sakai LY, Biery NJ, Bunton T *et al.* (1997) Targetting of the gene encoding fibrillin-1 recapitulates the vascular aspect of Marfan syndrome. *Nature genetics* **17**, 218–222.

37 Li DY, Sorensen LK, Brooke BS, Urness LD, Davis EC, Taylor DG, Boak BB & Wendel DP (1999) Defective angiogenesis in mice lacking endoglin. *Science* **284**, 1534–1537.

38 Urness LD, Sorensen LK & Li DY (2000) Arteriovenous malformations in mice lacking activin receptor-like kinase-1. *Nature genetics* **26**, 328–331.

39 Denier C, Gasc JM, Chapon F, Domenga V, Lescoat C, Joutel A & Tournier-Lasserve E (2002) Krit1/cerebral cavernous malformation 1 mRNA is preferentially expressed in neurons and epithelial cells in embryo and adult. *Mechanisms of development* **117**, 363–367.

40 Kehrer-Sawatzki H, Wilda M, Braun VM, Richter HP & Hameister H (2002) Mutation and expression analysis of the KRIT1 gene associated with cerebral cavernous malformations (CCM1). *Acta neuropathologica* **104**, 231–240.

41 Petit N, Blecon A, Denier C & Tournier-Lasserve E (2006) Patterns of expression of the three cerebral cavernous malformation (CCM) genes during embryonic and postnatal brain development. *Gene Expr Patterns* **6**, 495–503.

42 Seker A, Pricola KL, Guclu B, Ozturk AK, Louvi A & Gunel M (2006) CCM2 expression parallels that of CCM1. *Stroke* **37**, 518–523.

43 Park HJ, Kong D, Iruela-Arispe L, Begley U, Tang D & Galper JB (2002) 3-hydroxy-3-methylglutaryl coenzyme A reductase inhibitors interfere with angiogenesis by inhibiting the geranylgeranylation of RhoA. *Circ res* **91**, 143–150.

44 Plummer NW, Gallione CJ, Srinivasan S, Zawistowski JS, Louis DN & Marchuk DA (2004) Loss of p53 sensitizes mice with a mutation in Ccm1 (KRIT1) to development of cerebral vascular malformations. *The Am J pathol* **165**, 1509–1518.

45 Jacks T, Remington L, Williams BO, Schmitt EM, Halachmi S, Bronson RT & Weinberg RA (1994) Tumor spectrum analysis in p53-mutant mice. *Curr Biol* **4**, 1–7.

CHAPTER 2

THE CEREBRAL CAVERNOUS MALFORMATION SIGNALING PATHWAY PROMOTES VASCULAR INTEGRITY VIA RHO GTPASES

The following chapter was reprinted with permission from Nature Publishing Group. In addition to myself, the other authors were Kevin Whitehead, Sutip Navankasattusas, Wonshill Koh, Nyall London, Jing Ling, Anne Mayo, Stavros Drakos, Christopher Jones, Weiquan Zhu, Douglas Marchuk, George Davis, and Dean Li. It was originally published in Nature Medicine, 2009 Feb;15(2):177-84. Epub 2009 Jan 18. I participated in the design, execution, interpretation of data related to cell biology, biochemistry, and the adult *in vivo* phenotype.

nature medicine

The cerebral cavernous malformation signaling pathway promotes vascular integrity via Rho GTPases

Kevin J Whitehead[1,2], Aubrey C Chan[2], Sutip Navankasattusas[2], Wonshill Koh[3], Nyall R London[2], Jing Ling[2], Anne H Mayo[3], Stavros G Drakos[2], Christopher A Jones[2], Weiquan Zhu[2], Douglas A Marchuk[4], George E Davis[3] & Dean Y Li[1,2]

Cerebral cavernous malformation (CCM) is a common vascular dysplasia that affects both systemic and central nervous system blood vessels. Loss of function mutations in the *CCM2* gene cause CCM. Here we show that targeted disruption of *Ccm2* in mice results in failed lumen formation and early embryonic death through an endothelial cell autonomous mechanism. We show that *CCM2* regulates endothelial cytoskeletal architecture, cell-to-cell interactions and lumen formation. Heterozygosity at *Ccm2*, a genotype equivalent to that in human CCM, results in impaired endothelial barrier function. On the basis of our biochemical studies indicating that loss of *CCM2* results in activation of RHOA GTPase, we rescued the cellular phenotype and barrier function in heterozygous mice with simvastatin, a drug known to inhibit Rho GTPases. These data offer the prospect for pharmacological treatment of a human vascular dysplasia with a widely available and safe drug.

Cerebral cavernous malformations are common vascular malformations that affect the systemic and central nervous system (CNS) vasculature with a prevalence of 1 in 200 to 250 individuals[1,2] in unselected populations. CCM consists of enlarged microvascular channels lined by a single layer of endothelium without smooth muscle support. Individuals with these vascular lesions are subject to an unpredictable risk of hemorrhage for which no pharmacologic therapy currently exists[3]. Even before overt hemorrhage all lesions are surrounded by hemosiderin—iron-laden deposits that result from extravascular blood and that can be sensitively detected by magnetic resonance imaging[4]—suggesting abnormalities in endothelial barrier function[5]. Although lesions have been described in a variety of vascular beds[6], clinical manifestations are most common in the CNS, where the consequences of leak and hemorrhage can be stroke, seizure or death. A large proportion of cases are familial with an autosomal dominant pattern of inheritance. Genetic studies have shown that heterozygous loss of function mutations in *CCM2*—also known as osmosensing scaffold for mitogen-activated protein kinase kinase kinase-3 (*OSM*), and encoding a protein also known as malcavernin or MGC4607—cause cavernous malformations[7,8]. Two other structurally unrelated genes, KREV1 interaction trapped-1 (*KRIT1*)—also known as *CCM1* (refs. 9,10)—and programmed cell death 10 (*PDCD10*)—also known as *CCM3* (ref. 11)—have also been associated with CCM. Before the human genetic studies, there was little to recommend these genes as obvious candidate genes for any vascular disease.

CCM2 was identified in a screen for genes involved in the cellular response to osmotic shock[12]. These stress-activated pathways include signaling cascades involving Rho-family GTPases such as RHOA, RAC1 and CDC42, and mitogen-activated protein kinases (MAPKs) such as p38 and JNK. In fibroblasts, CCM2 is required for the assembly of a complex between the mitogen-activated protein kinase kinase kinase-3 and its substrate, mitogen-activated protein kinase kinase-3 (MKK3), to phosphorylate p38 in response to signaling from the GTPase RAC1 (ref. 12).

Efforts to incorporate these biochemical insights into a molecular model to explain the pathogenesis of CCM have been plagued by controversy over the identity of the cell type in which *CCM2* is required. Although a compromised vasculature defines CCM, there are compelling data to suggest a neuronal role in the etiology of the disease. First, the three genes involved in CCM are expressed neither specifically nor strongly in the endothelium in culture or in animal models[13–15]. Second, a precedent for a nonautonomous effect of a gene affecting vascular integrity exists: neural deletion of the gene encoding α_v integrin disrupts the cerebral vasculature and causes hemorrhage in mice[16]. Conversely, KRIT1 can act as an effector of the small GTPase RAP1A in cultured endothelial cells[17]. The tissue specificity of *Ccm2* function remains unknown. Here we seek to use genetically manipulated mice to understand the role of *Ccm2* in development, elucidate the mechanism of signaling and explore potential therapeutic strategies for ameliorating *CCM2* deficiency.

[1]Division of Cardiology, Department of Medicine, 30 North 1900 East, Room 4A100, University of Utah, Salt Lake City, Utah 84132, USA. [2]Molecular Medicine Program, 15 North 2030 East, Room 4140, University of Utah, Salt Lake City, Utah 84112, USA. [3]The Department of Medical Pharmacology and Physiology, University of Missouri School of Medicine, MA415 Medical Sciences Building, One Hospital Drive, Columbia, Missouri 65212, USA. [4]Department of Molecular Genetics and Microbiology, Box 3175, Duke University Medical Center, Durham, North Carolina 27710, USA. Correspondence should be addressed to K.J.W. (kevin.whitehead@hsc.utah.edu) or D.Y.L. (dean.li@hmbg.utah.edu).

Received 1 October 2008; accepted 2 December 2008; published online 18 January 2009; corrected after print 6 April 2009; doi:10.1038/nm.1911

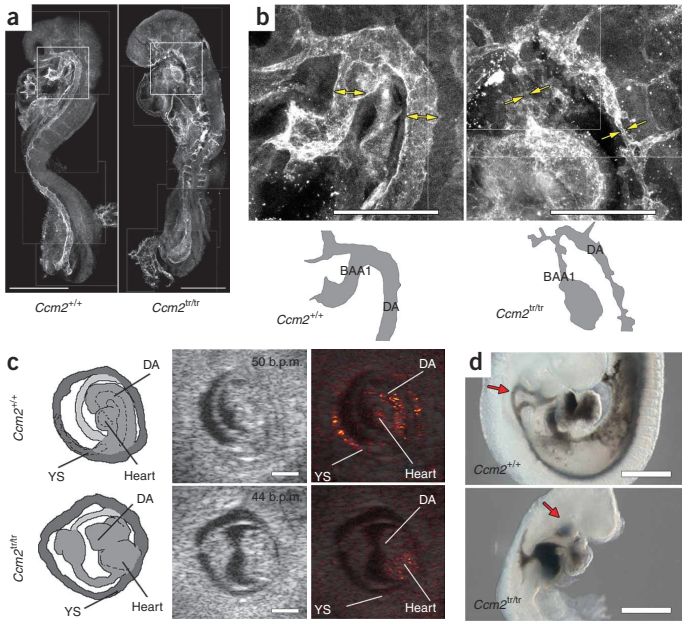

Figure 1 *Ccm2* is required for blood circulation. (**a**) Whole-mount confocal immunofluorescence micrographs of littermate embryos at E8.5 showing abnormal vasculature in $Ccm2^{tr/tr}$ (right). (**b**) Higher magnification of the first branchial arch arteries (BAA1) and dorsal aorta (DA). Cartoons at the bottom show orientation. *Ccm2*-mutant vessels (single arrows) are narrower at BAA1 and adjacent portions of the dorsal aorta than wild-type vessels (double arrows). (**c**) Fetal ultrasound showing no blood flow in a $Ccm2^{tr/tr}$ embryo (bottom row) at E8.5 despite a normal frequency of cardiac contractions (middle panels). Blood flow (colorized pixels) was observed in wild-type littermates (top row). Diagrams at left show orientation. DA, dorsal aorta; YS, yolk sac (also see **Supplementary Movies 1** and **2**). (**d**) Photographs after ink injection into the cardiac ventricle. Ink passage through the branchial arch arteries at E9.5 was observed in a wild-type embryo (top) but no anterograde passage through the branchial arches (red arrow) into the aorta was observed in a $Ccm2^{tr/tr}$ littermate (bottom). Scale bars: **a**,**c**,**d**, 500 μm; **b**, 200 μm. Results are representative of multiple (minimum eight) paired observations.

RESULTS

Ccm2 is required for angiogenesis

A putative null allele of *Ccm2* with a gene-trap–induced mutation was identified[14]. This allele has been termed $Ccm2^{Gt(RRG051)Byg}$ (hereafter designated $Ccm2^{tr}$), and consists of an insertion of the gene-trap vector into exon 6 of *Ccm2* and a 45-nucleotide deletion of the genomic sequence[14], disrupting transcription of *Ccm2* (**Supplementary Fig. 1a–c** online). Mice heterozygous for $Ccm2^{tr}$ are viable and fertile as previously reported[14]. We observed no homozygous mutant mice at weaning. We identified mutant embryos in mendelian ratios until embryonic day 9 (E9.0). Starting at E9.0, we noticed a gross phenotype in homozygous $Ccm2^{tr}$ mice (**Supplementary Table 1** online). The homozygous mutant embryos failed to organize the yolk sac vasculature and showed evidence of growth arrest at E9.0 (data not shown). Pericardial effusions subsequently developed before embryo resorption at E11.5. No viable homozygous mutants were observed at E9.5 and beyond. The timing of death in these embryos is consistent with failed angiogenesis.

We studied embryos at E8.5 before the mutant phenotype could be grossly detected. Embryos were stained with antibodies against the endothelial cell surface protein CD31 (PECAM) or α-smooth muscle actin and examined with whole-mount confocal immunofluorescence microscopy or sectioned and studied by immunohistochemistry. The initial patterning of the dorsal aorta (**Supplementary Fig. 1d**,**e**) and yolk sac primary vascular plexus (data not shown) by vasculogenesis[18] was intact in mutants. Heart development was also normal (data not shown). After the initial vascular pattern was established, however, profound defects occurred in the development of subsequent vessels by angiogenesis (**Fig. 1a**,**b**). The first defects observed in mutant embryos included abnormalities of the first branchial arch artery and the intersomitic arteries at E8.5 (**Fig. 1a**,**b** and **Supplementary Fig. 1e**,**f**). The first branchial arch artery, required to connect the dorsal aorta to the heart, failed to form a proper lumen. Adjacent portions of the aorta were also narrow and irregular, whereas the previously normal caudal portion of the dorsal aorta become enlarged (**Supplementary Fig. 1d**). Yolk sac vascular remodeling was abnormal (data not shown). The failure of the branchial arch arteries had profound physiologic consequences on the embryo. *In vivo* ultrasound studies showed that, despite normal frequency of cardiac contractions, circulation was not established in homozygous mutants (**Fig. 1c** and **Supplementary Movies 1** and **2** online). Branchial arch artery failure was not confined to the arteries of the first arch. The second and third pair of branchial arch arteries should normally form by E9.5. We injected India ink into the ventricles of mutant embryos at E9.5 and did not observe passage of ink into the dorsal aorta of mutants (**Fig. 1d**). Unlike the anterograde flow observed in wild-type littermates, ink passed retrogradely from the ventricle through the atrium and into the common cardinal vein in mutant embryos (**Fig. 1d**). Growth arrest and embryonic death resulted from the failed circulation first observed at E8.5.

Ccm2 is required in the endothelium

The phenotype of mice with gene-trap mutations in *Ccm2* establishes an essential role for this protein in angiogenesis. This mutation is present in all cells of the embryo and thus does not make clear which tissues require *Ccm2* for normal function. To determine the tissue requirement for *Ccm2*, we developed mice with a conditional mutation in *Ccm2* by Cre-*lox* technology (**Supplementary Fig. 2** online). This allele is termed $Ccm2^{tm1Kwhi}$ (hereafter referred to as $Ccm2^{fl}$). The *Ccm2* gene remains intact until the allele is exposed to Cre recombinase, which deletes exons 3–10 of *Ccm2*. Mating $Ccm2^{fl/+}$ mice with HPRT-Cre mice[19] expressing Cre recombinase in the germline resulted in a heritable mutant allele termed $Ccm2^{tm1.1Kwhi}$ hereafter referred to as $Ccm2^{-}$). Homozygous $Ccm2^{-/-}$ mutant mice phenocopy the gene-trap ($Ccm2^{tr/tr}$) mutants (**Supplementary Fig. 2e**). Cre recombinase can also be expressed in a tissue-specific manner under the control of a variety of promoters. We subsequently examined a number of

Table 1 Embryonic development in mice with tissue specific deletions of *Ccm2*

	Endothelial				Neural and glial				Smooth muscle			
	$Ccm2^{fl/+}$		$Ccm2^{fl/-}$		$Ccm2^{fl/+}$		$Ccm2^{fl/-}$		$Ccm2^{fl/+}$		$Ccm2^{fl/-}$	
Developmental stage	Tg(Tie2-Cre)	No Cre	Tg(Tie2-Cre)	No Cre	Tg(Nestin-Cre)	No Cre	Tg(Nestin-Cre)	No Cre	Tg(Tagln-Cre)	No Cre	Tg(Tagln-Cre)	No Cre
E9.0	4	12	13	9	6	7	7	5	6	4	6	2
E15.5	4	4	0	5	7	10	3	8	5	7	6	7
P0.5	17	18	0	7	4	4	7	2	9	11	3	8

Numbers represent the number of embryos or neonates of the indicated genotypes found at the indicated time points.

tissue-restricted, somatic mutants for defects in angiogenesis. Mice lacking *Ccm2* in the endothelium ($Ccm2^{fl/-}$;Tg(Tie2-Cre))[20] resemble germline mutants with similar vascular defects and timing of embryonic death (**Table 1** and **Fig. 2**). Endothelial cell–specific deletion of *Ccm2* is uniformly lethal during development (**Table 1** and data not shown).

The expression of *Ccm2* in neural tissues and the predominance of CCM lesions in the CNS suggest a possible role for *Ccm2* in neural cells. Mice lacking *Ccm2* in neural tissues were generated with Cre driven by a nestin promoter ($Ccm2^{fl/-}$;Tg(Nes-Cre))[21]. These mutant mice had no defects in angiogenesis at E9.0 and were found in the expected ratios at birth (**Table 1** and **Fig. 2**). Another key contributor to the milieu of endothelial cells *in vivo* is the smooth muscle cell. Mice lacking *Ccm2* in smooth muscle cells were generated with a transgelin-Cre ($Ccm2^{fl/-}$;Tg(Tagln-Cre))[22]. Like the mice lacking *Ccm2* in neural tissues, mice lacking *Ccm2* in smooth muscle were also found at birth, with normal vasculature at E9.0 (**Table 1** and **Fig. 2**). These data indicate an essential role for *Ccm2* only in endothelial cells for the initial events of angiogenesis.

CCM2 regulates lumen formation via the actin cytoskeleton

Our genetic studies led us to evaluate the function of *CCM2* in human endothelial cells. We detected *CCM2* expression by real-time quantitative RT-PCR in human mictrovascular (dermal) endothelial cells (HMVECs) and human umbilical vein endothelial cells (HUVECs; **Fig. 3a**). A single small interfering RNA (siRNA) construct specific for *CCM2* (*CCM2* siRNA) was able to decrease the amount of *CCM2* transcripts by 80–90% in HMVECs and HUVECs (**Fig. 3a**).

Endothelial cells in three-dimensional culture spontaneously develop tube-like structures that resemble the microvasculature and that model events in developmental angiogenesis[23]. We tested the role of *CCM2* in lumen formation *in vitro* by comparing HUVECs treated with *CCM2* siRNA with either a luciferase or a random negative control siRNA in this three-dimensional assay of tube morphogenesis (**Fig. 3b,c** and **Supplementary Movies 3** and **4** online). Control HUVECs formed vacuoles that coalesced into tube-like structures over the course of 24 h, whereas *CCM2*-depleted HUVECs formed fewer lumens with a much smaller lumen cross-sectional area (**Fig. 3d,e**). This defect was observed at the single-cell stage before the formation of multicellular structures (**Fig. 3d**). These observations suggest a crucial and endothelial intrinsic role for *CCM2* in the development of precursor vacuoles as well as in the coalescence and

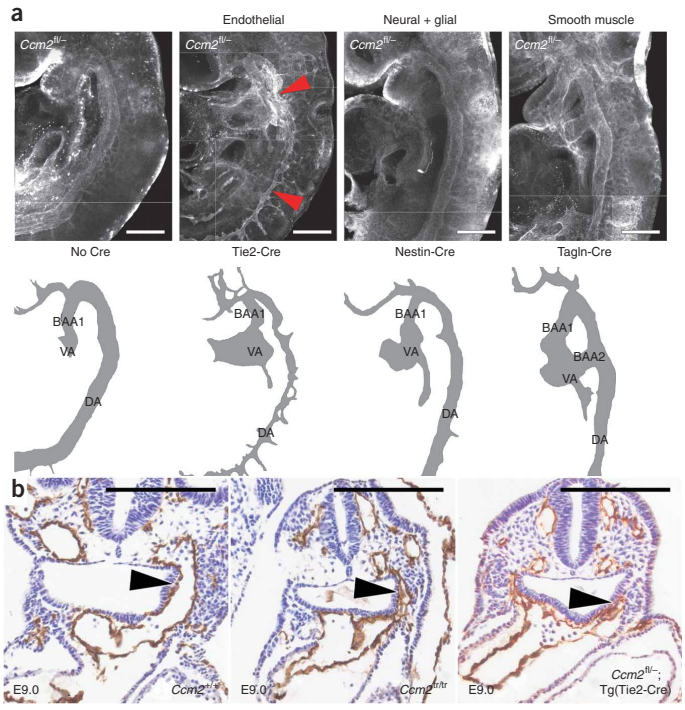

Figure 2 Vascular defects in mutant mice are endothelial cell autonomous. (**a**) Whole-mount immunofluorescence showing normal, uniform caliber branchial arch arteries and aortas in all $Ccm2^{fl/-}$ embryos except the endothelial (Tie2-Cre) mutant, which has an irregular, narrow lumen (red arrowheads). Cartoons at the bottom are provided for orientation. BAA1, first branchial arch artery; BAA2, second branchial arch artery; VA, ventral aorta (or aortic sac); DA, dorsal aorta. (**b**) Paraffin sections taken at E9.0 showing narrow branchial arch arteries in mutant embryos. In contrast to the wild-type embryo (left), the first branchial arch artery (arrowhead) is similarly narrowed and irregularly shaped in both complete knockout ($Ccm2^{tr/tr}$, middle) and endothelial mutant ($Ccm2^{fl/-}$;Tg(Tie2-Cre), right) embryos. Scale bars, 200 μm. Results are representative of multiple (minimum seven) independent observations.

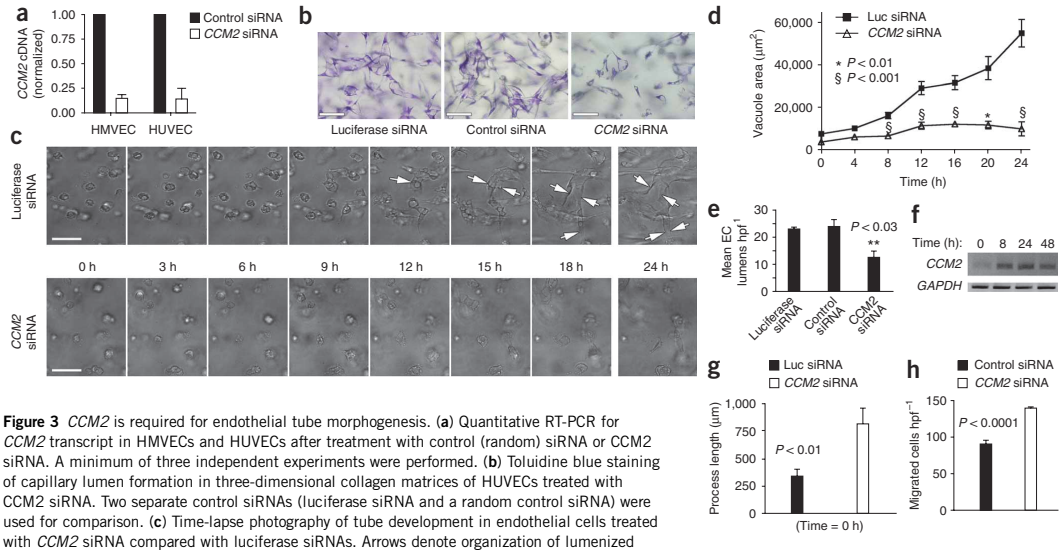

Figure 3 *CCM2* is required for endothelial tube morphogenesis. (**a**) Quantitative RT-PCR for *CCM2* transcript in HMVECs and HUVECs after treatment with control (random) siRNA or CCM2 siRNA. A minimum of three independent experiments were performed. (**b**) Toluidine blue staining of capillary lumen formation in three-dimensional collagen matrices of HUVECs treated with CCM2 siRNA. Two separate control siRNAs (luciferase siRNA and a random control siRNA) were used for comparison. (**c**) Time-lapse photography of tube development in endothelial cells treated with *CCM2* siRNA compared with luciferase siRNAs. Arrows denote organization of lumenized structures from vacuole precursors. (**d**) Quantification of lumen and vacuole development over time in HUVECs treated with *CCM2* siRNA as compared to a luciferase (Luc) siRNA control. Five fields were analyzed for each data point. (**e**) Quantification of lumen numbers at 24 h in HUVECs treated with *CCM2* siRNA compared to luciferase or random siRNA controls. EC, endothelial cell; hpf, high power field. Three fields were analyzed for each siRNA. (**f**) *CCM2* levels assayed by RT-PCR in control HUVECs undergoing tube formation at various stages of the vacuole and lumen formation assay. (**g**) Quantification of filopodial length in HUVECs treated with *CCM2* siRNA compared to a luciferase siRNA control. Ten fields were analyzed for each siRNA. (**h**) Haptotactic migration of HMVECs to fibronectin in *CCM2*-depleted cells versus random siRNA control–treated cells. Analysis was performed on twelve control and eight *CCM2* siRNA fields. Scale bars, 100 μm. Values are means ± s.e.m., except in **e**, where values are means ± s.d.

expansion of these structures to form the vascular lumen. Consistent with this hypothesis, we observed upregulation of *CCM2* messenger RNA by RT-PCR in a time course parallel with lumen formation in control HUVECs (**Fig. 3f**). The failure in lumen formation is not a consequence of insufficient endothelial migration or of an inability to form filopodial sprouts: HUVECs treated with *CCM2* siRNA showed increased sprouting of cell processes when initially plated in three-dimensional culture (**Fig. 3g**), and HMVECs treated with *CCM2* siRNA showed increased haptotactic migration (**Fig. 3h**).

Lumen formation is dependent upon the cellular cytoskeleton[24]. *CCM2*-deficient HMVECs had a marked increase in formation of actin stress fibers traversing the cell, with less cortical actin at the cell periphery (**Fig. 4a**). Actin redistribution correlated with a decrease in barrier function and increased permeability of the endothelial monolayer (**Fig. 4b,c**). We observed decreased electrical resistance and increased transit of macromolecules (horseradish peroxidase (HRP)) across *CCM2*-deficient monolayers compared to control cell monolayers (**Fig. 4b,c**).

CCM2 regulates actin and MAPK via RHOA

The Rho family of small GTPases regulates many aspects of the structure and function of the cellular cytoskeleton. Impaired lumen formation[24], increased formation of actin stress fibers and decreased barrier function[25] in endothelial cells suggest activation of RHOA. Consistent with the cellular phenotype, we observed increased active (GTP-bound) RHOA in *CCM2*-depleted HMVECs compared to control cells (**Fig. 4d**). We found no change in the activation of RAC1 and found less basal activation of CDC42 (**Fig. 4d**). By immunoprecipitation, we found that CCM2 binds RHOA and RAC1 but not CDC42 (**Fig. 4e**). Inhibition of RHOA signaling either at the level of RHOA with C3 transferase[26] or downstream at the level of Rho kinase (ROCK), with the ROCK inhibitor Y-27632 (ref. 27) blocked the stress fiber response of *CCM2*-depleted HMVECs (**Fig. 4f**). C3 transferase was also able to significantly rescue barrier function in these cells (**Fig. 4g**).

CCM2 has also been implicated in MAPK signaling[12]. We used phospho-specific antibodies to profile the activation state of MAPK family members in the absence of *CCM2* (**Fig. 4h**). The main families of MAP kinases are the extracellular signal regulated kinases (ERKs), p38 and JNK, with p38 and JNK also known as stress-regulated protein kinases[28]. A reduction in *CCM2* transcript levels did not affect the amount of either phosphorylated ERK or phosphorylated p38 but did increase phosphorylation of JNK and its upstream kinases MKK4 and MKK7. As GTPases can stimulate MAPK signaling, we tested whether increased JNK activation was the result of increased Rho activity by treating cells with the ROCK inhibitor Y-27632. ROCK inhibition decreased the activation of JNK (**Fig. 4i**). These observations suggest that the loss of *CCM2* leads to RHOA activation, causing activation of JNK with an associated change in endothelial phenotype including cytoskeletal changes, impaired lumen formation and increased migration and vascular permeability.

Simvastatin rescues *CCM2* deficiency *in vivo*

Humans with CCM have heterozygous mutations in *CCM2* and suffer from vascular hemorrhage or leakage, but not from severe developmental angiogenic defects as observed in mice with homozygous mutations in *Ccm2*. To examine the role of *Ccm2* in the disease state, we shifted our attention to mice heterozygous for *Ccm2*. We found no difference in vascular patterning (data not shown) or permeability to the intravascular dye Evans blue between heterozygous mice and wild-type controls (**Fig. 5a**). Clinical reports suggest that physiological[29–31]

or genetic[32] stressors may have a role in disease pathogenesis. An association was observed between accelerated progression of CCM and increasing amounts of vascular endothelial growth factor (VEGF)[29]. Consistent with this clinical observation, we observed significantly increased permeability to Evans blue in $Ccm2^{+/tr}$ mice in response to VEGF across a range of doses (**Fig. 5a**). Increased permeability was also observed in mice with endothelial-specific heterozygosity for *Ccm2* (**Fig. 5b**). These results demonstrate a role for *Ccm2* in the endothelium for the maintenance of normal *in vivo* barrier function in adults aside from its role in embryonic development.

Our observations *in vitro* suggested that Rho inhibition might rescue the increased permeability of *Ccm2*-heterozygous mice. However, mice do not tolerate the ROCK inhibitor Y-27632 (data not shown), and the Rho inhibitor C3 transferase has poor cellular penetration, limiting its usefulness *in vivo*. Inhibitors of 3-hydroxy-3-methyl-glutaryl-CoA reductase (statins) have pleiotropic effects that include the inhibition of Rho GTPases. Simvastatin disrupts the production of key intermediaries in the cholesterol synthesis pathway necessary for RHOA isoprenylation[33,34] and has been used as an inhibitor of Rho *in vivo*[35,36]. In culture, we found that simvastatin reduced formation of actin stress fibers in both control and *CCM2* siRNA–treated endothelial cells (**Fig. 5c**) and decreased haptotactic migration of *CCM2*-depleted HMVECs (**Fig. 5d**). Simvastatin also decreased the phosphorylation of JNK in both control and *CCM2* siRNA–treated cells (**Fig. 5e**). *In vivo*, we found that pretreatment of mice with simvastatin significantly reduced the permeability

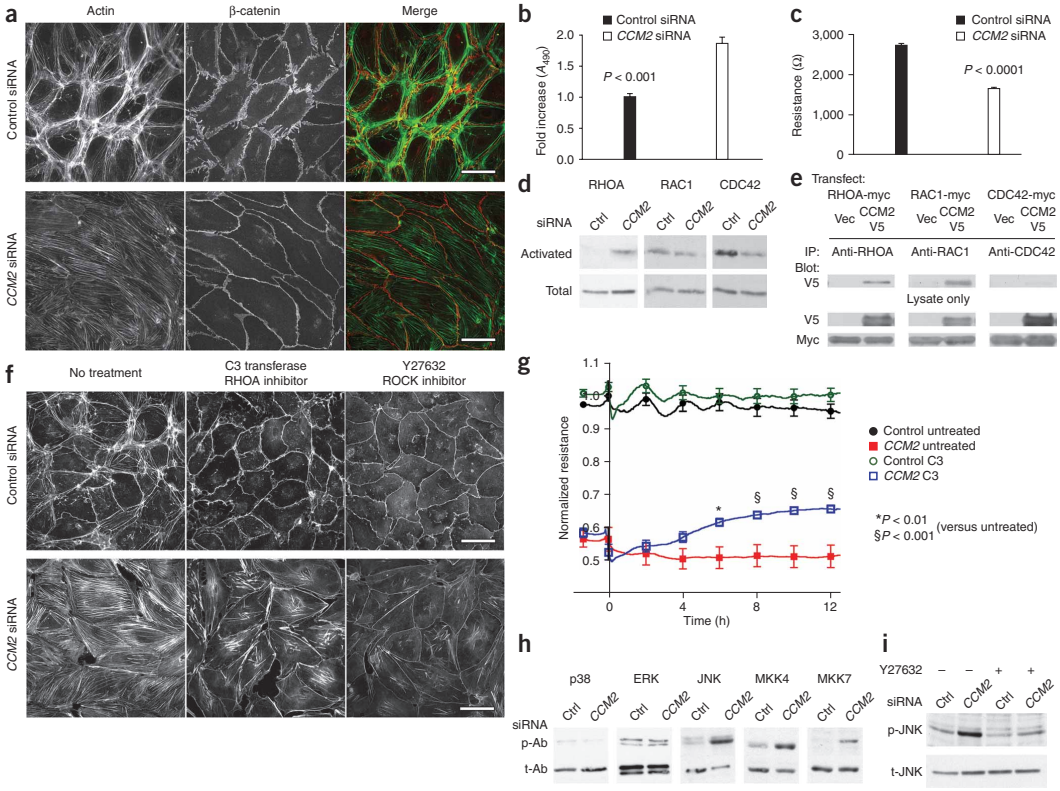

Figure 4 *CCM2* deficiency alters the endothelial cytoskeletal architecture and cell-cell interactions via activation of the small GTPase RHOA. (**a**) Confocal immunofluorescent visualization of cellular cytoskeleton (actin fibers) and cell junctions (β-catenin) in HMVECs treated with *CCM2* or random control siRNA. Results are representative of three independent experiments. (**b**) Endothelial monolayer permeability to HRP in HMVECs treated with *CCM2* or random control siRNA, as determined by absorbance at 490 nm (A_{490}). (**c**) Transendothelial resistance in *CCM2*-depleted HMVECs compared to control–treated cells. (**d**) GTPase pulldown assays for GTP-bound (active) RHOA, RAC1 and CDC42 in control and *CCM2*-depleted cells. Results are representative of three independent experiments. (**e**) Immunoprecipitation assays for CCM2 binding to Rho family GTPases. Myc, construct with myc epitope tag; Vec, empty vector control; V5, construct with V5 epitope tag; IP, immunoprecipitation; Anti, antibody to the indicated protein. Results are representative of three independent experiments. (**f**) Fluorescent phalloidin staining for actin stress fibers in HMVECs after treatment with inhibitors of Rho signaling. Results are representative of three independent experiments. (**g**) Time course of transendothelial electrical resistance in CCM2-depleted HMVECs compared to cells treated with either C3-transferase or control. (**h**) Immunoblot analyses of phosphorylated (active) MAP kinases and the JNK upstream kinases MKK4 and MKK7. p-Ab, phosphorylated kinase; t-Ab, total kinase. Results are representative of three independent experiments. (**i**) Immunoblot analysis of cell lysates for phosphorylated and total JNK after treatment with the Rho–kinase inhibitor Y-27632. Results are representative of three independent experiments. Scale bars, 50 μm. Values are means ± s.e.m. For **b**, **c** and **g**, a minimum of three independent experiments were performed.

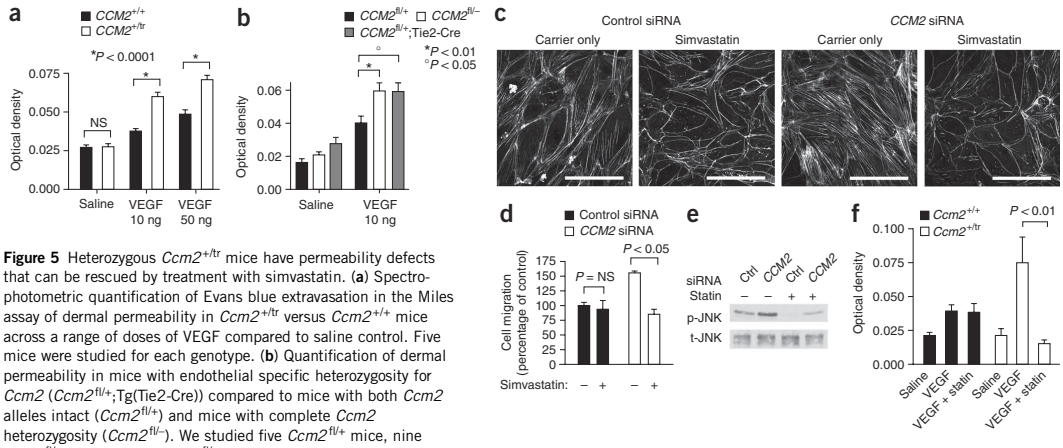

Figure 5 Heterozygous *Ccm2*$^{+/tr}$ mice have permeability defects that can be rescued by treatment with simvastatin. (**a**) Spectrophotometric quantification of Evans blue extravasation in the Miles assay of dermal permeability in *Ccm2*$^{+/tr}$ versus *Ccm2*$^{+/+}$ mice across a range of doses of VEGF compared to saline control. Five mice were studied for each genotype. (**b**) Quantification of dermal permeability in mice with endothelial specific heterozygosity for *Ccm2* (*Ccm2*$^{fl/+}$;Tg(Tie2-Cre)) compared to mice with both *Ccm2* alleles intact (*Ccm2*$^{fl/+}$) and mice with complete *Ccm2* heterozygosity (*Ccm2*$^{fl/–}$). We studied five *Ccm2*$^{fl/+}$ mice, nine *Ccm2*$^{fl/–}$ mice and ten *Ccm2*$^{fl/+}$;Tg(Tie2-Cre) mice. (**c**) Phalloidin staining for cellular actin fibers after treatment with carrier or simvastatin. Results are representative of three independent experiments. (**d**) Haptotactic migration of HMVECs to fibronectin after treatment with *CCM2* or random control siRNA and treatment with either simvastatin or ethanol carrier. A minimum of three independent experiments were performed. (**e**) Immunoblot for phosphorylated and total JNK in HMVECs treated with *CCM2* or random control siRNA and treated with either simvastatin or ethanol carrier. Results are representative of three independent experiments. (**f**) Quantification of Evans blue extravasation in the Miles assay in response to saline or VEGF after pretreatment with simvastatin or ethanol carrier. For both genotypes, we used three mice with control treatment and four mice with simvastatin treatment. Scale bars, 100 μm. Values are means ± s.e.m.

response of *Ccm2*$^{+/tr}$ mice to VEGF with no effect on the induced permeability of *Ccm2*$^{+/+}$ mice (**Fig. 5f**). These data suggest that the abnormal Rho GTPase activity observed in cells depleted of *CCM2* is also present in mice with reduced levels of Ccm2.

DISCUSSION

We show here that mice lacking *Ccm2* die in mid-gestation from failed angiogenesis and that these vascular defects are endothelial autonomous, providing what is to our knowledge the first *in vivo* evidence that any of the genes causing CCM are required in the endothelium. Using two distinct mutations in the *Ccm2* gene, we show that *Ccm2* is not required for the initial differentiation of endothelial cells from angioblast precursors (vasculogenesis)[18], but, rather, is required for subsequent vessel formation and remodeling (angiogenesis) In mice lacking Ccm2, the branchial arch arteries, the first essential angiogenic vessels, fail to form a stable lumen. As a result, the heart is not functionally connected with the vasculature, and circulation fails to initiate. Subsequent growth and development of the embryo is severely impaired, and death ensues. Tissue-specific mutants show that selective deletion of *Ccm2* in the endothelium is sufficient to reproduce the vascular defects, whereas mice lacking *Ccm2* in neural or smooth muscle cells develop normally. Thus, *Ccm2* is required in the endothelium for angiogenesis.

The recognition of an autonomous function for *Ccm2* in endothelial cells allowed us to examine previous biochemical studies in a new light. Such studies in fibroblasts and other nonendothelial cell types suggested a role for *CCM2* as a scaffold tying RAC1 GTPase activity to p38 activation in response to osmotic stress[12]. Endothelial cells face stressors in the context of a monolayer of interacting cells. In addition to the maintenance of individual cell size and shape in the face of stress, endothelial cells must also maintain contact and barrier function with adjacent cells in the monolayer. One might expect that *CCM2*, as a key molecule in response to stress, would have a role in maintaining stable endothelial cytoskeletal architecture and cell-to-cell interactions. Our observations in *CCM2*-depleted HMVECs support this hypothesis: these cells showed a loss of cortical actin, increased formation of actin stress fibers and decreased endothelial barrier function, changes that are typically caused by activated RHOA GTPase[25] and that can be reversed by inhibitors of RHOA signaling.

Our observations suggest a model whereby a dynamic equilibrium between vascular stability and instability exists. The endothelium of a stable blood vessel provides crucial barrier functions by controlling fluid, nutrient and cellular transport between intravascular and extravascular compartments. The formation and maintenance of strong cell-to-cell contacts is a favorable characteristic of endothelial cells in a stable blood vessel. However, when challenged by injury or inflammation, the endothelium alters its phenotype and temporarily disrupts cell-to-cell junctions. In this destabilized state, the endothelium can initiate the required migration and angiogenesis responses to the stressor. In this model, *CCM2* is required for endothelial cells to assume the stable phenotype, mediated at least in part by limiting RHOA activation[24,37,38]. Our cell culture data indicate that *CCM2* regulates key aspects of the stabilized endothelium, including cellular architecture, barrier function, migration and tube morphogenesis. Loss of *CCM2* favors the destabilized phenotype. In wild-type mice, with two functioning alleles of *CCM2*, the intensity and duration of instability after insult is limited. In heterozygous mice with only one functioning allele, there is a greater disruption of the stable state with increased permeability in response to VEGF. With the loss of both alleles of *Ccm2* in the endothelium, stability cannot be achieved—existing vessels enlarge and excessive but dysfunctional angiogenic sprouts form, which are unable to develop stable lumens to allow functional circulation.

This model might also explain the development of cavernous angiomas in familial CCM. Previously, a 'two-hit' hypothesis involving biallelic somatic and germline mutations was proposed to explain the focal nature of vascular lesions in human CCM, supported by a single case report[32]. The focal loss of the only remaining allele of *CCM2* would favor sustained instability of the affected endothelium, resulting

in a cavernous angioma. Our *in vivo* experiments suggest the possibility that the second hit may not be limited to genetic disruptions but could also take the form of recurrent exposure to cytokines such as VEGF that are released locally in response to stress or inflammation. The unique importance of strong endothelial cell-to-cell interaction in the central nervous system might render this vascular bed particularly sensitive to such perturbations. The importance of a physiologic response to stress as a second hit could explain the clinical association between elevated levels of VEGF and the rapid progression of CCM[29]. Thus, in retrospect, a gene originally identified for its role in the cytoskeletal response to stress should have been an obvious candidate gene for human vascular dysplasias. The efficacy of statins in rescuing *Ccm2*-related vascular pathology in mutant mice suggests a pharmacological strategy for treating patients whose therapeutic options are currently limited to brain surgery or radiation.

METHODS

Fetal ultrasound. We studied pregnant mice under isoflurane anesthesia on a heated stage, with continuous monitoring of electrocardiogram and respiration. After laparotomy, we studied embryos within 45 min. We determined genotype correlation with ultrasound findings by recording the position of the embryos in the uterus relative to the position in the abdomen by ultrasound. We used a Vevo 660 ultrasound machine (VisualSonics) with a 40-MHz transducer for imaging. We used digital subtraction to illustrate circulating blood in static images (**Supplementary Methods** online). We determined heart rates by M-mode ultrasound.

Ink injection. We injected India ink as previously described[39].

Endothelial cell vasculogenesis in three-dimensional collagen matrices. We suspended HUVECs (passages 2–5) within 3.75 mg ml^{-1} of collagen type I matrices and allowed them to undergo morphogenesis as described[40]. We fixed cultures with 3% glutaraldehyde for 30 min. We stained some cultures with 0.1% toluidine blue in 30% methanol and destained before photography and visualization. We performed time-lapse microscopy as previously described[41] with a Nikon TE2000U microscope with attached environmental chamber. We examined time-lapse images for total area of both vacuoles and lumens ($n = 5$ independent fields) and total process length from all cells ($n = 10$ fields). We quantified the number of lumens per field at 24 h ($n = 3$ fields). We used Metamorph (Molecular Devices) software to trace and quantify lumen area and process length.

Endothelial cell haptotaxis. We examined haptotactic migration with a modified Boyden chamber assay (Neuro Probe). We coated polycarbonate membranes (8-μm pores) with human fibronectin (1 μg ml^{-1}, Biomedical Technologies) on the lower surface. We added HMVECs to the upper well (20,000 cells per well) in endothelial growth medium-2 and allowed them to migrate for 3 h. We fixed and stained the membranes (Hema3 kit, Fisher), removed nonmigrated cells and mounted the membrane on a glass slide. We counted the number of migrated cells per high-power field for multiple fields and replicates (control, $n = 12$ fields; *CCM2*, $n = 8$ fields). For simvastatin rescue experiments, we treated cells with either 10 μM simvastatin (Calbiochem) or ethanol carrier for 24 h before the assay ($n = 3$ fields per condition).

Horseradish peroxidase permeability. We coated transwell inserts (Corning, 48-well, 3-μm pore) with human fibronectin and seeded them with 30,000 cells per well. We added HRP (25 μg ml^{-1}, Sigma) to the top of the insert. We asssayed solution from the bottom of the well for HRP 6 h later by colorimetric assay. We mixed the sample with guaicol (Sigma) and hydrogen peroxide (Fisher) and measured for absorbance at 490 nm ($n = 6$ wells each).

Transendothelial resistance. We coated an electrode culture array (Applied Biophysics) with human fibronectin and seeded it at 50,000 cells per well. Three days after seeding, we serum-starved cells in endothelial basal medium-2 with 0.2% BSA overnight. We measured transendothelial resistance with an electric cell-substrate impedance sensing system (Applied Biophysics). We added cell-permeable C3 transferase (1 μg ml^{-1}) to inhibit RHOA. For basal resistance, we measured 40 wells each; for Rho inhibition experiments, we measured six control wells each and ten C3 transferase wells each.

Miles assay. We performed tail vein injections of Evans blue (0.5% in normal saline, Sigma) in 8–12-week-old mice. Thirty minutes later, we injected either saline or VEGF-165 (R&D Systems, 10 ng) in multiple dermal sites. After an additional 30 min, we killed the mice, performed punch biopsies and eluted Evans blue from the biopsies in formamide (Invitrogen) overnight at 60 °C. We measured the absorbance of Evans blue at 620 nm, subtracting the background absorbance at 740 nm. We gave simvastatin (20 mg kg^{-1}) as an intraperitoneal injection 26 h before and 2 h before the intradermal stimuli. For the VEGF dose-response experiment, we used five mice per group. For the permeability experiment with conditional *Ccm2*, we used five *Ccm2*$^{fl/+}$ mice, nine *Ccm2*$^{fl/-}$ mice and ten *Ccm2*$^{fl/+}$;Tg(Tie2-Cre) mice. For the simvastatin experiment, we used three mice with control treatment and four mice with simvastatin treatment.

Additional methodology. Mouse strains, histology, confocal immunofluorescence of embryos, cell culture, transfection of endothelial cells with siRNAs, RT-PCR, immunofluorescent cell staining, GTPase activation assays, immunoprecipitation and MAPK profiling are described in the **Supplementary Methods** online.

Mouse experiments. All mouse experiments were approved by the University of Utah Institutional Animal Care and Use Committee.

Statistical analyses. For *in vitro* lumen formation and cell process formation in three-dimensional culture, we performed statistical comparisons between treatment groups with a two-tailed paired samples *t*-test with an α value of 0.05. For transwell *in vitro* permeability, transendothelial resistance, endothelial cell migration and the Miles assay of dermal permeability, we made group comparisons by two-tailed Student's *t*-test with an α value of 0.05.

Note: Supplementary information is available on the Nature Medicine website.

ACKNOWLEDGMENTS

We thank C. Colvin and A. Frias for technical assistance; M. Sanguinetti, S. Odelberg and I. Benjamin for critical comments; M. Kahn, K. Thomas, M. Ginsberg and R. Stockton for helpful scientific discussions; and A. Hall (Memorial Sloan-Kettering Cancer Center) for GTPase complementary DNA constructs. This work was funded by the US National Institutes of Health (K.J.W., D.A.M., G.E.D. and D.Y.L.), including training grant T32-GM007464 (A.C.C.) and a Ruth L. Kirschstein National Research Service award (N.R.L.), the American Heart Association (K.J.W. and D.Y.L.), the H.A. and Edna Benning Foundation, the Juvenile Diabetes Research Foundation, the Burroughs Wellcome Fund and the Flight Attendants Medical Research Institute (D.Y.L.).

COMPETING INTERESTS STATEMENT

The authors declare competing financial interests: details accompany the full-text HTML version of the paper at http://www.nature.com/naturemedicine/.

Published online at http://www.nature.com/naturemedicine/
Reprints and permissions information is available online at http://npg.nature.com/reprintsandpermissions/

1. Otten, P., Pizzolato, G.P., Rilliet, B. & Berney, J. A propos de 131 cas d'angiomes caverneux (cavernomes) du S.N.C. repérés par l'analyse rétrospective de 24 535 autopsies. *Neurochirurgie* **35**, 82–83 128–131 (1989).
2. Robinson, J.R., Awad, I.A. & Little, J.R. Natural history of the cavernous angioma. *J. Neurosurg.* **75**, 709–714 (1991).
3. Hasegawa, T. *et al.* Long-term results after stereotactic radiosurgery for patients with cavernous malformations. *Neurosurgery* **50**, 1190–1197 discussion 1197–1198 (2002).
4. Chappell, P.M., Steinberg, G.K. & Marks, M.P. Clinically documented hemorrhage in cerebral arteriovenous malformations: MR characteristics. *Radiology* **183**, 719–724 (1992).
5. Clatterbuck, R.E., Eberhart, C.G., Crain, B.J. & Rigamonti, D. Ultrastructural and immunocytochemical evidence that an incompetent blood-brain barrier is related to the pathophysiology of cavernous malformations. *J. Neurol. Neurosurg. Psychiatry* **71**, 188–192 (2001).
6. Toldo, I., Drigo, P., Mammi, I., Marini, V. & Carollo, C. Vertebral and spinal cavernous angiomas associated with familial cerebral cavernous malformation. *Surg. Neurol.* published online, doi:10.1016/j.surneu.2007.07.067 (22 January 2008).

7. Liquori, C.L. *et al.* Mutations in a gene encoding a novel protein containing a phosphotyrosine-binding domain cause type 2 cerebral cavernous malformations. *Am. J. Hum. Genet.* **73**, 1459–1464 (2003).
8. Denier, C. *et al.* Mutations within the *MGC4607* gene cause cerebral cavernous malformations. *Am. J. Hum. Genet.* **74**, 326–337 (2004).
9. Sahoo, T. *et al.* Mutations in the gene encoding KRIT1, a Krev-1/rap1a binding protein, cause cerebral cavernous malformations (CCM1). *Hum. Mol. Genet.* **8**, 2325–2333 (1999).
10. Laberge-le Couteulx, S. *et al.* Truncating mutations in *CCM1*, encoding KRIT1, cause hereditary cavernous angiomas. *Nat. Genet.* **23**, 189–193 (1999).
11. Bergametti, F. *et al.* Mutations within the programmed cell death 10 gene cause cerebral cavernous malformations. *Am. J. Hum. Genet.* **76**, 42–51 (2005).
12. Uhlik, M.T. *et al.* Rac-MEKK3–MKK3 scaffolding for p38 MAPK activation during hyperosmotic shock. *Nat. Cell Biol.* **5**, 1104–1110 (2003).
13. Petit, N., Blecon, A., Denier, C. & Tournier-Lasserve, E. Patterns of expression of the three cerebral cavernous malformation (CCM) genes during embryonic and postnatal brain development. *Gene Expr. Patterns* **6**, 495–503 (2006).
14. Plummer, N.W. *et al.* Neuronal expression of the *Ccm2* gene in a new mouse model of cerebral cavernous malformations. *Mamm. Genome* **17**, 119–128 (2006).
15. Seker, A. *et al.* CCM2 expression parallels that of CCM1. *Stroke* **37**, 518–523 (2006).
16. McCarty, J.H. *et al.* Selective ablation of α_v integrins in the central nervous system leads to cerebral hemorrhage, seizures, axonal degeneration and premature death. *Development* **132**, 165–176 (2005).
17. Glading, A., Han, J., Stockton, R.A. & Ginsberg, M.H. KRIT-1/CCM1 is a Rap1 effector that regulates endothelial cell cell junctions. *J. Cell Biol.* **179**, 247–254 (2007).
18. Risau, W. Mechanisms of angiogenesis. *Nature* **386**, 671–674 (1997).
19. Su, H., Mills, A.A., Wang, X. & Bradley, A. A targeted X-linked CMV-Cre line. *Genesis* **32**, 187–188 (2002).
20. Kisanuki, Y.Y. *et al.* Tie2-Cre transgenic mice: a new model for endothelial cell-lineage analysis in vivo. *Dev. Biol.* **230**, 230–242 (2001).
21. Sclafani, A.M. *et al.* Nestin-Cre mediated deletion of *Pitx2* in the mouse. *Genesis* **44**, 336–344 (2006).
22. Lepore, J.J. *et al.* High-efficiency somatic mutagenesis in smooth muscle cells and cardiac myocytes in SM22α-Cre transgenic mice. *Genesis* **41**, 179–184 (2005).
23. Kamei, M. *et al.* Endothelial tubes assemble from intracellular vacuoles in vivo. *Nature* **442**, 453–456 (2006).
24. Bayless, K.J. & Davis, G.E. Microtubule depolymerization rapidly collapses capillary tube networks *in vitro* and angiogenic vessels *in vivo* through the small GTPase Rho. *J. Biol. Chem.* **279**, 11686–11695 (2004).
25. Wojciak-Stothard, B., Potempa, S., Eichholtz, T. & Ridley, A.J. Rho and Rac but not Cdc42 regulate endothelial cell permeability. *J. Cell Sci.* **114**, 1343–1355 (2001).
26. Mohr, C., Koch, G., Just, I. & Aktories, K. ADP-ribosylation by Clostridium botulinum C3 exoenzyme increases steady-state GTPase activities of recombinant rhoA and rhoB proteins. *FEBS Lett.* **297**, 95–99 (1992).
27. Hirose, M. *et al.* Molecular dissection of the Rho-associated protein kinase (p160ROCK)-regulated neurite remodeling in neuroblastoma N1E–115 cells. *J. Cell Biol.* **141**, 1625–1636 (1998).
28. Kyriakis, J.M. & Avruch, J. Sounding the alarm: protein kinase cascades activated by stress and inflammation. *J. Biol. Chem.* **271**, 24313–24316 (1996).
29. Jung, K.H. *et al.* Cerebral cavernous malformations with dynamic and progressive course: correlation study with vascular endothelial growth factor. *Arch. Neurol.* **60**, 1613–1618 (2003).
30. Larson, J.J., Ball, W.S., Bove, K.E., Crone, K.R. & Tew, J.M.,, Jr. Formation of intracerebral cavernous malformations after radiation treatment for central nervous system neoplasia in children. *J. Neurosurg.* **88**, 51–56 (1998).
31. Shi, C., Shenkar, R., Batjer, H.H., Check, I.J. & Awad, I.A. Oligoclonal immune response in cerebral cavernous malformations. Laboratory investigation. *J. Neurosurg.* **107**, 1023–1026 (2007).
32. Gault, J., Shenkar, R., Recksiek, P. & Awad, I.A. Biallelic somatic and germ line CCM1 truncating mutations in a cerebral cavernous malformation lesion. *Stroke* **36**, 872–874 (2005).
33. Zeng, L. *et al.* HMG CoA reductase inhibition modulates VEGF-induced endothelial cell hyperpermeability by preventing RhoA activation and myosin regulatory light chain phosphorylation. *FASEB J.* **19**, 1845–1847 (2005).
34. Park, H.J. *et al.* 3-hydroxy-3-methylglutaryl coenzyme A reductase inhibitors interfere with angiogenesis by inhibiting the geranylgeranylation of RhoA. *Circ. Res.* **91**, 143–150 (2002).
35. Kranenburg, O., Poland, M., Gebbink, M., Oomen, L. & Moolenaar, W.H. Dissociation of LPA-induced cytoskeletal contraction from stress fiber formation by differential localization of RhoA. *J. Cell Sci.* **110**, 2417–2427 (1997).
36. Collisson, E.A., Carranza, D.C., Chen, I.Y. & Kolodney, M.S. Isoprenylation is necessary for the full invasive potential of RhoA overexpression in human melanoma cells. *J. Invest. Dermatol.* **119**, 1172–1176 (2002).
37. Im, E. & Kazlauskas, A. Src family kinases promote vessel stability by antagonizing the Rho/ROCK pathway. *J. Biol. Chem.* **282**, 29122–29129 (2007).
38. Mavria, G. *et al.* ERK-MAPK signaling opposes Rho-kinase to promote endothelial cell survival and sprouting during angiogenesis. *Cancer Cell* **9**, 33–44 (2006).
39. Whitehead, K.J., Plummer, N.W., Adams, J.A., Marchuk, D.A. & Li, D.Y. Ccm1 is required for arterial morphogenesis: implications for the etiology of human cavernous malformations. *Development* **131**, 1437–1448 (2004).
40. Davis, G.E. & Camarillo, C.W. An $\alpha_2\beta_1$ integrin-dependent pinocytic mechanism involving intracellular vacuole formation and coalescence regulates capillary lumen and tube formation in three-dimensional collagen matrix. *Exp. Cell Res.* **224**, 39–51 (1996).
41. Saunders, W.B. *et al.* Coregulation of vascular tube stabilization by endothelial cell TIMP-2 and pericyte TIMP-3. *J. Cell Biol.* **175**, 179–191 (2006).

The *Cerebral Cavernous Malformation* signaling pathway promotes vascular integrity via Rho GTPases

Kevin J. Whitehead, Aubrey C. Chan, Sutip Navankasattusas, Wonshill Koh, Nyall R. London, Jing Ling, Anne H. Mayo, Stavros G. Drakos, Douglas A. Marchuk, George E. Davis & Dean Y. Li

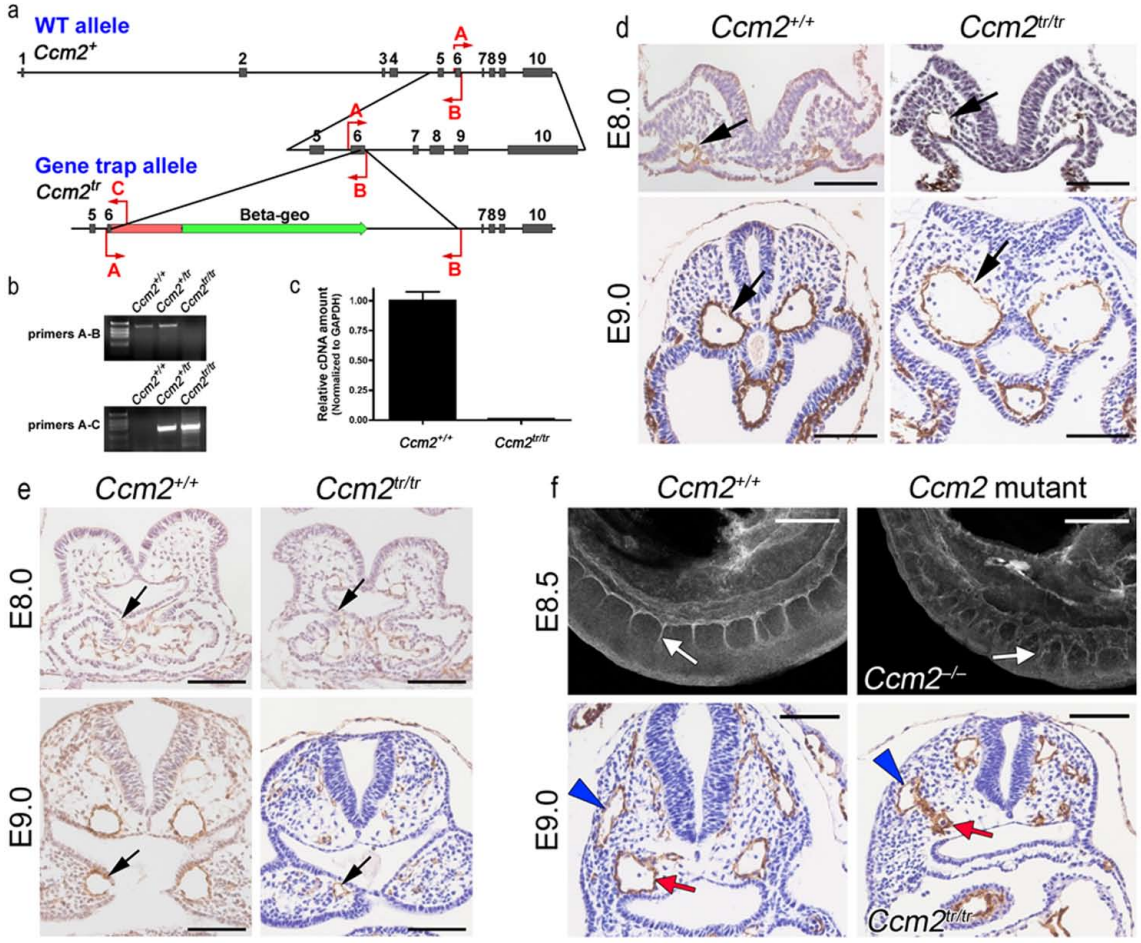

Supplementary figure 1 – A gene trap mutation results in loss of *Ccm2* expression and angiogenesis defects. (**a**) The genomic structure of wild type *Ccm2* is disrupted by insertion of the gene trap vector within exon 6. The location of genotype primers is demonstrated. (**b**) The results of PCR genotyping for the three possible genotypes is illustrated. (**c**) Real-time quantitative RT PCR with primers in exons 8 and 9 for *Ccm2* message in total RNA derived from $Ccm2^{tr/tr}$ embryos. The quantity of *Ccm2* cDNA was normalized to *Gapdh* (values +/- s.d.). (**d**) The aorta of the embryo (arrows) caudal to the heart and venous inflow in wild type and mutant embryos. The aortae of the mutant enlarge by E9.0 (lower right). (**e**) Development of the first branchial arch artery in mice lacking *Ccm2*. A cord of endothelial cells is present at E8.0 in both wild type and mutant embryos (arrows, upper panels). The mutant has endothelial cells without proper lumen at E9.0 (arrows, lower panels). (**f**) Angiogenesis defects involve the intersomitic arteries in mice lacking *Ccm2*. Intersomitic artery sprouts (white arrows) are broad and irregular in mutant embryos. An abnormal, direct connection between the cardinal vein (blue arrowheads) and dorsal aorta (red arrows) is seen in a mutant E9.0 embryo (lower right). Scale bars: 100 μm.

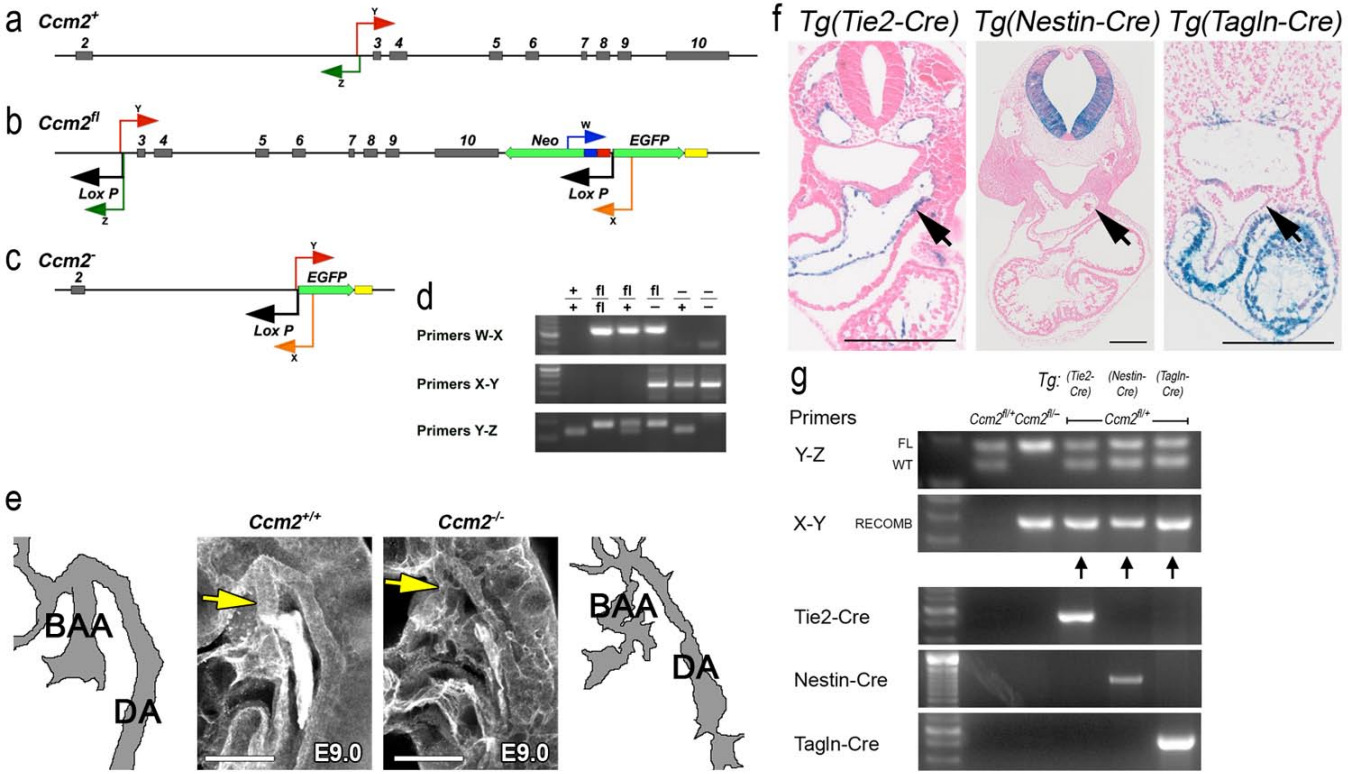

Supplementary figure 2. Conditional targeting of *Ccm2*. The three alleles of *Ccm2* that result from our targeting strategy are shown. (**a**) Wild type *Ccm2* has 10 exons, the final 9 of which are shown. (**b**) The conditional (floxed) allele includes LoxP sites that flank exons 3 through 10 of *Ccm2*. The floxed allele can be detected with primers W and X, or can be recognized by the upward shift in band size with primers Y and Z relative to wild type due to LoxP insertion. (**c**) Cre recombinase deletes exons 3–10 of *Ccm2*. The mutant allele can be detected with primers X and Y. (**d**) PCR genotyping results are shown for all 6 possible combinations. (**e**) Confocal immunofluorescence (CD31 antibody) of branchial arch arteries (yellow arrows) and aorta in an embryo homozygous for a germline recombined allele of *Ccm2* compared to a wild type littermate. Scale bars: 100 μm. (**f**) X-gal staining of embryos containing LacZ reporter allele and tissue specific Cre drivers as specified. The branchial arch artery endothelium is indicated (arrows). Scale bars: 500 μm. (**g**) PCR for the recombined allele in embryos (primers X-Y, "RECOMB"). Primers Y-Z also define the status of the wild type ("WT") and floxed ("FL") alleles. The appearance of PCR product for the recombined allele in $Ccm2^{fl/+}$ embryos (arrows) indicates Cre-mediated recombination for each of the tissue specific drivers.

Supplementary table 1. *Ccm2*$^{tr/tr}$ mutant phenotype: normal appearing embryos.

	Ccm2$^{+/+}$	*Ccm2*$^{+/tr}$	*Ccm2*$^{tr/tr}$
<E8.5	72	161	79
E8.5	217	362	177
E9.0	48	80	2
>E9.0	79	121	0

Supplementary Methods

Mouse strains.

Mice with gene trap mutations of *Ccm2* were derived from an embryonic stem cell clone (Bay Genomics). A construct for the conditional allele of *Ccm2* was derived from genomic sequence obtained from a BAC clone (RP22 library, Invitrogen). The construct extended from a *Sal*I site 5' of exon 3 through a *Bam*HI site 3' of exon 10. The construct contained inserts as outlined in Fig. S2. All mice were backcrossed into the C57BL6/J strain. Experiments performed prior to the 5th cross were performed with littermate controls. LacZ reporter mice (*R26R1*) and *Tie2-Cre* mice were generously provided by Phil Soriano and Masashi Yanagisawa respectively. *HPRT-Cre*, *Nestin-Cre* and *Tagln-Cre* mice were obtained from The Jackson Laboratory. Genotypes were determined by PCR analysis of genomic DNA isolated from either ear biopsies or yolk sac tissues using primers outlined in **Supplementary Fig. 1** and **2** (sequences available upon request).

Confocal immunofluorescence of embryos.

Embryos were prepared for confocal immunofluorescent detection of PECAM antigen as previously described[1] with the following exception. For improved signal detection in thick specimens, following the final wash steps after applying secondary antibody, embryos were processed through graded methanols before mounting in benzyl alcohol – benzyl benzoate (BABB) based mounting medium. Images were aquired with an Olympus FV300 confocal microscope, and stacks were chosen to visualize only one of the paired dorsal aortae. Multiple images were required to visualize the entire embryo. Photoshop was used to assemble source images into a final composite (image junctions shown in final assembly).

Digital Subtraction.

Ultrasound images were selected for digital subtraction by choosing frames unaffected by motion from maternal respiration. Sequential images were applied to each other in Photoshop (Adobe Systems, Inc.) using a subtractive filter to remove static portions of the image. Several resulting images of dynamic pixels were merged together using an additive filter. This composite of dynamic pixels was colorized using a gradient overlay. To provide some anatomic perspective, the colorized image was given 75% opacity and projected over an unfiltered source image.

Histology.

Embryos were studied with antibodies to PECAM (1:250 dilution, clone MEC13.3, BD Biosciences). Improved visualization on paraffin sections was obtained using a biotinylated tyramide signal amplification (TSA) kit (PerkinElmer) according to the manufacturer's instructions. Cardiac smooth muscle was demonstrated with antibodies to alpha smooth muscle actin (1:500 dilution, clone 1A4, Sigma) without signal amplification. To demonstrate tissue specificity of transgenic Cre

lines, embryos with appropriate LacZ reporter alleles were stained with X-gal as previously described[2].

Cell culture.
Human umbilical vein endothelial cells (HUVEC) and human dermal microvascular endothelial cells (HMVEC) were obtained from Lonza and grown according to the manufacturer's instructions in EGM-2 media (HUVEC) or EGM-2MV media (HMVEC). Human embryonic kidney (HEK 293T) cells (from ATCC) were grown in Dulbecco's Modified Eagle Medium (DMEM, Gibco) with 10% fetal bovine serum (Hyclone) supplemented with antibiotics.

Transfection of ECs with siRNAs.
Human *CCM2* siRNA was obtained from Dharmacon. Luciferase GL2 duplex or scramble siRNA (Dharmacon) were used as a control. EC transfection with siRNAs was carried out in growth media with 1% serum. Details of the siRNA transfection protocol have been described previously[3].

Reverse transcription-polymerase chain reaction (RT-PCR).
Total RNA was extracted from EC vasculogenesis assay at indicated time points or from siRNA-treated (Luciferase or *CCM2*) ECs using the Totally RNA Isolation kit (Ambion) according to the manufacturer's instructions. RNA (1 µg) was reverse transcribed using AccuScript High Fidelity 1st strand cDNA synthesis kit (Stratagene). RT-PCR amplification primer sequences are available upon request. For quantitative real-time PCR, total RNA was extracted from cultured endothelial cells or from embryos using the NucleoSpin RNA II kit (Clontech) according to the manufacturer's instructions. Reverse transcription was performed with random primers using the RetroScript kit (Ambion). Quantitative PCR was performed with TaqMan assays (Applied Biosystems) for human *CCM2* and *GAPDH*, or mouse *Ccm2* and *Gapdh*. Quantification was performed by standard curve method, and *CCM2* transcripts were normalized to *GAPDH* for comparisons.

Immunofluorescent Cell Staining.
Glass chamber slides were coated with human fibronectin (Biomedical Technologies, Inc.), and transfected cells were seeded at 50,000 cells per well. For the RHOA and ROCK experiment, cells were treated 4 d after seeding with 40 µg mL^{-1} of cell-permeable C3 transferase (Cytoskeleton, Inc.) or 20 µM Y-27632 (Santa Cruz Biotechnology) for 4 h. For the simvastatin experiment, cells were treated 3 d after seeding with 40 µM simvastatin or equivalent amounts of ethanol in growth media for 24 h. Cells were fixed in 4% formaldehyde and incubated with an antibody against β-catenin (BD Biosciences). Fluorescent secondary antibody (Molecular Probes) was used to visualize β-catenin staining. Actin cytoskeleton was visualized using fluorescently-conjugated phalloidin (Molecular Probes). Images were obtained with an Olympus FV300 confocal microscope.

GTPase Activation Assays.
Activity of RHOA, RAC1, and CDC42 were measured using activation assay kits (Upstate) according to manufacturer's instructions. Briefly, transfected cells were scraped into Mg^{2+} lysis buffer supplemented with protease inhibitors (Roche) and phosphatase inhibitors (Sigma). A small portion of the lysate was retained as total cell lysate and the rest was incubated with the assay reagent. GTP-bound forms were eluted from the assay reagent using Laemmli sample buffer and analyzed by western blotting. The total cell lysate was analyzed by western blotting for total GTPase input.

Immunoprecipitation.
An EST for *CCM2* (IMAGE: 2924210) was obtained from ATCC and cloned into a pcDNA3.1 Hygro+ plasmid modified to encode a C-terminal V5 tag. Constructs for myc-tagged RHOA, RAC1, and CDC42 were obtained from Addgene[4] (Addgene plasmid 15899, Addgene plasmid 15902, and Addgene plasmid 15905 respectively). Plasmids were transfected into HEK 293T cells using Lipofectamine 2000 (Invitrogen) according to the manufacturer's instructions. 3 d post transfection, cells were scraped into lysis buffer (50 mM Tris-HCl at pH 7.5, 100 mM NaCl, 0.5% Triton X-100) supplemented with protease and phosphatase inhibitors. A portion of cell lysate was retained as whole cell lysate, and the rest incubated with antibodies against RHOA (Santa Cruz Biotechnology), RAC1, or CDC42 (Upstate) as indicated at 4°C for 2 h, followed by incubation with Protein A/G beads (Santa Cruz Biotechnology). The beads were washed three times with lysis buffer and bound proteins were eluted using Laemmli sample buffer. Presence of CCM2-V5 was detected using an anti-V5 antibody (Invitrogen). Presence of myc-tagged RHOA, RAC1, and CDC42 were detected using an anti-myc antibody (Santa Cruz Biotechnology).

MAPK Profiling.
siRNA transfected cells were lysed in RIPA buffer (50 mM Tris pH 7.4, 150 mM NaCl, 1% NP-40) supplemented with protease and phosphatase inhibitors. Lysates were then analyzed by western blotting. Antibodies to phospho-JNK and total JNK were from Santa Cruz Biotechnology. Antibodies to phospho-ERK, phospho-p38, phospho-MKK4, phospho-MKK7, total ERK, total p38, total MKK4, and total MKK7 were from Cell Signaling Technology. The effect of ROCK inhibitor on JNK was tested by treating cells with 10 μM Y-27632 for 30 min prior to cell lysis. The effect of simvastatin on JNK was determined by treating cells with 10 μM simvastatin for 24 h prior to cell lysis.

References:

1. Whitehead, K.J., Plummer, N.W., Adams, J.A., Marchuk, D.A. & Li, D.Y. Ccm1 is required for arterial morphogenesis: implications for the etiology of human cavernous malformations. *Development* **131**, 1437-1448 (2004).

2. Navankasattusas, S.*, et al.* The netrin receptor UNC5B promotes angiogenesis in specific vascular beds. *Development* **135**, 659-667 (2008).
3. Saunders, W.B., Bayless, K.J. & Davis, G.E. MMP-1 activation by serine proteases and MMP-10 induces human capillary tubular network collapse and regression in 3D collagen matrices. *Journal of cell science* **118**, 2325-2340 (2005).
4. Nobes, C.D. & Hall, A. Rho GTPases control polarity, protrusion, and adhesion during cell movement. *J Cell Biol* **144**, 1235-1244 (1999).

CORRIGENDA AND ERRATA

Corrigendum: VEGF modulates erythropoiesis through regulation of adult hepatic erythropoietin synthesis

Betty YFY Tam, Kevin Wei, John S Rudge, Jana Hoffman, Joceyln Holash, Sang-ki Park, Jenny Yuan, Colleen Hefner, Cecile Chartier, Jeng-Shin Lee, Shelly Jiang, Nihar R Nayak, Frans A Kuypers, Lisa Ma, Uma Sundram, Grace Wu, Joseph A Garcia, Stanley L Schrier, Jacquelyn J Maher, Randall S Johnson, George D Yancopoulos, Richard C Mulligan & Calvin J Kuo
Nat. Med. **12, 793–800 (2006); published online 25 June 2006; corrected after print 6 April 2009**

In the version of this article initially published, the name of one of the authors, Nihar R. Nayak, was misspelled as Nihar R. Niyak. The error has been corrected in the HTML and PDF versions of the article.

Corrigendum: Bone marrow stromal cells attenuate sepsis via prostaglandin E_2–dependent reprogramming of host macrophages to increase their interleukin-10 production

Krisztián Németh, Asada Leelahavanichkul, Peter S T Yuen, Balázs Mayer, Alissa Parmelee, Kent Doi, Pamela G Robey, Kantima Leelahavanichkul, Beverly H Koller, Jared M Brown, Xuzhen Hu, Ivett Jelinek, Robert A Star & Éva Mezey
Nat. Med. **15, 42–49 (2009); published online 21 November 2008; corrected after print 6 April 2009**

In the version of this article initially published, the labeling in (Figure 4) was incorrect. In panel (b), the cells in the left two FACS plots are shown based on their size (FSC, *y* axis) and CD11b expression (*x* axis), and the cells in the right two FACS plots are shown based on their F4/80 expression (*y* axis) and GR1 expression (*x* axis). In panel (c), the curves should start at 1 h. In panel (d), the text labeling the *y* axis should read "*in vitro*," not "*in vivo*." The errors have been corrected in the HTML and PDF versions of this article.

Corrigendum: The cerebral cavernous malformation signaling pathway promotes vascular integrity via Rho GTPases

Kevin J Whitehead, Aubrey C Chan, Sutip Navankasattusas, Wonshill Koh, Nyall R London, Jing Ling, Anne H Mayo, Stavros G Drakos, Christopher A Jones, Weiquan Zhu, Douglas A Marchuk, George E Davis & Dean Y Li
Nat. Med. **15, 177–184 (2009); published online 18 January; corrected after print 6 April 2009**

In the version of this article initially published, Christopher A. Jones and Weiquan Zhu were not included in the list of authors. The error has been corrected in the HTML and PDF versions of the article.

Corrigendum: Effector memory T cell responses are associated with protection of rhesus monkeys from mucosal simian immunodeficiency virus challenge.

Scott G Hansen, Cassandra Vieville, Nathan Whizin, Lia Coyne-Johnson, Don C Siess, Derek D Drummond, Alfred W Legasse, Michael K Axthelm, Kelli Oswald, Charles M Trubey, Michael Piatak Jr, Jeffrey D Lifson, Jay A Nelson, Michael A Jarvis & Louis J Picker
Nat. Med. **15, 293–299 (2009); published online 15 February 2009; corrected after print 6 April 2009**

In the version of this article initially published, a "left" and "right" designation was switched in the legend for Figure 4d. The legend should read "FCICA of peripheral blood $CD8^+$ T cells from the four protected vaccinees, examining the response of these cells to SIV proteins that were (Rev-Tat-Nef) or were not (Pol and Vif) expressed by the administered RhCMV vectors before (left) and 133 d after (right) initiation of the SIVmac239 intrarectal challenge protocol." The error has been corrected in the HTML and PDF versions of the article.

Erratum: Straight talk with...Mac Cowell and Jason Bobe

Prashant Nair
Nat. Med. **15, 230–231 (2009); published online 5 March 2009; corrected after print 6 April 2009**

In the print version of this interview, the first response contained an unrelated excerpt from the previous month's Q & A. The text begins with "who could mobilize..." and ends with "…results and more results." The error did not appear online in the HTML and PDF versions of the article.

CHAPTER 3

MUTATIONS IN 2 DISTINCT GENETIC PATHWAYS RESULT IN CEREBRAL CAVERNOUS MALFORMATIONS IN MICE

The following chapter was reprinted with permission from the American Society for Clinical Investigation. In addition to myself, the other authors were Stavros Drakos, Oscar Ruiz, Alexandra Smith, Christopher Gibson, Jing Ling, Samuel Passi, Amber Stratman, Anastasia Sacharidou, M. Patricia Revelo, Allie Grossmann, Nikolaos Diakos, George Davis, Mark Metzstein, Kevin Whitehead, and Dean Li. It was originally published in the Jouranl of Clinical Investigation, 2011 May 2;121(5):1871-81. doi: 10.1172/JCI44393, Epub 2011 Apr 1. I participated in the design, execution, interpretation of data, and preparation of the manuscript.

Research article

Mutations in 2 distinct genetic pathways result in cerebral cavernous malformations in mice

Aubrey C. Chan,[1,2] Stavros G. Drakos,[1,3] Oscar E. Ruiz,[4] Alexandra C.H. Smith,[1,4] Christopher C. Gibson,[1,5] Jing Ling,[1] Samuel F. Passi,[1] Amber N. Stratman,[6] Anastasia Sacharidou,[6] M. Patricia Revelo,[7] Allie H. Grossmann,[1,7] Nikolaos A. Diakos,[1] George E. Davis,[6] Mark M. Metzstein,[4] Kevin J. Whitehead,[1,3] and Dean Y. Li[1,2,3,4]

[1]Molecular Medicine Program, [2]Department of Oncological Sciences, [3]Division of Cardiology, Department of Medicine, [4]Department of Human Genetics, and [5]Department of Bioengineering, University of Utah, Salt Lake City, Utah, USA. [6]Department of Medical Pharmacology and Physiology, School of Medicine, University of Missouri School of Medicine, Columbia, Missouri, USA. [7]Division of Anatomic Pathology, Department of Pathology, University of Utah, Salt Lake City, Utah, USA.

Cerebral cavernous malformations (CCMs) are a common type of vascular malformation in the brain that are a major cause of hemorrhagic stroke. This condition has been independently linked to 3 separate genes: Krev1 interaction trapped (*KRIT1*), Cerebral cavernous malformation 2 (*CCM2*), and Programmed cell death 10 (*PDCD10*). Despite the commonality in disease pathology caused by mutations in these 3 genes, we found that the loss of *Pdcd10* results in significantly different developmental, cell biological, and signaling phenotypes from those seen in the absence of *Ccm2* and *Krit1*. PDCD10 bound to germinal center kinase III (GCKIII) family members, a subset of serine-threonine kinases, and facilitated lumen formation by endothelial cells both in vivo and in vitro. These findings suggest that CCM may be a common tissue manifestation of distinct mechanistic pathways. Nevertheless, loss of heterozygosity (LOH) for either *Pdcd10* or *Ccm2* resulted in CCMs in mice. The murine phenotype induced by loss of either protein reproduced all of the key clinical features observed in human patients with CCM, as determined by direct comparison with genotype-specific human surgical specimens. These results suggest that CCM may be more effectively treated by directing therapies based on the underlying genetic mutation rather than treating the condition as a single clinical entity.

Introduction

Cerebral cavernous malformations (CCMs) are common vascular malformations with a prevalence of 1 in 200 to 250 individuals in unselected populations (1, 2). CCMs can lead to focal neurological deficits, seizures, and hemorrhagic stroke, but no pharmacologic therapy currently exists (3). CCMs predominantly occur in the central nervous system and are characterized by subclinical bleeding and consequential hemosiderin deposits that are detected by MRI (4). MRI is the primary clinical modality for detection, diagnosis, and management of CCMs. Hemosiderin deposits give CCMs an MRI appearance of a central mass with a dark perilesional halo, whose appearance is nearly diagnostic (pathognomonic) of cavernous malformation (5). Cavernous malformations are characterized by a complex of vascular channels of varying sizes lined by a single layer of endothelial cells without any abnormally large arteries, arterialized veins, or large venous outflow vessels. Although dense fibrillary neuroglial tissue may penetrate the mass, vascular channels are generally arranged in a back-to-back pattern with little or no intervening brain parenchyma. There is often a peripheral margin of gliotic tissue containing hemosiderin-laden macrophages (6).

CCMs can occur sporadically or be inherited in an autosomal dominant pattern. Familial CCM has been linked to heterozygosity for any of 3 genes: Krev1 interaction trapped (*KRIT1*), Cerebral cavernous malformation 2 (*CCM2*), and Programmed cell death 10 (*PDCD10*) (7). All 3 proteins bind each other in coimmunoprecipitation experiments on cells overexpressing these proteins, leading to the hypothesis that they function as a complex to affect a common signaling mechanism (8). Both Krit1 and Ccm2 are required for proper connection of the developing heart with the aorta to establish circulation in the mouse embryo (9, 10). Mice lacking either Krit1 or Ccm2 fail to form a lumenized first branchial arch artery to link the heart and aorta; as a result, mice lacking either gene die at the same age. The requirement for Ccm2 is endothelial autonomous (9, 11). In the endothelium, both KRIT1 and CCM2 suppress the activity of the small GTPase RhoA (9, 12). Loss of either gene leads to RhoA activation and signaling through Rho kinase (ROCK) resulting in increased actin stress fibers, impaired cell-cell interactions, and increased vascular permeability (9, 12, 13). These defects can be reversed in cell culture and in mice with inhibitors of RhoA including HMG-CoA reductase inhibitors (statins) (9, 12).

A recent report suggested a similar mechanism of Rho activation for PDCD10 (14). However, other studies have suggested a different cell-signaling role for PDCD10. While KRIT1, CCM2, and PDCD10 all occupy the cytoplasmic compartment of the cell, unique subcellular localization for each has been described, including nuclear localization of KRIT1 (15) and Golgi localization of PDCD10 (16). Each protein has also been found to have unique binding partners (17–19). PDCD10's binding partners include members of the germinal center kinase III (GCKIII) subfamily of serine-threonine kinases with homology to yeast sterile-20 (STE20) kinase (16, 20–23). Furthermore, the clinical features of CCM in *KRIT1*, *CCM2*, and *PDCD10* families have important differences (24, 25), with *PDCD10* resulting in the most severe disease (24, 26). It is possible that CCM disease is the common result of multiple unique mechanisms and may require unique therapeutic strategies to target the underlying disturbed cellular and signaling pathways.

Conflict of interest: The University of Utah seeks to commercialize this technology and has filed patent applications related to this manuscript.

Citation for this article: *J Clin Invest.* 2011;121(5):1871–1881. doi:10.1172/JCI44393.

Table 1
Early growth arrest and death in embryos lacking *Pdcd10*

Cross	*Pdcd10*$^{+/-}$ × *Pdcd10*$^{+/-}$			
Genotype	***Pdcd10***$^{+/+}$	***Pdcd10***$^{+/-}$	***Pdcd10***$^{-/-}$	**Total litters**
No. of progeny				
E7.5	75	114	52	27
E8.0	9	13	0[A]	4
E8.5	27	45	0[A]	13
E9.0	1	5	0	1
>E9.0	7	8	0	3

The numbers of normal-appearing and viable offspring by genotype in matings between *Pdcd10*$^{+/-}$ parents are shown. [A]Ages at which growth-arrested embryos could be obtained.

Though the signaling and cellular mechanisms associated with the 3 known CCM proteins may be different, a common genetic mechanism of loss of heterozygosity (LOH) has been suggested for familial CCM disease (27–29). Familial CCM is more aggressive than sporadic disease, with an earlier age of onset, increased risk of hemorrhage and seizure, and an increased number of lesions (3, 30–32). These observations have led to the hypothesis that CCM disease occurs by the Knudson 2-hit mechanism, similar to retinoblastoma (33). There is limited evidence from human pathologic specimens to support an association of LOH with CCM lesions. In a series of challenging experiments, a number of investigators have identified biallelic mutations, 1 somatic and 1 germline, in the endothelium of a subset of patient samples (27, 28, 34). While LOH could not be confirmed for a number of samples, a total of 4 cases have been described for *KRIT1* and 1 case each for *CCM2* and *PDCD10*. Mice heterozygous for *Krit1* or *Ccm2* do not develop cavernous malformations, and no examples of secondary somatic mutations have been reported (35, 36).

To determine whether endothelial LOH is not simply associated with, but is causative for, CCM pathology, requires an animal model with a controlled genetic mutation that can be directed and detected in a tissue-specific manner. In this work, we use drug-inducible, tissue-specific strains of Cre recombinase to target conditional null alleles of the CCM genes to test directly the 2-hit hypothesis for cavernous malformations. We demonstrate that *Pdcd10* differs substantially from *Ccm2* in development, cell biology, and signaling, yet LOH is the common genetic mechanism to cause CCMs in both genotypes. These findings suggest that PDCD10 influences different endothelial signaling pathways from KRIT1/CCM2 to lead to a common histopathology and imply that medical treatment to stabilize familial CCM may need to be developed and evaluated in a genotype-specific manner.

Results

Loss of Pdcd10 results in embryonic lethal phenotypes distinct from loss of Krit1 or Ccm2. To determine the role of *Pdcd10* in development and disease, we developed a conditional null allele, *Pdcd10*^{flox}, in which exons 4–8 are flanked with LoxP sites (Supplemental Figure 1; supplemental material available online with this article; doi:10.1172/JCI44393DS1). This strategy also allowed us to generate a constitutive null allele, *Pdcd10*$^{-}$, by crossing mice carrying *Pdcd10*^{flox} with a mouse strain expressing Cre recombinase in the germline (37). To characterize the role of *Pdcd10* in development, we intercrossed *Pdcd10*$^{+/-}$ mice and harvested embryos at varying stages of development. Surprisingly, we found that mice lacking *Pdcd10* died at a much earlier age than those deficient for either *Krit1* or *Ccm2*. Whereas *Krit1* and *Ccm2* mice show growth arrest at E9.0 and die at E11 (9–11), the loss of *Pdcd10* leads to growth arrest at E8.0, after gastrulation, but prior to the onset of circulation or the requirement for cardiovascular function (Table 1 and Supplemental Figure 1).

An earlier requirement for *Pdcd10* than *Krit1* or *Ccm2* in development does not preclude a shared role in the vascular system. Mice with endothelial loss of *Ccm2* phenocopy the constitutive null mutant (9, 11), so we sought to determine whether mice with endothelial loss of *Pdcd10* would also recapitulate the *Ccm2* phenotype. Using the endothelial Tie2-Cre driver, the same Cre driver that we used to ablate *Ccm2* (9), we found that although mice with endothelial loss of *Pdcd10* (*Pdcd10*$^{flox/-}$*;Tie2-Cre*) did not survive to birth, they had patent branchial arch arteries, a developed circulatory system, and were indistinguishable from control littermates at E9.5 (Supplemental Figure 2). Instead, we found that loss of *Pdcd10* in the endothelium leads to progressive enlargement of the cardinal vein and other veins of the rostral embryo at E11.5 (Figure 1). Venous enlargement was not due to abnormal cardiac structure or function (Figure 1 and Supplemental Figure 2), nor were defects observed in arteries of the embryo (Figure 1 and Supplemental Figure 2). Death occurred due to hemorrhage from venous rupture by E13.5 (Table 2). Additionally, mice with loss of *Pdcd10* in neural and glial tissues induced by Nestin-Cre showed no vascular or any other obvious defects and were born alive (Supplemental Figure 2 and Supplemental Table 1). These observations suggest that *Pdcd10* is required in the endothelium for control of venous size and integrity, yet *Pdcd10* differs from *Ccm2* in that it is not required for the establishment of circulation.

Loss of PDCD10 does not affect RhoA signaling but results in lumen formation defects. To explore the role of PDCD10 in endothelial cells, we depleted *PDCD10* in human dermal microvascular endothelial cells (HMVEC) with siRNA (Supplemental Figure 3). Whereas the loss of CCM2 leads to an increase in actin stress fibers as a result of RhoA activation (9, 12, 13) and phosphorylation of myosin light chain-2 by Rho kinase (Figure 2), we observed none of these indicators of RhoA activation with the loss of PDCD10 (Figure 2). Thus, the role of PDCD10 in endothelial cell biology and signaling differs from that of CCM2.

Having found that PDCD10's function in development differs from that of CCM2, we sought to identify defects associated with PDCD10 depletion in assays relevant to vascular development. PDCD10-depleted HUVECs showed defective function in a 3D angiogenesis assay. Endothelial cells plated in a collagen matrix spontaneously organize into complex multicellular capillary-like networks with lumens (38), but cells depleted of PDCD10 failed to organize themselves into a lumenized network (Supplemental Figure 4, A and B). We explored potential downstream signaling pathways using this assay. A growing body of evidence suggests that PDCD10 interacts with the GCKIII subfamily of serine-threonine kinases (16, 21–23); we used siRNA to deplete cells of each of the subfamily members (Supplemental Figure 3). We observed no effect on lumen formation with the knockdown of STK25, STK24, or MST4 in HUVECs (Supplemental Figure 4C).

Pdcd10 functionally associates with GCKIII in lumen formation. Because the GCKIII family members may be functionally redundant, we sought to validate the importance of the PDCD10-GCKIII interaction in vivo and in a simpler genetic model. We chose the fruit fly, *Drosophila melanogaster*, in which the GCKIII family is represented by

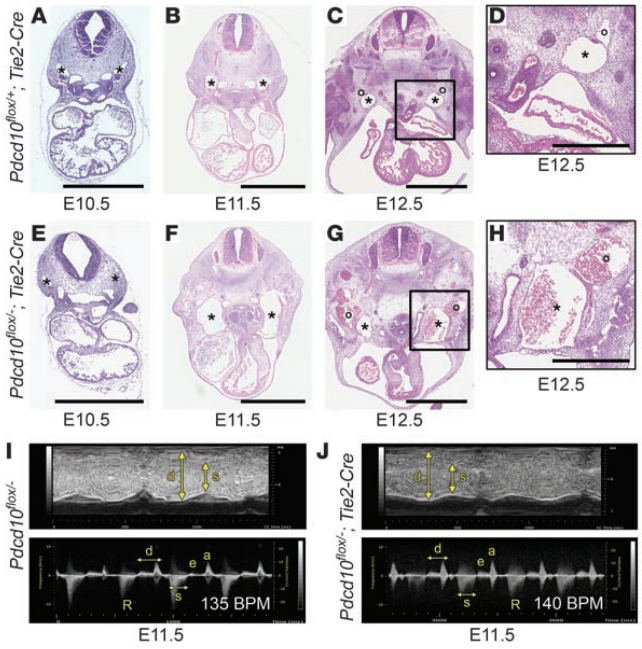

Figure 1
Pdcd10 is required in the endothelium for venous integrity. (**A**–**H**) H&E staining of developmental time course of *Pdcd10* endothelial knockout. *Pdcd10*$^{flox/+}$*;Tie2-Cre* is shown in **A**–**D**. *Pdcd10*$^{flox/–}$*;Tie2-Cre* is shown in **E**–**H**. Close-up images of the cardinal vein at E12.5 are shown in **D** and **H**. Asterisks denote the cardinal veins. Circles denote the external jugular veins. (**I** and **J**) Echocardiography of hearts from *Pdcd10*$^{flox/–}$ (**I**) and *Pdcd10*$^{flox/–}$*;Tie2-Cre* (**J**) mice at E11.5. Top panels show M-mode images of hearts contracting over time. Bottom panels show waveforms corresponding to blood flow across the atrioventricular valves. s, systole; d, diastole; e, early filling; a, atrial contraction; R, valvular regurgitation. Scale bars: 1 mm (**A**–**C** and **E**–**G**); 500 μm (**D** and **H**). $n \geq 6$ embryos at each age.

a single protein, GCKIII. This model avoids the complexity of human or mouse, which has 3 GCKIII kinases, or zebrafish, which has 2 orthologs for *Pdcd10*, 2 orthologs for *STK25*, and single orthologs for *STK24* and *MST4* (23). Furthermore, the *Drosophila* genome contains a single ortholog of *PDCD10*, but no orthologs for *KRIT1* or *CCM2*. Thus, *Drosophila* represents a simple model organism for studying Pdcd10-specific biology. To ensure that the biochemical interaction between PDCD10 and GCKIII was conserved in *Drosophila*, we performed immunoprecipitation assays with the *Drosophila* proteins. *Drosophila* Pdcd10 binds to GCKIII (Supplemental Figure 4D) in a manner analogous to that of human, mouse, or zebrafish protein (21, 23). A human disease PDCD10 mutation exists, which deletes 18 amino acids crucial for PDCD10-GCKIII binding (21). Removal of the analogous 18 amino acids from the *Drosophila* Pdcd10 protein abrogated binding to GCKIII (Supplemental Figure 4D).

Whereas *Drosophila* do not develop a vascular system, they do form a branched, lumenized network of tubes in the tracheal (respiratory) system. This epithelial network requires coordinated cell-cell interactions and specialized cell-cell junctions, analogous to the mammalian vascular system (39, 40). To determine the necessity of Pdcd10 in developing fly tracheal tubes, we expressed a dsRNA directed against *Pdcd10* (41) under the control of the tracheal-specific *Breathless* promoter (42) using the GAL4-UAS system (43). We found that tracheal tubes lacking Pdcd10 grow and branch normally, but fail to lumenize and fill with air (Supplemental Figure 5), indicating that Pdcd10 is required for normal lumen formation in fly tracheal tubes as it is in human endothelial tubes. This effect is highly penetrant; nearly all dsRNA-expressing flies show lack of lumenization in multiple tracheal tubes (Supplemental Figure 4E). The specificity of this effect is confirmed, as it could be rescued by coexpression of *Drosophila* Pdcd10 in RNAi-expressing cells (Supplemental Figure 4E). Notably, coexpression of the 18–amino acid deletion form of *Drosophila* Pdcd10, which does not bind to GCKIII, fails to rescue this phenotype (Supplemental Figure 4E). We used the same RNAi strategy to inactivate *GCKIII* (44) in the developing tracheal system. Tracheal tubes lacking GCKIII exhibit failure of lumenization (Supplemental Figure 5), and the phenotype appears very similar to that of Pdcd10-deficient tubes. Thus, Pdcd10 is essential for normal lumen formation in the absence of Krit1 and Ccm2 and in a manner that requires interaction with GCKIII kinases.

Our experiments in *Drosophila* suggested that GCKIII kinases are required for lumen formation but that functional redundancy in mammalian cells may have accounted for the lack of a lumen formation defect when any single kinase was lost. We therefore performed combinatorial knockdown experiments for pairs of the GCKIII kinases. Consistent with our hypothesis, we found that the loss of STK25, if coupled with the loss of either STK24 or MST4, was sufficient to reproduce the lumen formation defects seen with PDCD10 depletion (Supplemental Figure 4). Thus, PDCD10 interaction with GCKIII kinases is critical in lumen formation.

LOH of either Pdcd10 or Ccm2 causes murine cavernous malformations that phenocopy human CCMs. Pdcd10 and Ccm2's functions clearly differ in embryonic development, in endothelial cell culture, and in signaling, and Pdcd10 is necessary for lumen formation in a system that lacks Ccm2 or Krit1. The 3 genes, however, are linked

Table 2
Loss of *Pdcd10* in the endothelium leads to embryonic death after E12.5

Cross	*Pdcd10*$^{flox/flox}$ × *Pdcd10*$^{+/–}$*;Tie2-Cre*			
Genotype	***Pdcd10***$^{flox/+}$	***Pdcd10***$^{flox/–}$	***Pdcd10***$^{flox/+}$***;Tie2-Cre***	***Pdcd10***$^{flox/–}$***;Tie2-Cre***
No. of progeny				
E9.5	14	14	7	11
E12.5	13	28	16	16
E15.5	8	8	20	0
P21	26	20	20	0

Live offspring by genotype at embryonic and postnatal time points resulting from matings between *Pdcd10*$^{flox/flox}$ and *Pdcd10*$^{+/–}$*;Tie2-Cre* parents.

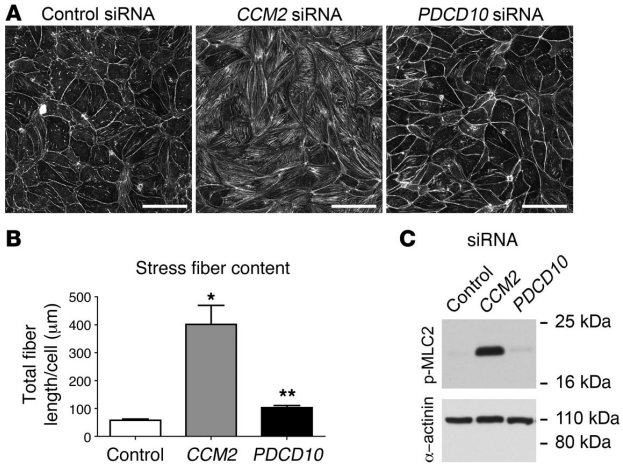

Figure 2
PDCD10 differs from CCM2 in downstream signaling. (**A**) Phalloidin staining of human microvascular endothelial cells treated with siRNA directed against *CCM2*, *PDCD10*, or nonsense control. (**B**) Quantification of stress fiber response of HMVEC cells. Stress fiber content is determined by adding the total length of stress fibers divided by the total number of cells. Results indicate mean ± SEM and are representative of at least 3 independent experiments. **P* < 0.001 versus control or *PDCD10*; ***P* = NS versus control. (**C**) Immunoblot for phospho-myosin light chain-2 (with α-actinin immunoblot as a loading control). Results are representative of 3 independent experiments. Scale bars: 100 μm.

to the same human disease. Limited human genetics suggested an association between LOH and CCM disease, so we investigated whether *Pdcd10* and *Ccm2* share this genetic mechanism for causing disease. To control the timing of the endothelial "second-hit," we used a drug-inducible Cre strain under the control of the *PDGF-B* promoter. This *PDGFb-iCreER*^{T2} strain expresses a Cre recombinase activated only after administration of the drug tamoxifen. Consistent with the original report describing this recombinase (37), we found that the administration of tamoxifen on the first postnatal day (P1) led to efficient, endothelial-specific recombination throughout the entire brain vasculature (Supplemental Figure 6). The induction of endothelial LOH of either *Pdcd10* or *Ccm2* by this Cre at birth resulted in CCMs in mice as early as 1 month of age (Figure 3). Induction of endothelial LOH of either *Pdcd10* or *Ccm2* resulted in a spectrum of vascular malformations, from capillary telangiectasias, to isolated caverns, to multiple back-to-back caverns with thrombosis, hemorrhage, and formation of secondary channels (Supplemental Figure 7). Loss of protein product via LOH was confirmed by antibody staining (Supplemental Figure 8). The retinal vasculature is another location for human CCMs, and murine cavernous malformations were also observed in mouse retinal vasculature (Supplemental Figure 9). To formally prove LOH in the endothelium of these CCMs, we performed laser capture microdissection to obtain tissue-specific DNA as previously done in human studies of CCM (28). We found that DNA from lesion endothelium had lost the conditional allele for either *Pdcd10* or *Ccm2*, confirming LOH, whereas this allele could still be detected in adjacent neuronal tissue (Figure 3). In contrast, loss of *Ccm2* in neural tissues using Nestin-Cre did not result in the development of vascular malformations (Supplemental Figure 10).

We characterized the histopathologic features of cavernous malformations in mice with induced endothelial loss of either *Pdcd10* (Figure 4) or *Ccm2* (Figure 5). We compared mouse CCMs with surgical specimens from CCM patients with germline mutations of either *PDCD10* (Figure 4) or *CCM2* (Figure 5). Cavernous malformations in these induced mouse models share all of the key histologic features of CCM lesions with human specimens. Furthermore, both *Pdcd10* and *Ccm2* resulted in identical pathologic findings for all of these defining characteristics in both human and mouse (Table 3). Mouse specimens showed numerous

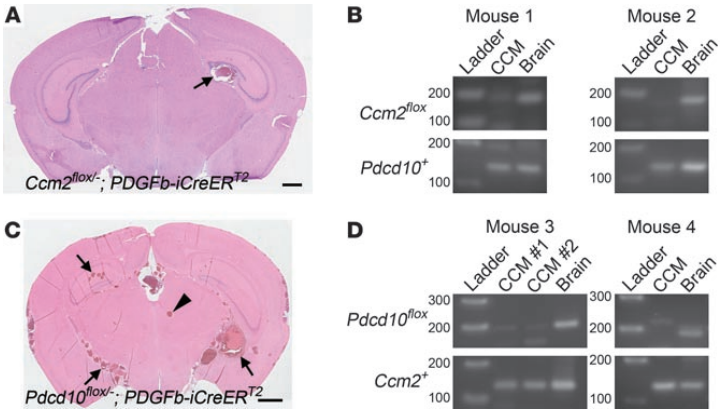

Figure 3
Cavernous malformations result from LOH of either *Ccm2* or *Pdcd10*. (**A**) Cavernous malformation (arrow) shown in an H&E-stained section of brain cerebrum from a mouse with induced endothelial knockout of *Ccm2*. (**B**) Confirmation of LOH of *Ccm2* in 2 mice with loss of *Ccm2*^{flox} allele by PCR, compared with *Pdcd10* wild-type allele as a control. (**C**) Cavernous malformations (arrows) and a less complex telangiectasia (arrowhead) shown in an H&E-stained section of brain cerebrum from a mouse with induced endothelial knockout of *Pdcd10*. (**D**) Confirmation of LOH of *Pdcd10* in 2 mice by PCR with loss of *Pdcd10*^{flox} allele compared with *Ccm2* wild-type allele as a control. Samples in **B** and **D** were obtained via laser capture microdissection of sectioned mouse brains. Scale bars: 1 mm.

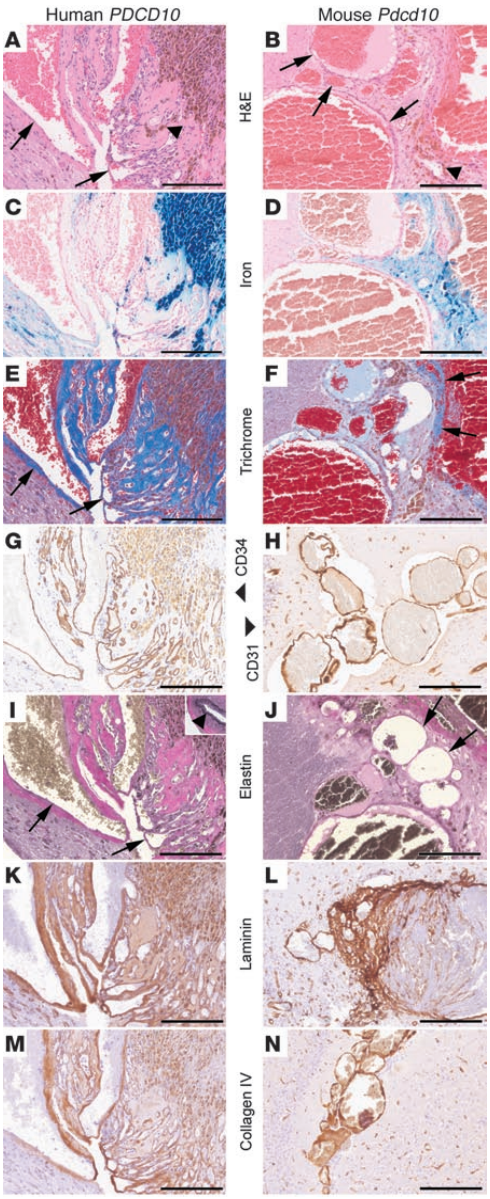

Figure 4
Pathologic analysis of mouse and human *PDCD10*-associated CCM. Paired analysis of histologic sections with human tissue on the left and mouse on the right. (**A** and **B**) H&E staining revealing back-to-back vascular channels (arrows) and hemosiderin pigment (arrowheads) in surrounding tissues. (**C** and **D**) Iron (blue) detected by Prussian blue stain highlights hemosiderin deposits in macrophages and surrounding brain tissue. (**E** and **F**) Fibrous matrix deposits (blue) identified by Masson's trichrome staining with fibrous tissue surrounding vascular channels (arrows) and in surrounding gliotic brain. (**G** and **H**) Endothelial staining for CD34 (**G**) or CD31 (**H**) is positive in the cells lining the channels. (**I** and **J**) Elastin staining shows that vascular channels lack elastic laminae (arrows) unlike normal vessels of similar caliber (arrowhead, inset in **I**). The fibrous matrix surrounding channels includes laminin (**K** and **L**) and collagen IV (**M** and **N**). Scale bars: 200 μm.

vascular channels of variable diameter (Figure 4, A and B, and Figure 5, A and B), some of them with organized thrombi. Immunohistochemical stains for endothelium highlighted endothelial cells in the channels, with focal attenuation or loss of endothelial cells in larger channels (Figure 4, G and H, and Figure 5, G and H). Iron stain highlighted the presence of hemosiderin-laden macrophages and hemosiderin in the wall of the channels as well as in the periphery and brain tissue (Figure 4, C and D, and Figure 5, C and D). Additionally, we also examined gliosis, trichrome staining, elastin, laminin, and collagen type IV, and these features were all identical between mouse and human lesions (Figure 4, E and N, Figure 5, E and N, and Table 3).

We also examined mouse lesions at the ultrastructural level using transmission electron microscopy. Murine cavernous malformations showed endothelial cells lining vascular channels with associated basal lamina (Figure 6A). Some of the larger channels showed segmental multilayering (lamellated appearance) of the basal lamina (Figure 6B). The most dilated channels showed focally marked attenuation of the endothelial cells (Figure 6C); however, tight junctions were identified between cells, and definitive gaps were not seen. Connective tissue composed mainly of collagen fibers separated the vascular channels (Figure 6D). Pericytes or astrocytic foot processes were missing, as seen in human lesions. Foci of mononuclear inflammatory cells were also seen (Figure 6E), including hemosiderin-laden macrophages (Figure 6F). Ultrastructural analysis of murine CCM lesions was similar to that described in human CCMs (45), further solidifying the fidelity of the mouse model to the human disease.

Murine cavernous malformations can be detected and followed noninvasively by MRI. MRI is used to document the natural history of human cavernous malformations and will be necessary for prospective therapeutic trials in both mice and humans. We thus employed monthly live MRI studies to follow the onset and progression of disease in mice until at least 6 months of age (Figure 7). As in humans (24), mice lacking *Pdcd10* had an earlier onset of disease, with a more severe phenotype than *Ccm2*. All *Pdcd10* mice studied at 1 month of age had lesions, whereas no *Ccm2* mice had yet developed lesions by 2 months of age (Figure 7K). Mice with *Pdcd10* mutations had a greater disease burden when assessed by total lesion burden (Figure 7L) or by number of complex lesions (increased signal intensity within the lesion; Figure 7M). Cavernous malformations were fully penetrant in mice with *Ccm2* LOH at 6 months of age and most had lesions at 4 months, at which time the disparity between the genotypes began to narrow. This parity reflected not only the increased burden of disease in *Ccm2*, but also the onset of death in the most severely affected *Pdcd10* mice. Mice of both genotypes began to die of hemorrhage, but mortality was greater in mice with LOH for *Pdcd10* (Figure 7N), a finding that reflects the reported experience in humans (24).

Discussion

Although CCM has been associated with mutations in 3 distinct loci, it has been clinically treated as a single pathophysiologic entity. In this manuscript, we describe for what we believe is the first time the pathologic features of CCM in a genotype-specific manner. We

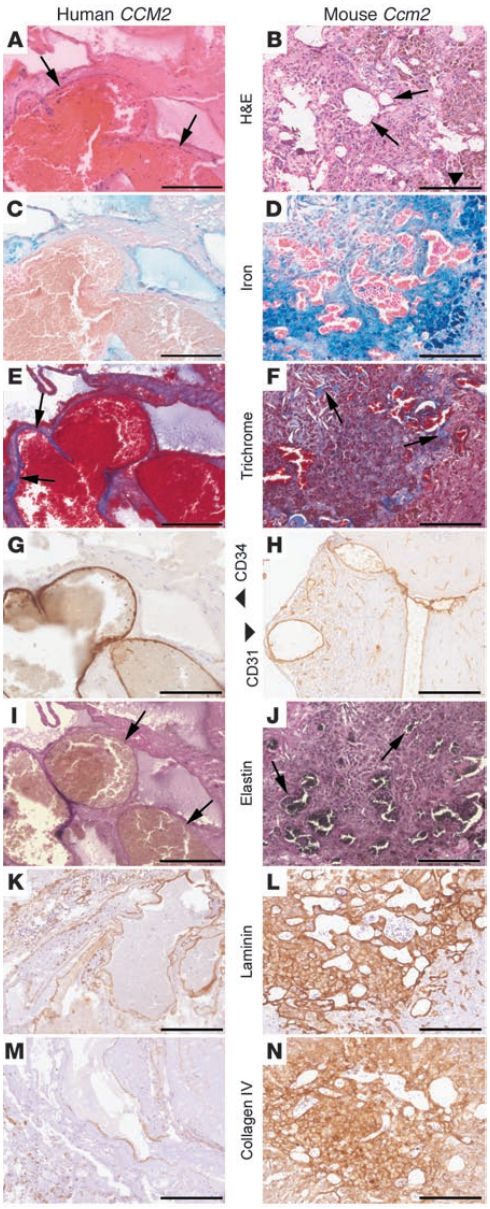

Figure 5
Pathologic analysis of mouse and human *CCM2*-associated CCM. Paired analysis of histologic sections with human tissue on the left and mouse on the right. (**A** and **B**) H&E staining revealing back-to-back vascular channels (arrows) and hemosiderin pigment (arrowhead) in surrounding tissues. (**C** and **D**) Iron (blue) detected by Prussian blue stain highlights hemosiderin deposits in macrophages and surrounding brain tissue. (**E** and **F**) Fibrous matrix deposits (blue) identified by Masson's trichrome staining with fibrous tissue surrounding vascular channels (arrows) and in surrounding gliotic brain. (**G** and **H**) Endothelial staining for CD34 (**G**) or CD31 (**H**) is positive in the cells lining the channels. (**I** and **J**) Elastin staining shows that vascular channels lack elastic laminae (arrows). The fibrous matrix surrounding channels includes laminin (**K** and **L**) and collagen IV (**M** and **N**). Scale bars: 200 μm.

find that mutations of both *PDCD10* and *CCM2* result in a common pathologic expression of disease in both humans and mice. Surprisingly, this common disease endpoint does not constitute proof of a common disease mechanism. Whereas our previous work and the work of others found that Ccm2 and Krit1 play similar roles in embryonic development, in vitro cell biology, and cell signaling (9, 10, 12, 13), these roles differ from those we observe with Pdcd10. Unlike Krit1 and Ccm2, Pdcd10 is not required for development of the branchial arch arteries that connect the heart to the aorta. Rather, Pdcd10 has an essential, nonendothelial role in development not shared with Krit1 or Ccm2 as well as an essential function in venous maturation. We further observe differences in cell biology and signaling between PDCD10 and KRIT1 or CCM2; whereas the loss of KRIT1 or CCM2 leads to RhoA activation, increased Rho kinase activity, myosin light chain phosphorylation, and actin stress fiber formation (9, 12, 13), we do not observe activation of this signaling pathway in cells depleted of PDCD10. Instead, we found that PDCD10 signals primarily through the GCKIII family of kinases.

The similarity in human CCM disease caused by mutations in *KRIT1*, *CCM2*, and *PDCD10* have led to an assumption that the proteins encoded by these genes function in a common signaling pathway. This assumption has been supported by experimental evidence showing binding between ectopically expressed, epitope-tagged proteins (7, 8). However, the complexities of signaling pathways and pathophysiology allow for multiple mechanisms to converge on a common disease phenotype (Figure 8A). An example is hypertrophic cardiomyopathy, which was considered 1 disease until molecular genetics revealed that 2 different mechanisms (sarcomere function or metabolism), each affected by distinct genes, both result in pathologic hypertrophy (Figure 8B and ref. 46). We propose that a similar scenario is involved in the pathogenesis of CCM (Figure 8C).

There is controversy concerning the signaling pathways affected by PDCD10. Several reports suggest an essential role for binding GCKIII family serine-threonine kinases (16, 21–23). However, a recent characterization of mice carrying a different conditional allele of *Pdcd10* showed that the loss of Pdcd10 in endothelial cells substantially blocks VEGFR2 signaling and inhibits the earliest stages of developmental angiogenesis (47). The implication of VEGFR2 signaling through MAP kinases agrees with a previous report linking GCKIII kinases and ERK signaling (20). Our data contrast with these reports; we observe that the absence of Pdcd10 in vivo leads to a localized vascular defect at a much later developmental stage, inconsistent with a panendothelial block of VEGF signaling. In cell culture, we have not found any interaction between PDCD10 and VEGF or ERK signaling (Supplemental Figure 11). We suspect that this disparity may be due to a difference in knockout strategy; however, our confidence in our allele is bolstered by our ability to induce CCM disease. Our data support the model that PDCD10 signals through the GCKIII family kinases, as we have observed in human endothelial cells and in *Drosophila* that PDCD10 binds to GCKIII family kinases and both are required for lumen formation. Previous reports have further suggested that GCKIII signals through RhoA to converge

Table 3
Pathologic findings in human and murine CCMs

Genotype	Human *CCM2*	Murine *Ccm2*	Human *PDCD10*	Murine *Pdcd10*
Trichrome	+	+	++	++
Iron	+	+	++	++
Elastin	–	–	–	–
CD34	+	NA	+	NA
CD31	NA	+	NA	+
Laminin	+	+	+	+
Collagen IV	+	+	+	+

The pathologic findings compared for human and murine CCMs associated with mutations of either *CCM2* or *PDCD10*.

with KRIT1/CCM2 signaling (23). By direct comparison of Ccm2 and Pdcd10 in mouse and cell biology, however, our data suggest that PDCD10 signaling is distinct from the CCM2-RhoA axis.

The nature and severity of disease in familial forms of CCM in comparison with sporadic CCM suggested a genetic mechanism consistent with Knudson's 2-hit hypothesis (33): LOH for a CCM gene induces lesions. Limited evidence to support this theory has come from a few human surgical samples amid multiple cases in which the second genetic hit could not be found (27, 28). Further supportive evidence comes from mice with heterozygous mutations for *Krit1* or *Ccm2* that have been mated into strains with high rates of spontaneous mutations. Mice heterozygous for *Krit1* develop CCM lesions on either a p53- or Msh2-null background, whereas mice heterozygous for *Ccm2* develop lesions only on the p53-, but not the Msh2-null background (35, 36). Whereas these models provide suggestive evidence of LOH and employ stochastic events to induce CCM formation, LOH was not demonstrated at either locus, nor can the LOH hypothesis be supported for all CCM genes, as $Ccm2^{+/-};Msh2^{-/-}$ mice do not develop CCMs. These models also do not rule out a role for mutations in other, non-CCM genes and do not control tissue specificity of mutation. The penetrance of CCMs in these models is incomplete, complicating the use of these models in prospective trials to study therapeutics or natural history of CCM disease. Concurrent development of neoplasms in both the p53- and the Msh2-null backgrounds also adds confounding physiological stressors and increases the mortality of the animals. In contrast, we employ a strategy that allows direct testing of the LOH mechanism in CCM disease. Using an inducible Cre-recombinase, we have targeted gene-specific LOH for both *Pdcd10* and *Ccm2* to the endothelium of mice. In the case of both genes, we have found that LOH is sufficient to cause a fully penetrant CCM phenotype that recapitulates every key pathologic and radiologic hallmark of human disease.

Much work remains to translate the observations and insights regarding disease signaling mechanisms into viable therapeutic strategies in patients. This work underscores the importance of carefully considering disease mechanisms in a genotype-specific manner. The availability of faithful, genotype-specific, and highly penetrant mouse models of CCM disease unlocks the tremendous opportunities to study the natural history of lesion genesis and progression as well as opportunities for preclinical testing of therapeutic interventions. In order for mouse models of CCM disease to be useful in informing human studies, the same tools used to follow patients with CCM need to be developed for serial observation of affected mice. We have demonstrated that noninvasive MRI of live mice, the same modality used to follow CCM in humans, can detect and follow murine CCMs. Although our mouse models share a measurable mortality, as with humans, they are compatible with prolonged survival and serial, noninvasive observation. The ability to follow these mice noninvasively over time is a crucial prerequisite for judging the effectiveness of any preclinical therapeutic strategy in the future and for testing the timing and intensity of LOH required for lesion formation. Our mouse models of CCM phenocopy human disease closely, supplanting previously available surrogate phenotypes, and are a powerful new tool in the armamentarium to decipher and combat CCM disease.

Methods

Mouse strains. The *Ccm2* conditional knockout mice have been previously described (9). A construct for the conditional allele of *Pdcd10* was derived from genomic sequence obtained from a BAC clone (RP22 library; Invitrogen). The construct extended from a SacII site 5′ of exon 4 through an ApaI site 3′ of exon 8. The construct contained inserts as outlined in Supplemental Figure 1, including LoxP sequences at a KasI site just 5′ of exon 4 and at a EcoRI site just 3′ of exon 8. All mice were backcrossed into the C57BL/6J strain. Experiments performed prior to the fifth cross were performed with littermate controls. *LacZ* reporter mice (R26R1), *Tie2-Cre*

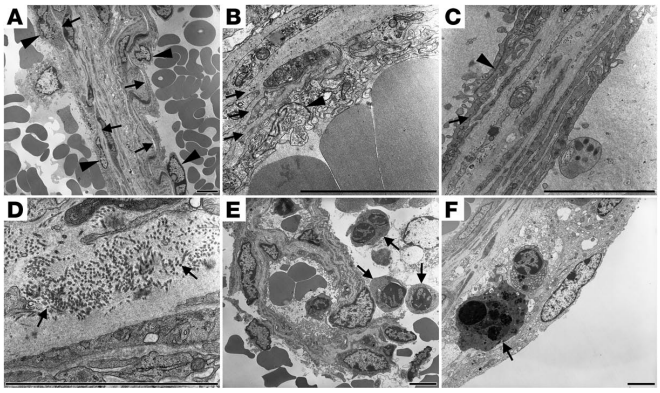

Figure 6
Ultrastructural findings in murine cavernous malformations. (**A**) Dilated vascular channels are lined by endothelial cells (arrowheads) with associated basal lamina (arrows). (**B**) Occasional channels have segments with a multilayered appearance (arrows indicate lamellae of endothelium with basal laminae). Tight junctions appear intact (arrowhead). (**C**) Focal areas of endothelial attenuation are observed (arrow) without apparent gaps or disruption of tight junctions (arrowhead indicates a junctional complex). (**D**) Channels are separated by loose connective tissue composed mostly of collagen (arrows). (**E**) Foci of mononuclear inflammatory cells are present (arrows). (**F**) Hemosiderin-laden macrophages (arrow) are among the inflammatory cells observed. Images are representative of 5 lesions from 3 *Pdcd10* mice. Scale bars: 4 μm.

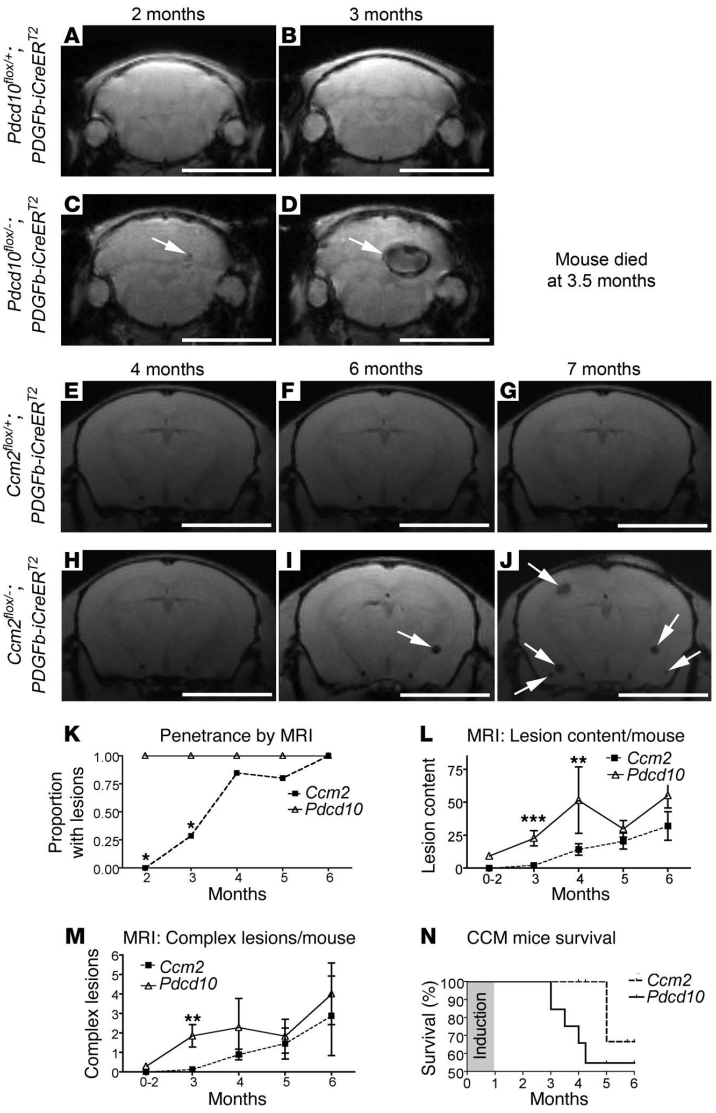

Figure 7
Natural history of murine CCM by MRI — *Pdcd10* onsets earlier and is more severe than *Ccm2*. (**A**–**D**) Live MRI scans of the same *Pdcd10*$^{flox/+}$*; PDGFb-iCreER*^{T2} mouse at 2 months and 3 months (**A** and **B**) and its *Pdcd10*$^{flox/-}$*;PDGFb-iCreER*^{T2} littermate (**C** and **D**). Both mice were given tamoxifen at birth. (**E**–**J**) Live MRI scans of the same *Ccm2*$^{flox/+}$*;PDGFb-iCreER*^{T2} mouse (**E**–**G**) and its *Ccm2*$^{flox/-}$*;PDGFb-iCreER*^{T2} littermate (**H**–**J**) at 4, 6, and 7 months. Both mice were given tamoxifen at birth. Arrows indicate CCM lesions. (**K**) Disease penetrance (proportion affected) by age in *Ccm2* and *Pdcd10* induced knockout mice as assessed by live MRI. (**L**) Lesion burden assessed as total number of lesions observed on each tomographic view (slice) of the MRI per mouse. (**M**) Number of complex lesions (lesions with bright cores) per mouse. (**N**) Kaplan-Meier survival curve of *Ccm2* and *Pdcd10* induced knockout mice. For **K**–**N**, $n = 11$ *Ccm2*, $n = 13$ *Pdcd10*. Data in **L** and **M** represent mean ± SEM. $^{*}P < 0.01$; $^{**}P < 0.05$; $^{***}P < 0.001$. Scale bars: 1 mm.

mice, and *PDGFb-iCreER*^{T2} mice were generously provided by Phil Soriano (Fred Hutchinson Cancer Research Center, Seattle, Washington, USA, and Mount Sinai School of Medicine, New York, New York, USA), Masashi Yanagisawa (University of Texas Southwestern Medical Center at Dallas, Dallas, Texas, USA), and Marcus Fruttiger (University College London Institute of Ophthalmology, London, United Kingdom) via Holger Gerhardt (London Research Institute – Cancer Research UK, London, United Kingdom), respectively. *HPRT-Cre*, *Nestin-Cre*, and *Tomato-EGFP* reporter mice were obtained from The Jackson Laboratory. Genotypes were determined by PCR analysis of genomic DNA isolated from either ear biopsies or yolk sac tissues using primers outlined in Supplemental Figure 1. Primer sequences were as follows: primer W: 5′-GCAATCCATCTTGTTCAATGGC-3′, primer X: 5′-CGTAGGTCAGGGTGGTCACG-3′, primer Y: 5′-TGAAAGAGGACATACTGGAGAGGC-3′, primer Z: 5′-AAGGACAAGAAAGCACTGTTGACC-3′. Tamoxifen (Sigma-Aldrich) was resuspended in corn oil (Sigma-Aldrich), and 40 ng was given as an i.p. injection to mouse pups on perinatal day 1.

MRI of mouse brains. All MRI experiments were conducted on a 7T Bruker Biospec 70/30 USR scanner (Bruker Biospin MRI Inc.) equipped with a BGA12S gradients set. A combination of volume-transmit–only radio frequency coil (internal diameter: 72 mm) and a quad-surface-receive–only coil (internal diameter: 1.5 cm) were used. For live scans, mice were anesthetized in 2.5% isoflurane and then placed into the scanner on top of circulating heated water. During the scans, mice were monitored for temperature and respiration, with isoflurane concentration and water bath temperature adjusted to maintain a body temperature between 35.8°C and 37.6°C and respiration between 75 and 100 breaths/min. A gradient recalled echo sequence was used to acquire coronal slices spanning the whole brain. Sequence parameters were as follows: repetition time, 328 ms; echo time, 5.4 ms; flip-angle, 40°; 12 averages, in-plane-resolution, 125 μm × 125 μm; and slice thickness, 0.5 mm.

For postmortem specimens, mouse skulls were fixed in 4% formaldehyde for at least 3 days before the brain was imaged with the skull intact. Postmortem MRI scanning allows a high-resolution coverage of the brain at the expense of longer scan time. High-resolution 3D gradient echo was acquired using the same scanner configuration described above, with isotropic voxel size of 78 μm × 78 μm × 78 μm over 9 hours. Other sequence parameters were as follows: repetition time, 250 ms; echo time, 7.5 ms; flip angle, 30°; and 2 averages.

Histology. Embryo and mouse CCM lesions were studied with antibodies to PECAM (1:250 dilution, clone MEC13.3; BD Biosciences) and PDCD10 (1:50 dilution, Prestige Antibody; Sigma-Aldrich). Improved visualization on paraffin sections was obtained using a biotinylated tyramide signal

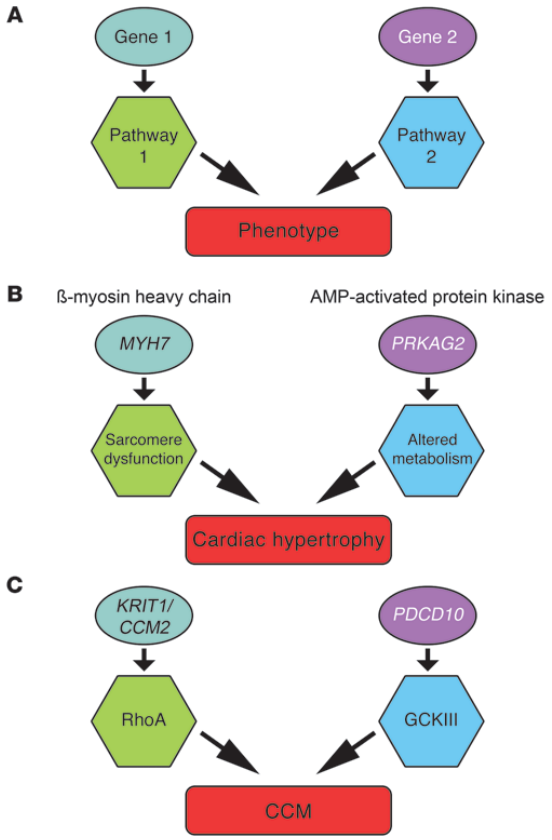

Figure 8
Convergence of different mechanistic pathways in common pathology. (**A**) Proposed schema for different genes acting on separate mechanistic pathways, yet ultimately resulting in a common expression of disease. (**B**) Genetic studies of hypertrophic cardiomyopathy highlight genes that can be grouped broadly into 2 separate mechanistic pathways: sarcomeric proteins such as β-myosin heavy chain (MYH7), and metabolic genes including adenosine monophosphate-activated protein kinase (PRKAG2). (**C**) Studies of mouse development, cell biology, and signaling suggest that KRIT1 and CCM2 signal through RhoA GTPase, while PDCD10 signals through GCKIII kinases to lead to cavernous malformations.

amplification (TSA) kit (PerkinElmer) according to the manufacturer's instructions. To demonstrate tissue specificity of *PDFGb-iCreER*^{T2}, brains from mice carrying a *LacZ* reporter allele were fixed and then stained with X-gal as previously described (48). Brains from mice carrying the *Tomato-EGFP* reporter allele were fixed and then embedded into OCT (Fisher Scientific) for fluorescent frozen sections. H&E staining of embryos was performed using standard procedures.

For histology of adult mouse brains, mouse skulls were fixed in 4% formaldehyde for at least 3 days or zinc-buffered formalin overnight before the brain was removed and sliced into 4 coronal sections. These sections were embedded into paraffin by standard techniques. Prussian blue staining for iron and Masson's trichrome staining of mouse brain sections were performed using the Artisan system (DAKO) according to manufacturer's instructions. Staining for elastin, laminin, and collagen IV was performed by the Immunohistochemistry Research and Development Lab at ARUP Laboratories. Human CCM samples were stained in the same way as adult mouse brains except for CD34 staining, which was performed by the Central Labs at Intermountain Medical Center (Murray, Utah, USA).

Fluorescent staining of mouse retinas. Mice were anesthetized using Avertin (2,2,2-tribromoethanol, 0.4 mg/g; Acros Organics) and perfused with fluorescently conjugated tomato lectin (Vector Labs) as previously described (49) at a dose of 5 μg/g body weight. After 5 minutes, mice were perfused with saline and then with 4% formaldehyde. Retinas were then extracted, stained, and mounted as previously described (50).

Analysis of mouse embryos. Confocal immunofluorescence of embryos and fetal ultrasound were performed as previously described (9).

Transmission electron microscopy. Samples were fixed in 1% formaldehyde, 2.5% glutaraldehyde in 0.1 M sodium cacodylate buffer with 8 mM $CaCl_2$ and 2.4% sucrose, pH 7.4, for at least 3 days. Samples were then rinsed in 0.1 M cacodylate buffer, postfixed in 2% osmium tetroxide in 0.1 M cacodylate buffer, rinsed in type I water, and then enbloc stained with saturated aqueous uranyl acetate. Samples were dehydrated through a graded series of ethanols, followed with final dehydration in acetone, and then infiltrated and embedded in an epoxy resin.

Thick sections and thin sections were cut on a Leica EM UC6 ultramicrotome (Leica Microsystems). The thick sections were cut with glass and the thin sections were cut with a diatome diamond knife. Thick sections were dried on glass slides and were stained with 1% toluidine blue O in 1% aqueous sodium borate. Thin sections were placed on 135 mesh copper hex grids and stained sequentially with saturated aqueous uranyl acetate and Reynolds lead citrate.

Sections were examined on an FEI Tecnai T-12 transmission electron microscope (FEI) at 80 KV. Images were taken on Kodak 4489 electron microscope film, developed with Kodak D-19 developer, fixed, washed, and dried. The negatives were scanned on an Epson Perfection Photo 4990 flatbed scanner.

Cell culture. HUVEC and HMVEC were obtained from Lonza and grown according to the manufacturer's instructions in EGM-2 media (HUVEC) or EGM-2MV media (HMVEC). Human embryonic kidney (HEK 293T) cells (ATCC) were grown in DMEM (Gibco; Invitrogen) with 10% fetal bovine serum (Bio-West) supplemented with antibiotics. EAHY cells were generously provided by Andrew Weyrich (University of Utah) and were grown in DMEM with 10% fetal bovine serum and HAT supplement (Sigma-Aldrich).

Transfection of ECs with siRNAs. Human *CCM2* and *PDCD10* siRNAs were obtained from Dharmacon. Luciferase GL2 duplex or nontargeting siRNA (Dharmacon) were used as controls. EC transfection with siRNAs was carried out in growth media with 1% serum. Details of the siRNA transfection protocol have been described previously (51).

RT-PCR. Total RNA was extracted from EC vasculogenesis assay at indicated time points or from siRNA-treated ECs using the ToTALLY RNA Isolation Kit (Ambion) according to the manufacturer's instructions. RNA (1 μg) was reverse transcribed using AccuScript High Fidelity 1st strand cDNA synthesis kit (Stratagene; Agilent). RT-PCR amplification used the following primers: forward: 5′-AGACTTCACGGAGTCCCTTC-3′, reverse: 5′-AGAAGGTCTGAAGTATTAAGTTGG-3′. For quantitative real-time PCR, total RNA was extracted from cultured endothelial cells or from embryos using the NucleoSpin RNA II Kit (Clontech) according to the manufacturer's instructions. Reverse transcription was performed with random primers using the RETROScript Kit (Ambion). Quantitative PCR was performed with TaqMan assays (Applied Biosystems) for human *CCM2*, *PDCD10*, *GAPDH*, *STK24*, *STK25*, and *MST4* or mouse *Pdcd10* and *Gapdh*. Quantification was performed by standard curve method, and

CCM2 and *PDCD10* transcripts were normalized to *GAPDH* for comparisons. RT-PCR primers for embryonic *Pdcd10* transcripts were as follows: primer 4F: 5′-TTCACCGAGTCCCTCCTTCG-3′; primer 7/8R: 5′-GAACACATTTATTGCCTTGCCATC-3′; primer 1F: 5′-AAGTCCGTGCCTCAGTTGCC-3′; and primer EGFP-R: 5′-TCCTCGCCCTTGCTCACC-3′.

Immunofluorescent cell staining. Glass chamber slides (Nalge Nunc; Thermo Fisher) were coated with human fibronectin (Biomedical Technologies Inc.), and transfected cells were seeded at 50,000 cells per well. Cells were fixed in 4% formaldehyde and actin cytoskeleton was visualized using fluorescently conjugated phalloidin (Molecular Probes; Invitrogen). Images were obtained with an Olympus FV300 confocal microscope.

Endothelial cell vasculogenesis in 3D collagen matrices. This assay was performed as previously described (9, 38).

Immunoprecipitation and Western blotting. An expressed sequence tag (EST) for human *PDCD10* (IMAGE: 3050540) was obtained from ATCC and cloned into a pcDNA3.1 Hygro$^+$ plasmid (Invitrogen) modified to encode an N-terminal FLAG tag. ESTs for *Drosophila Pdcd10* and *GCKIII* were obtained from the Drosophila Genomics Resource Center and cloned into a pcDNA3.1 Hygro$^+$ plasmid modified to encode an N-terminal FLAG tag (*Pdcd10*) or HA tag (*GCKIII*). PDCD10Δ18 constructs were made using nested PCR with primers designed to overlap and omit the 54 nucleotides encoding those 18 amino acids. Plasmids were transfected into EAHY or HEK 293T cells using Lipofectamine 2000 (Invitrogen) according to the manufacturer's instructions, with a reduced dosage of DNA and lipofectamine for EAHY cells. Two days after transfection, cells were scraped into lysis buffer (50 mM Tris-HCl at pH 7.5, 100 mM NaCl, 0.5% Triton X-100) supplemented with protease and phosphatase inhibitors and 1 mM DTT. A portion of cell lysate was retained as whole cell lysate and the rest precleared with normal mouse IgG conjugated to agarose beads (Santa Cruz Biotechnology Inc.) at 4°C for 1 hour, then incubated with anti-FLAG resin at 4°C for 2 hours. The beads were washed 3 times with lysis buffer, and bound proteins were eluted using Laemmli sample buffer. Presence of FLAG-tagged PDCD10 proteins was detected using the anti-FLAG M2 antibody (Sigma-Aldrich). Presence of HA-tagged GCKIII was detected using an anti-HA antibody (Santa Cruz Biotechnology Inc.). Near-infrared secondary antibodies (LI-COR Biosciences) were used to probe the blots, which were visualized using the Odyssey system (LI-COR Biosciences).

Rabbit polyclonal antibody against PDCD10 was from Proteintech Group. Rabbit antibodies against phospho-myosin light chain (Thr18/Ser19), phospho-VEGFR2 (Tyr1175), total VEGFR2, phospho-PLCγ (Tyr783), total PLCγ, phospho-ERK1/2 (Thr202/Tyr204), and total ERK1/2 were from Cell Signaling Technology. α-Actinin antibody (clone H-2) was from Santa Cruz Biotechnology Inc. HRP-conjugated secondary antibodies were from Jackson ImmunoResearch. Western blots were developed using the ECL Plus Western blotting reagent (GE Healthcare) and Kodak Biomax MR film.

Drosophila strains. The GAL4/UAS system was used for tissue-specific RNAi knockdown (43). The driver used was *btl-GAL4* (42), and RNAi targeting constructs v109453 (against *Pdcd10*) (41), v106841 (against *Pdcd10*) (41), and v49559 (against *GCKIII*) (44) were obtained from the Vienna Drosophila RNAi Center. For rescue experiments, full-length cDNAs for *Drosophila Pdcd10* were cloned into a pUAST transformation vector containing an attb site for site-specific transformation (52) provided by Carl Thummel (University of Utah). Transgenes were injected into docking sites VK00027 (53) and attp0016 (52) by Genetic Services Inc., and homozygous lines were established by standard methods.

For cDNA rescue experiments, flies homozygous for the cDNA rescuing construct on the third chromosome were crossed to a homozygous *btl-GAL4*, *UAS-GFP* driver line on the second chromosome to generate transheterozygote flies (*btl-GAL4*, *UAS-GFP/+*; *UAS-Rescue/+*). Males of this genotype were then crossed to virgin females homozygous for the RNAi targeting construct located on the second chromosome. GFP expression indicated the presence of the *btl-GAL4*, *UAS-GFP* transgenes. All of these larvae contain 1 copy of the RNAi targeting construct, and half also have the cDNA rescue transgene. Results shown used the v109453 line, which targets the 3′ UTR of *Pdcd10*. The v106841 line showed similar results.

Analysis of tracheal tube formation in Drosophila larvae. Animals were scored at the prewandering third instar larval stage for tracheal defects. Animals were graded by scoring air filling in primary sprouts emanating from the dorsal trunk. All primary sprouts were scored bilaterally (at least 12 per larva). The animals were categorized as having severe, moderate, or mild defects or wild-type if they had 3 or more of the following defects: (a) severe defects were truncations before the first bifurcation of the primary side branches or immediately after branching; (b) moderate defects represented gaps in air filling with filled tubes on both sides; (c) mild defects were loss of air filling only in the fine terminal tubes. In the event that more than 1 criterion was met, the more severe category was selected. If animals had fewer than 3 branches with a given defect, the less severe category was selected. Only animals with no defects were categorized as wild type.

Mouse and human experiments. All mouse experiments were approved by the University of Utah Institutional Animal Care and Use Committee. Human tissue samples were obtained with written informed consent and provided by Connie Lee and Amy Akers (Angioma Alliance, Norfolk, Virginia, USA) and Randy Jensen (University of Utah). Human experiments were approved by the Institutional Review Board of the University of Utah.

Statistics. For actin stress fiber content, and for in vitro lumen formation with GCKIII kinases, we performed ANOVA with Tukey's post hoc analysis with an α value of 0.05. For in vitro lumen formation time course for PDCD10, we performed statistical comparisons between treatment groups with a 2-tailed paired-sample *t* test with an α value of 0.05. For the tracheal tube formation rescue experiment, we performed a χ^2 test for independence with an α value of 0.05 (degrees of freedom = 9). For CCM penetrance and lesion content, we performed a 2-tailed *t* test with an α value of 0.05.

Acknowledgments

We thank N. London, S. Navankasattusas, L. Shi, Y. Xiong, C. Jensen, J. Zhu, D. Zurcher, A. Fang, T. Mleynek, and D. Lim for technical assistance; O. Abdullah and E. Hsu and the University of Utah Small Animal Imaging Facility; C. Rodesch and the University of Utah Cell Imaging/Fluorescence Facility; N. Chandler and the University of Utah Electron Microscopy Facility; S. Tripp and the Immunohistochemistry Research and Development Lab at ARUP Laboratories; J. Hansen at Central Labs at Intermountain Medical Center; K. Thomas and S. Odelberg for critical comments and helpful scientific discussions; and S. Chin for helpful scientific discussions. This work was funded by the US NIH (to G.E. Davis, M.M. Metzstein, K.J. Whitehead, and D.Y. Li), including training grant T32-GM007464 (to A.C. Chan and O.E. Ruiz), the Hellenic Cardiological Society (to N.A. Diakos), the American Heart Association (to K.J. Whitehead and D.Y. Li), the H.A. and Edna Benning Foundation, the Juvenile Diabetes Research Foundation, and the Burroughs Wellcome Fund (to D.Y. Li).

Received for publication July 16, 2010, and accepted in revised form March 2, 2011.

Address correspondence to: Kevin J. Whitehead, Room 4A100, 30 N 1900 East, Salt Lake City, Utah 84132, USA. Phone: 801.581.7715; Fax: 801.581.7735; E-mail: kevin.whitehead@u2m2.utah.edu. Or to: Dean Y. Li, Building 533 Room 4220, 15 N 2030 East, Salt Lake City, Utah 84112, USA. Phone: 801.585.5505; Fax: 801.585.0701; E-mail: dean.li@u2m2.utah.edu.

1. Otten P, Pizzolato GP, Rilliet B, Berney J. A propos de 131 cas d'angiomes caverneux (cavernomes) du S.N.C. repérés par l'analyse rétrospective de 24 535 autopsies. *Neurochirurgie*. 1989;35(2):82–83.
2. Vernooij MW, et al. Incidental findings on brain MRI in the general population. *N Engl J Med*. 2007;357(18):1821–1828.
3. Hasegawa T, McInerney J, Kondziolka D, Lee JY, Flickinger JC, Lunsford LD. Long–term results after stereotactic radiosurgery for patients with cavernous malformations. *Neurosurgery*. 2002;50(6):1190–1197.
4. Chappell PM, Steinberg GK, Marks MP. Clinically documented hemorrhage in cerebral arteriovenous malformations: MR characteristics. *Radiology*. 1992;183(3):719–724.
5. Burger PC, Scheithauer BW. *Tumors of the Central Nervous System*. Washington, DC, USA: American Registry of Pathology; 2007.
6. Wang H, Gujrati M. Pathology of cerebral cavernous malformations. In: Lanzino G, Spetzler RF, eds. *Cavernous Malformations of the Brain and Spinal Cord*. New York, New York, USA: Thieme Medical Publishers, Inc; 2008:22–25.
7. Faurobert E, Albiges-Rizo C. Recent insights into cerebral cavernous malformations: a complex jigsaw puzzle under construction. *FEBS J*. 2010;277(5):1084–1096.
8. Hilder TL, et al. Proteomic identification of the cerebral cavernous malformation signaling complex. *J Proteome Res*. 2007;6(11):4343–4355.
9. Whitehead KJ, et al. The cerebral cavernous malformation signaling pathway promotes vascular integrity via Rho GTPases. *Nat Med*. 2009;15(2):177–184.
10. Whitehead KJ, Plummer NW, Adams JA, Marchuk DA, Li DY. Ccm1 is required for arterial morphogenesis: implications for the etiology of human cavernous malformations. *Development*. 2004; 131(6):1437–1448.
11. Boulday G, et al. Tissue-specific conditional CCM2 knockout mice establish the essential role of endothelial CCM2 in angiogenesis: implications for human cerebral cavernous malformations. *Dis Model Mech*. 2009;2(3–4):168–177.
12. Stockton RA, Shenkar R, Awad IA, Ginsberg MH. Cerebral cavernous malformations proteins inhibit Rho kinase to stabilize vascular integrity. *J Exp Med*. 2010;207(4):881–896.
13. Glading A, Han J, Stockton RA, Ginsberg MH. KRIT-1/CCM1 is a Rap1 effector that regulates endothelial cell cell junctions. *J Cell Biol*. 2007; 179(2):247–254.
14. Borikova AL, et al. Rho kinase inhibition rescues the endothelial cell cerebral cavernous malformation phenotype. *J Biol Chem*. 2010;285(16):11760–11764.
15. Zawistowski JS, et al. CCM1 and CCM2 protein interactions in cell signaling: implications for cerebral cavernous malformations pathogenesis. *Hum Mol Genet*. 2005;14(17):2521–2531.
16. Fidalgo M, Fraile M, Pires A, Force T, Pombo C, Zalvide J. CCM3/PDCD10 stabilizes GCKIII proteins to promote Golgi assembly and cell orientation. *J Cell Sci*. 2010;123(pt 8):1274–1284.
17. Zhang J, Clatterbuck RE, Rigamonti D, Chang DD, Dietz HC. Interaction between krit1 and icap1alpha infers perturbation of integrin beta1-mediated angiogenesis in the pathogenesis of cerebral cavernous malformation. *Hum Mol Genet*. 2001;10(25):2953–2960.
18. Zawistowski JS, Serebriiskii IG, Lee MF, Golemis EA, Marchuk DA. KRIT1 association with the integrin-binding protein ICAP-1: a new direction in the elucidation of cerebral cavernous malformations (CCM1) pathogenesis. *Hum Mol Genet*. 2002;11(4):389–396.
19. Uhlik MT, et al. Rac-MEKK3-MKK3 scaffolding for p38 MAPK activation during hyperosmotic shock. *Nat Cell Biol*. 2003;5(12):1104–1110.
20. Ma X, et al. PDCD10 interacts with Ste20-related kinase MST4 to promote cell growth and transformation via modulation of the ERK pathway. *Mol Biol Cell*. 2007;18(6):1965–1978.
21. Voss K, et al. Functional analyses of human and zebrafish 18-amino acid in-frame deletion pave the way for domain mapping of the cerebral cavernous malformation 3 protein. *Hum Mutat*. 2009;30(6):1003–1011.
22. Goudreault M, et al. A PP2A phosphatase high-density interaction network identifies a novel striatin-interacting phosphatase and kinase complex linked to the cerebral cavernous malformation 3 (CCM3) protein. *Mol Cell Proteomics*. 2008;8(1):157–171.
23. Zheng X, et al. CCM3 signaling through sterile 20-like kinases plays an essential role during zebrafish cardiovascular development and cerebral cavernous malformations. *J Clin Invest*. 2010;120(8):2795–2804.
24. Denier C, et al. Genotype-phenotype correlations in cerebral cavernous malformations patients. *Ann Neurol*. 2006;60(5):550–556.
25. Sirvente J, Enjolras O, Wassef M, Tournier-Lasserve E, Labauge P. Frequency and phenotypes of cutaneous vascular malformations in a consecutive series of 417 patients with familial cerebral cavernous malformations. *J Eur Acad Dermatol Venereol*. 2009;23(9):1066–1072.
26. Labauge P, et al. Multiple dural lesions mimicking meningiomas in patients with CCM3/PDCD10 mutations. *Neurology*. 2009;72(23):2044–2046.
27. Akers AL, Johnson E, Steinberg GK, Zabramski JM, Marchuk DA. Biallelic somatic and germline mutations in cerebral cavernous malformations (CCMs): evidence for a two-hit mechanism of CCM pathogenesis. *Hum Mol Genet*. 2009;18(5):919–930.
28. Gault J, et al. Cerebral cavernous malformations: somatic mutations in vascular endothelial cells. *Neurosurgery*. 2009;65(1):138–144.
29. Pagenstecher A, Stahl S, Sure U, Felbor U. A two-hit mechanism causes cerebral cavernous malformations: complete inactivation of CCM1, CCM2 or CCM3 in affected endothelial cells. *Hum Mol Genet*. 2009;18(5):911–918.
30. Rigamonti D, et al. Cerebral cavernous malformations. Incidence and familial occurrence. *N Engl J Med*. 1988;319(6):343–347.
31. Labauge P, Brunereau L, Levy C, Laberge S, Houtteville JP. The natural history of familial cerebral cavernomas: a retrospective MRI study of 40 patients. *Neuroradiology*. 2000;42(5):327–332.
32. Del Curling O Jr, Kelly DL Jr, Elster AD, Craven TE. An analysis of the natural history of cavernous angiomas. *J Neurosurg*. 1991;75(5):702–708.
33. Knudson AG Jr. Mutation and cancer: statistical study of retinoblastoma. *Proc Natl Acad Sci U S A*. 1971;68(4):820–823.
34. Gault J, Shenkar R, Recksiek P, Awad IA. Biallelic somatic and germ line CCM1 truncating mutations in a cerebral cavernous malformation lesion. *Stroke*. 2005;36(4):872–874.
35. Shenkar R, et al. Advanced magnetic resonance imaging of cerebral cavernous malformations: part II. Imaging of lesions in murine models. *Neurosurgery*. 2008;63(4):790–797.
36. McDonald DA, et al. A novel mouse model of cerebral cavernous malformations based on the two-hit mutation hypothesis recapitulates the human disease. *Hum Mol Genet*. 2011;20(2):211–222.
37. Claxton S, Kostourou V, Jadeja S, Chambon P, Hodivala-Dilke K, Fruttiger M. Efficient, inducible Cre-recombinase activation in vascular endothelium. *Genesis*. 2008;46(2):74–80.
38. Davis GE, Camarillo CW. An alpha 2 beta 1 integrin-dependent pinocytic mechanism involving intracellular vacuole formation and coalescence regulates capillary lumen and tube formation in three-dimensional collagen matrix. *Exp Cell Res*. 1996;224(1):39–51.
39. Ghabrial A, Luschnig S, Metzstein MM, Krasnow MA. Branching morphogenesis of the Drosophila tracheal system. *Annu Rev Cell Dev Biol*. 2003;19:623–647.
40. Manning G, Krasnow MA. Development of the Drosophila tracheal system. In *The Development of Drosophila melanogaster*. Bate M, Martinez Arias A, eds. Plainview, New York, USA: Cold Spring Harbor Laboratory Press; 1993:609–685.
41. Mummery-Widmer JL, et al. Genome-wide analysis of Notch signalling in Drosophila by transgenic RNAi. *Nature*. 2009;458(7241):987–992.
42. Shiga Y, Tanaka-Matakatsu M, Hayashi S. A nuclear GFP/beta-galactosidase fusion protein as a marker for morphogenesis in living Drosophila. *Dev Growth Differ*. 1996;38(1):99–106.
43. Brand AH, Perrimon N. Targeted gene expression as a means of altering cell fates and generating dominant phenotypes. *Development*. 1993;118(2):401–415.
44. Dietzl G, et al. A genome-wide transgenic RNAi library for conditional gene inactivation in Drosophila. *Nature*. 2007;448(7150):151–156.
45. Clatterbuck RE, Eberhart CG, Crain BJ, Rigamonti D. Ultrastructural and immunocytochemical evidence that an incompetent blood-brain barrier is related to the pathophysiology of cavernous malformations. *J Neurol Neurosurg Psychiatry*. 2001;71(2):188–192.
46. Wang L, Seidman JG, Seidman CE. Narrative review: harnessing molecular genetics for the diagnosis and management of hypertrophic cardiomyopathy. *Ann Intern Med*. 2010;152(8):513–520.
47. He Y, et al. Stabilization of VEGFR2 signaling by cerebral cavernous malformation 3 is critical for vascular development. *Sci Signal*. 2010;3(116):ra26.
48. Navankasattusas S, et al. The netrin receptor UNC5B promotes angiogenesis in specific vascular beds. *Development*. 2008;135(4):659–667.
49. di Tomaso E, et al. PDGF-C induces maturation of blood vessels in a model of glioblastoma and attenuates the response to anti-VEGF treatment. *PLoS ONE*. 2009;4(4):e5123.
50. Jones CA, et al. Robo4 stabilizes the vascular network by inhibiting pathologic angiogenesis and endothelial hyperpermeability. *Nat Med*. 2008;14(4):448–453.
51. Saunders WB, Bayless KJ, Davis GE. MMP-1 activation by serine proteases and MMP-10 induces human capillary tubular network collapse and regression in 3D collagen matrices. *J Cell Sci*. 2005;118(pt 10):2325–2340.
52. Groth AC, Fish M, Nusse R, Calos MP. Construction of transgenic Drosophila by using the site-specific integrase from phage phiC31. *Genetics*. 2004;166(4):1775–1782.
53. Venken KJ, He Y, Hoskins RA, Bellen HJ. P[acman]: a BAC transgenic platform for targeted insertion of large DNA fragments in D. melanogaster. *Science*. 2006;314(5806):1747–1751.

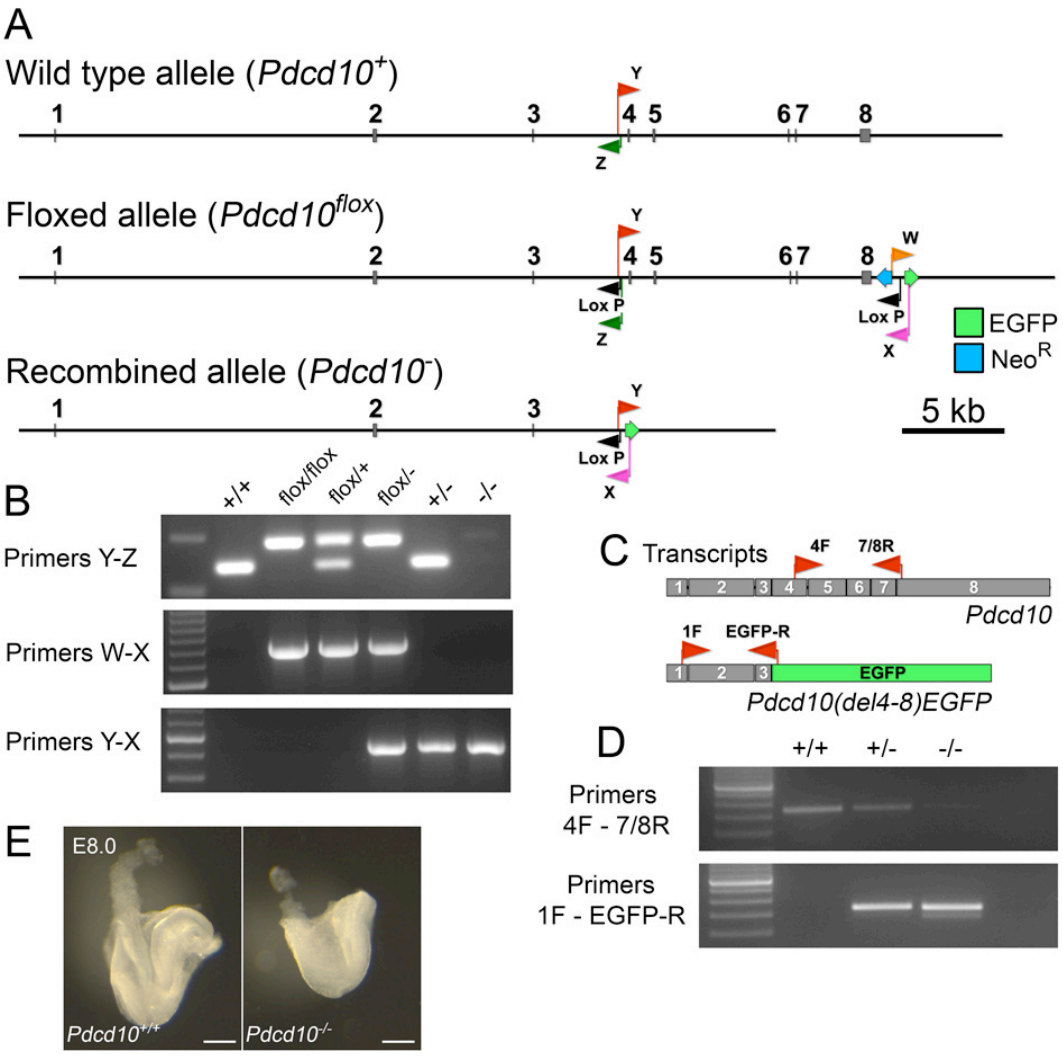

Supplemental Figure 1. Knockout design for *Pdcd10*. Ubiquitous deletion of *Pdcd10* results in early embryonic death. (**A**) Alleles of *Pdcd10* are shown. The floxed allele resulting from the targeting strategy includes loxP sites flanking exons 4-8 and places the enhanced green fluorescent protein (EGFP) in position to splice onto exon 3 in a fusion transcript resulting from the recombined allele. Genotyping primers are indicated by the letters W, X, Y and Z. (**B**) Genotyping by PCR using combinations of primers W, X, Y, and Z distinguishes the possible genotypes. (**C**) The wildtype and fusion transcripts are illustrated with exons outlined. The location of primers for RT-PCR are shown. (**D**) Results of RT-PCR performed on cDNA from embryos pooled by genotype that resulted from a mating of $Pdcd10^{+/-}$ vs. $Pdcd10^{+/-}$ mice. (**E**) Gross photos of E8.0 mouse embryos on dissection. Wildtype is shown in (**E**, left panel), *Pdcd10* knockout in (**E**, right panel). Even at this early stage, the knockout embryo has growth arrested and is smaller than its wildtype littermate. Scale bars = 200 μm.

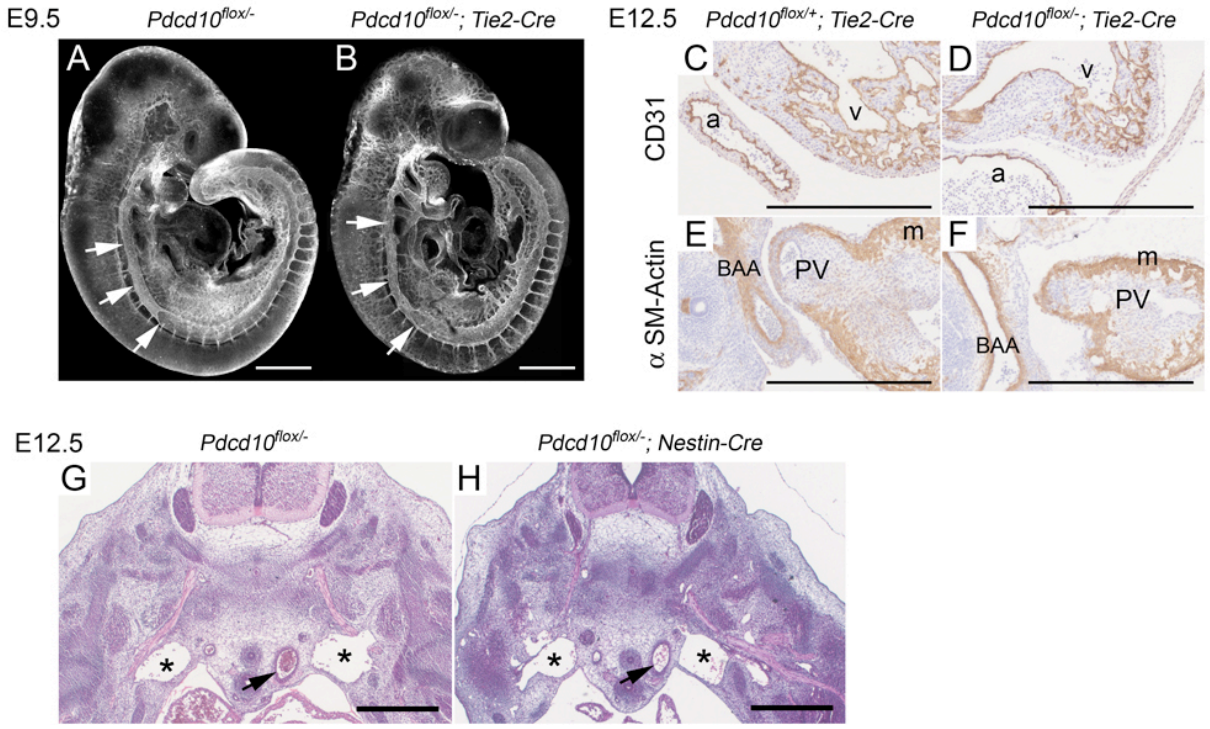

Supplemental Figure 2. Endothelial knockout of *Pdcd10* does not affect establishment of circulation or cardiac structure. Neural knockout of *Pdcd10* is viable. (**A-B**) Whole-mount fluorescent staining for CD31 in E9.5 *Pdcd10*$^{flox/-}$ (**A**) and *Pdcd10*$^{flox/-}$*; Tie2-Cre* (**B**) embryos. Arrows denote the dorsal aorta. (**C-D**) Hematoxylin and CD31 staining in E12.5 *Pdcd10*$^{flox/+}$*; Tie2-Cre* (**C**) and *Pdcd10*$^{flox/-}$*; Tie2-Cre* (**D**) embryos. (**E-F**) Hematoxylin and α-smooth muscle actin staining in E12.5 *Pdcd10*$^{flox/+}$*; Tie2-Cre* (**E**) and *Pdcd10*$^{flox/-}$*; Tie2-Cre* (**F**) embryos. a, atrium; v, ventricle; BAA, branchial arch artery; m, myocardium; PV, pulmonary valve. (**G-H**) Hematoxylin and eosin staining in E12.5 *Pdcd10*$^{flox/+}$*; Nestin-Cre* (**G**) and *Pdcd10*$^{flox/-}$*; Nestin-Cre* (**H**) embryos. Asterisks denote the cardinal veins. Arrows denote the dorsal aorta. Scale bars = 500 μm.

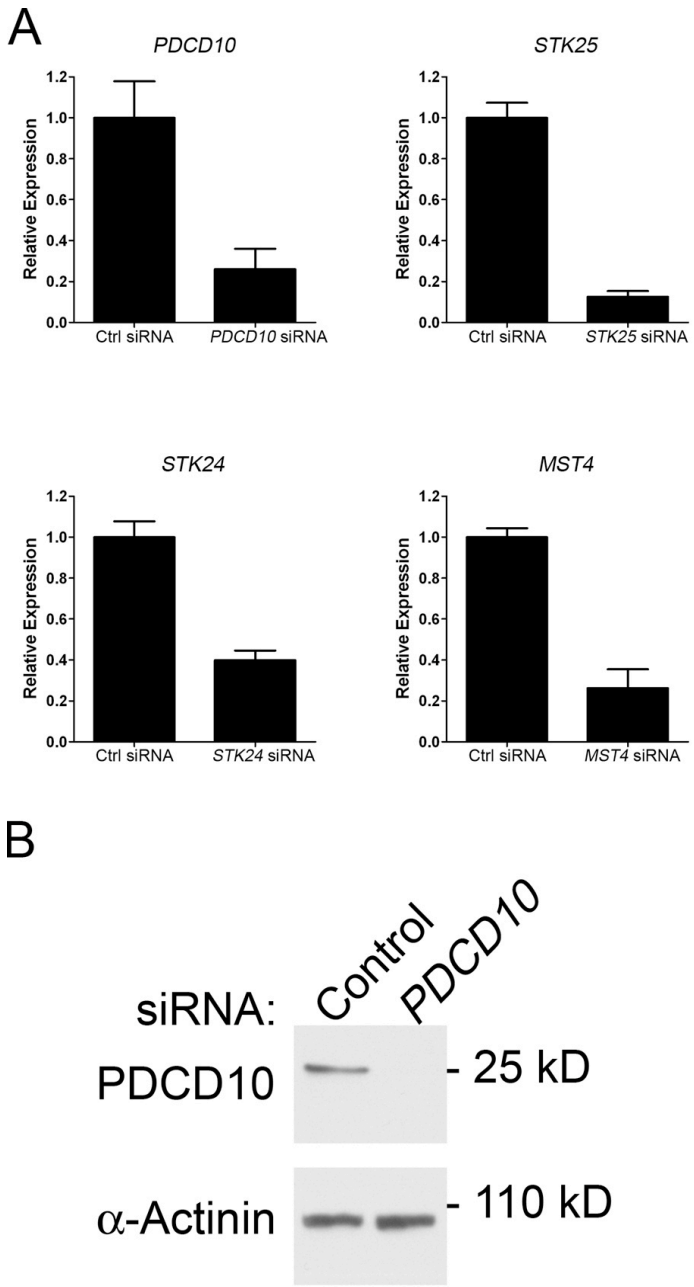

Supplemental Figure 3. siRNA effectively reduces levels of *PDCD10*, *STK25*, *STK24*, and *MST4*. (**A**) Quantitative PCR to detect *PDCD10*, *STK25*, *STK24*, and *MST4* was performed on cDNA made from the RNA of human endothelial cells to assess knockdown. (**B**) Western blot for PDCD10 to confirm knockdown.

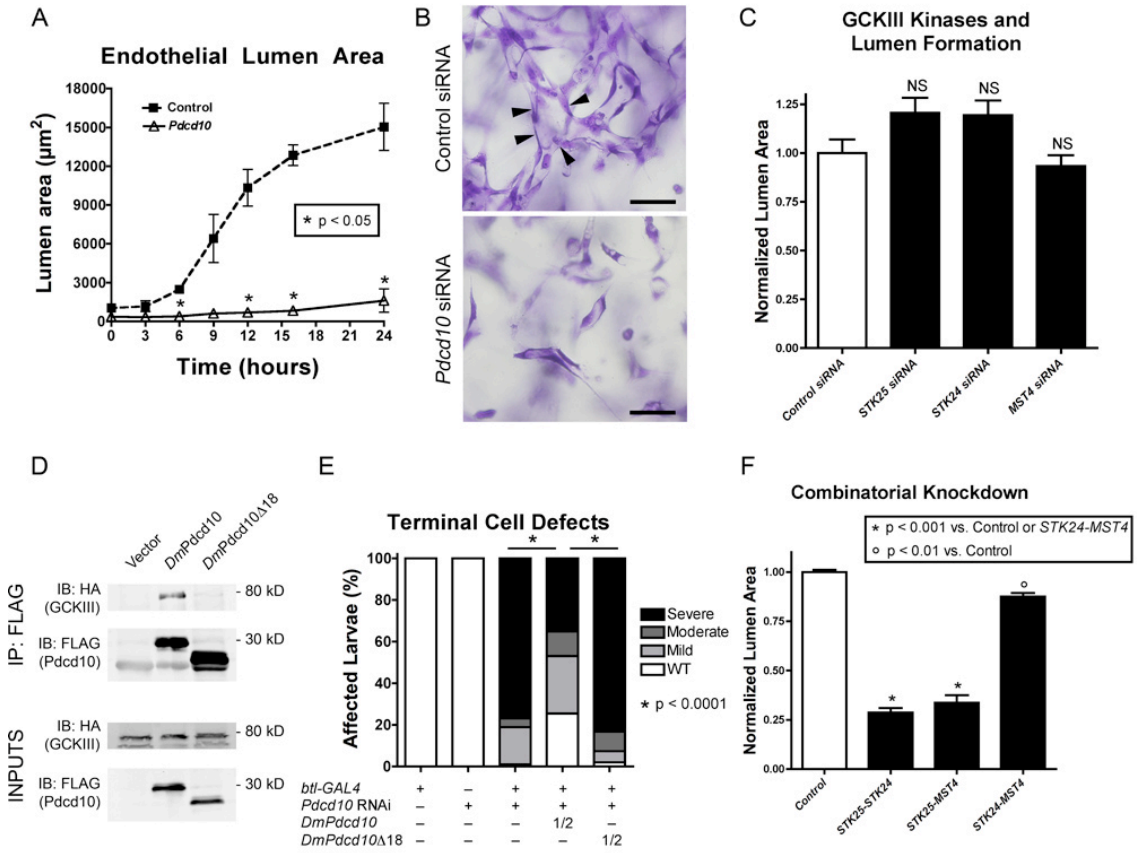

Supplemental Figure 4. Pdcd10 signals through GCKIII kinases in lumen formation. (**A**) Quantification of lumen area over time for human umbilical vein endothelial cells after treatment with *PDCD10* siRNA or control siRNA directed against Luciferase. (**B**) Toluidine blue staining of lumen formation assay. Lumens are shown with arrowheads. (**C**) Quantification of lumen area at 24 hours for cells treated with siRNA directed against each of the GCKIII kinases or Luciferase control (5 fields per time point in 3 independent experiments). (**D**) Immunoprecipitation for HA-tagged *Drosophila* GCKIII using full length *Drosophila* Pdcd10 (*Dm*Pdcd10) or *Drosophila* Pdcd10 with 18 amino acid deletion (*Dm*Pdcd10Δ18). Results are representative of 3 independent experiments. (**E**) Quantification of tracheal tube lumen formation defects in *Drosophila* with RNAi knockdown of *Pdcd10* with or without rescue constructs (N ≥ 64 for each genotype). Note: for rescue experiments only ~50% of all larvae contained the corresponding rescue transgene since they were generated by mating rescue heterozygous males (*btl-GAL4*, *UAS-GFP/+*; *UAS-Rescue/+*) to homozygous *UAS-RNAi* virgin females. (**F**) Quantification of 3D endothelial cell lumen area with combinatorial knockdown of human GCKIII kinases (5 fields per time point in 3 independent experiments). Data indicate mean ± SD. Scale bars = 50 μm.

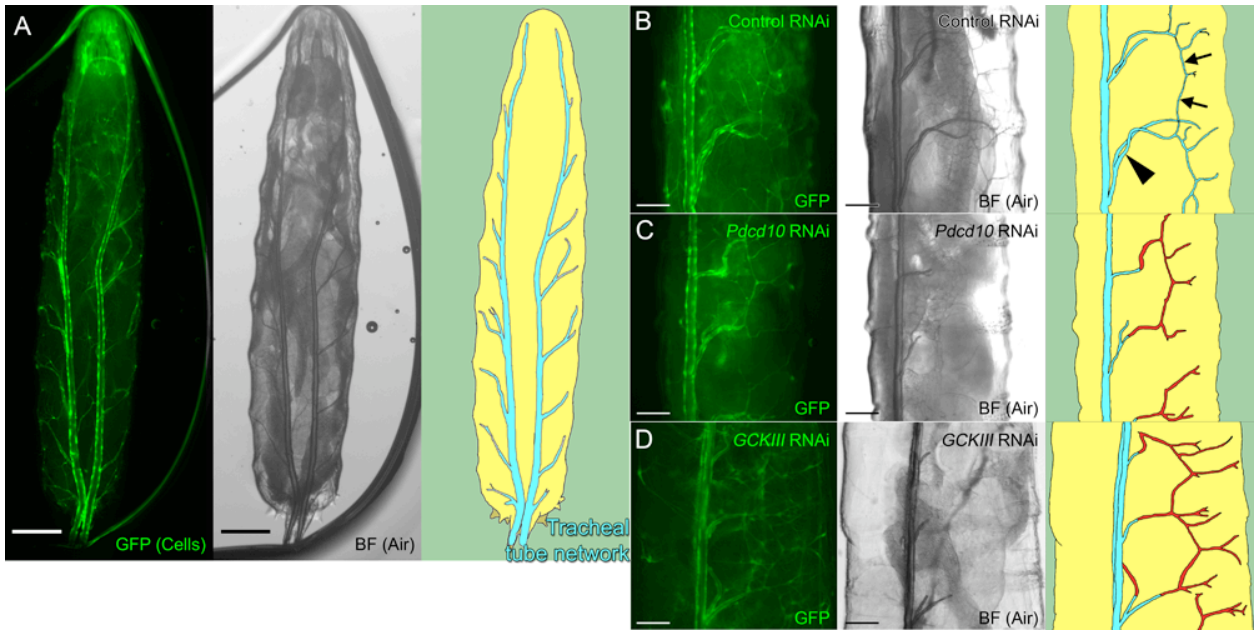

Supplemental Figure 5. Loss of Pdcd10 or GCKIII results in failure of tracheal tube lumenization in *Drosophila*. (**A**) The tracheal network of a *Drosophila* larva. A *UAS-GFP* transgene was used to label tracheal cells (left panel). Brightfield images of the same larva show air filling in lumens (middle panel). A cartoon representing the lumenized tube network (cyan) appears in the rightmost panel. (**B-D**) Tracheal tube lumen formation in flies expressing control RNAi (**B**), RNAi directed against *Pdcd10* (**C**), or RNAi directed against *GCKIII* (**D**) under the control of the tracheal-specific *btl-GAL4* driver. Arrowhead (in cartoon panel of **B**) indicates the primary trunk of a tracheal tube (where lumen truncation would indicate a severe phenotype), and arrows indicate the fine terminal branches (where lumen truncation would indicate a mild phenotype). Loss of *Pdcd10* or *GCKIII* results in similar air-filling defects. GFP expressing tracheal cells that lack air-filled lumens are outlined in red on the cartoon panels of **C-D**. Scale bars in (**A**) = 500 μm. Scale bars in (**B-D**) = 200 μm.

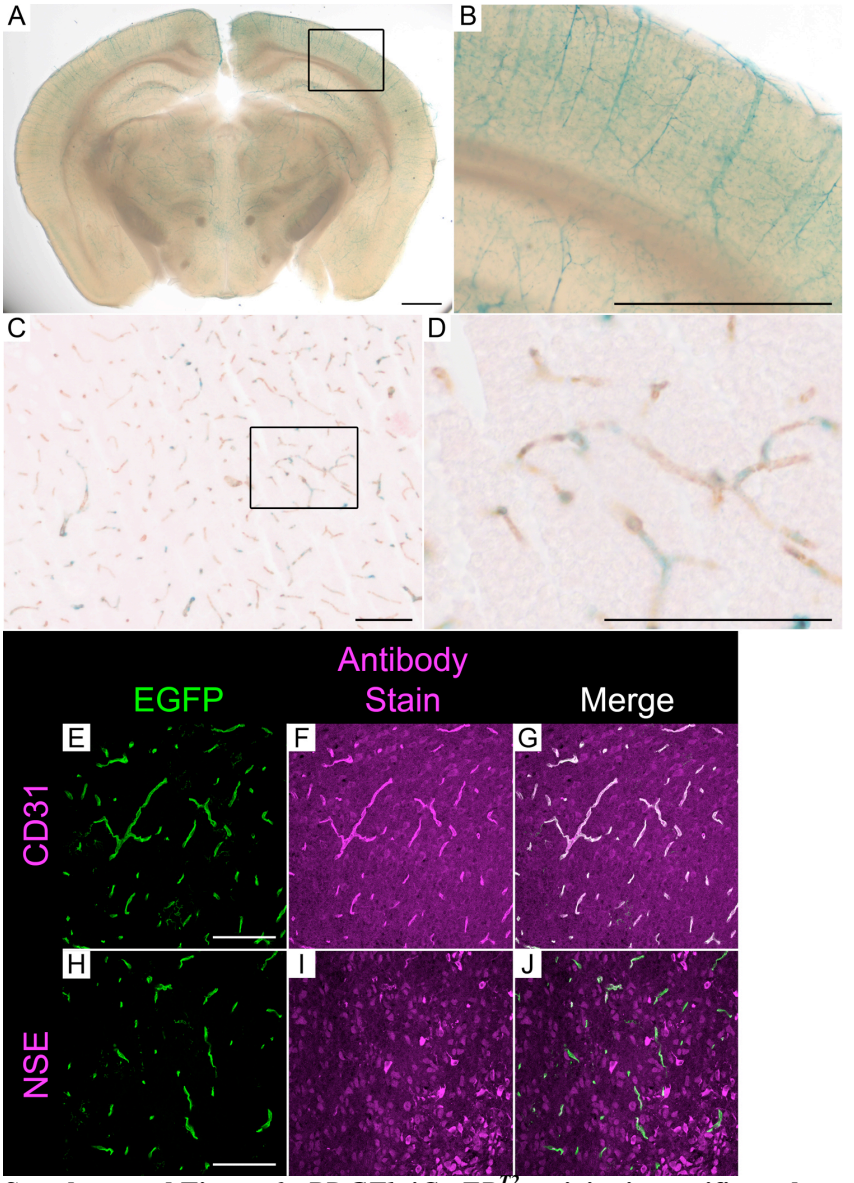

Supplemental Figure 6. *PDGFb-iCreER^{T2}* activity is specific to the endothelium. (**A**) X-gal staining (blue) of brain from a 6 month old *PDGFb-iCreER^{T2}; Rosa26-LacZ* mouse that was given tamoxifen at birth. (**B**) Close-up of the boxed area in panel (**A**). (**C-D**) X-gal (blue) and CD31 (brown) staining of brain from a 6 month old *PDGFb-iCreER^{T2}; Rosa26-LacZ* mouse that was given tamoxifen at birth. (**E-G**) CD31 (magenta) staining of brain from a 12 day old *PDGFb-iCreER^{T2}; Rosa26-ACTB-tdTomato,-EGFP* mouse that was given tamoxifen at birth. Cre activation converts ubiquitous tomato expression (not shown) to EGFP expression (green). (**H-J**) Neuron-specific enolase (NSE, magenta) staining of brain from a 12 day old *PDGFb-iCreER^{T2}; Rosa26-ACTB-tdTomato,-EGFP* mouse that was given tamoxifen at birth. Cre activation converts ubiquitous tomato expression (not shown) to EGFP expression (green). Scale bars in (**A-B**) = 1 mm. Scale bars in (**C-J**) = 100 μm.

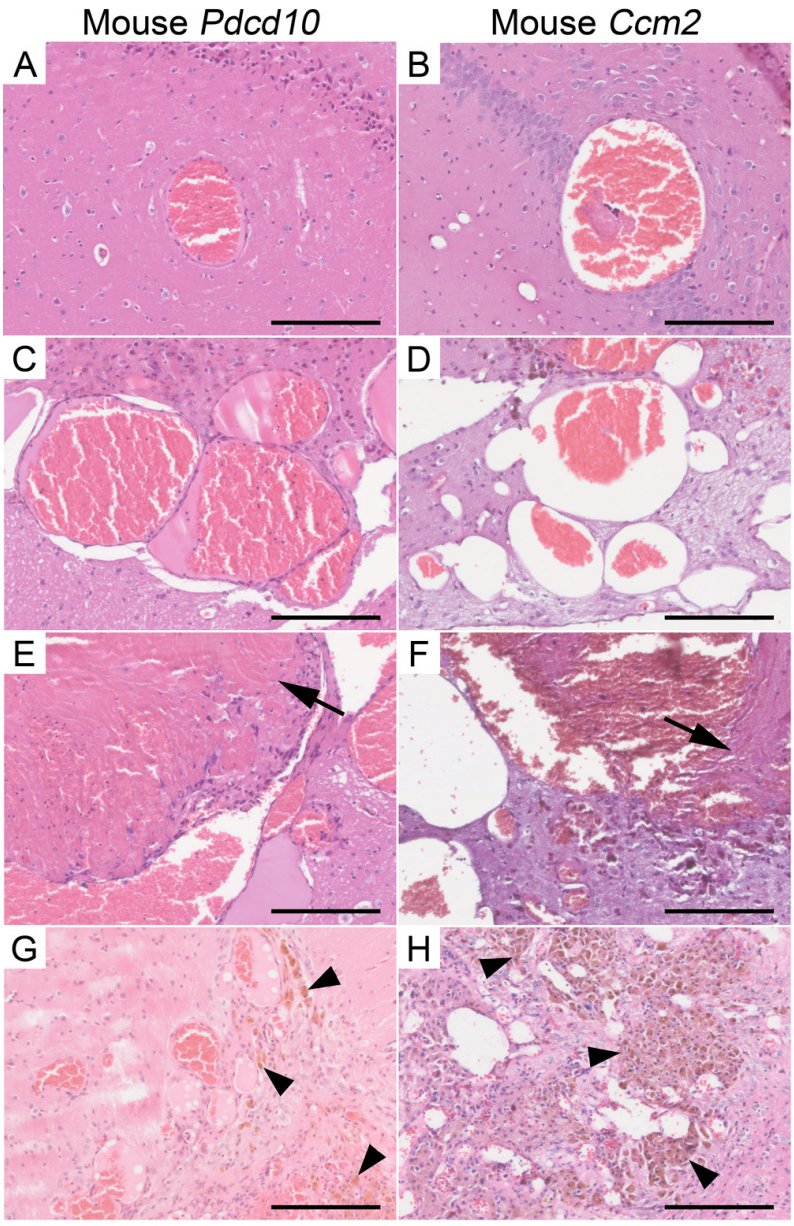

Supplemental Figure 7. LOH of either *Ccm2* or *Pdcd10* results in a range of vascular malformations. Both mouse models of CCM exhibit the same spectrum of pathology. Both the *Pdcd10* (**A**, **C**, **E**, and **G**) and *Ccm2* (**B**, **D**, **F**, and **H**) induced endothelial knockout models develop vascular lesions that exhibit the previously described spectrum of CCM pathology. Examples shown here include lesions consistent with solitary telangiectasias (**A-B**), multichannel "pristine" caverns (**C-D**), complex multichannel lesions with organizing thromboses (arrows in **E-F**), and multiple small caverns associated with heavy hemosiderin staining (arrowheads in **G-H**). Scale bars = 200 µm.

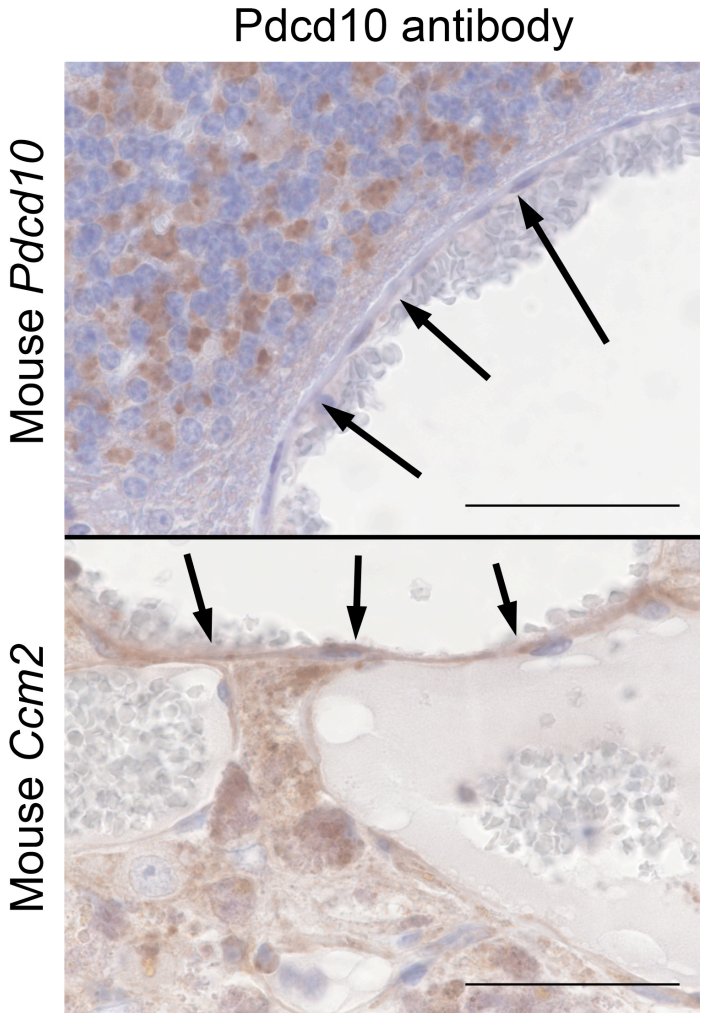

Supplemental Figure 8. Loss of Pdcd10 protein from *Pdcd10* (but not *Ccm2*) vascular lesions. An antibody against Pdcd10 does not stain endothelial cells of a CCM lesion from a *Pdcd10* induced knockout mouse (upper panel) but does stain the endothelial cells of a CCM from a *Ccm2* induced knockout mouse (bottom panel). Arrows indicate endothelial cells. Scale bars = 50 μm.

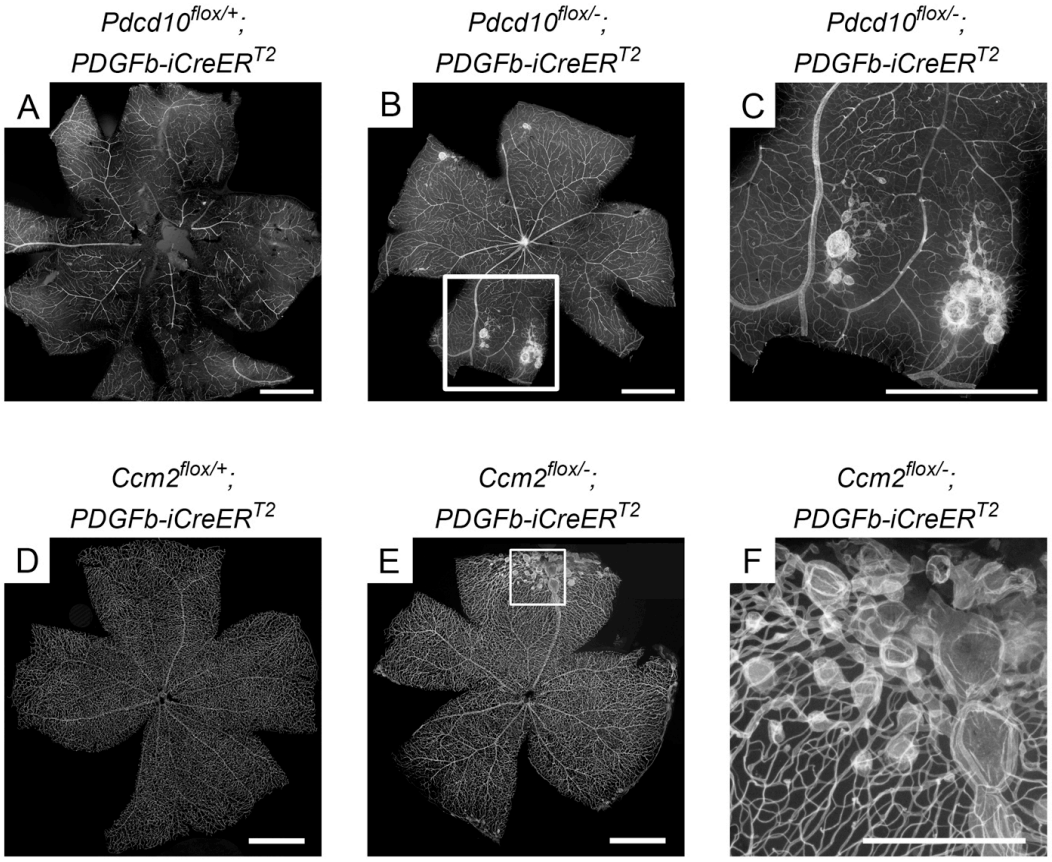

Supplemental Figure 9. Murine CCMs occur in the retinal vasculature. Lectin stained retinal flat mounts from a 5 month old *Pdcd10$^{flox/+}$; PDGFb-iCreER^{T2}* mouse (**A**), a 5 month old *Pdcd10$^{flox/-}$; PDGFb-iCreER^{T2}* mouse (**B-C**), a 7 month old *Ccm2$^{flox/+}$; PDGFb-iCreER^{T2}* mouse (**D**), and a 7 month old *Ccm2$^{flox/-}$; PDGFb-iCreER^{T2}* mouse (**E-F**). All mice were given tamoxifen at birth. (**C**) Close-up of the boxed, CCM-containing area in (**B**). (**F**) Close-up of the boxed, CCM-containing area in (**E**). Scale bars for all panels = 1 mm, except for panel (**F**), which is 500 μm.

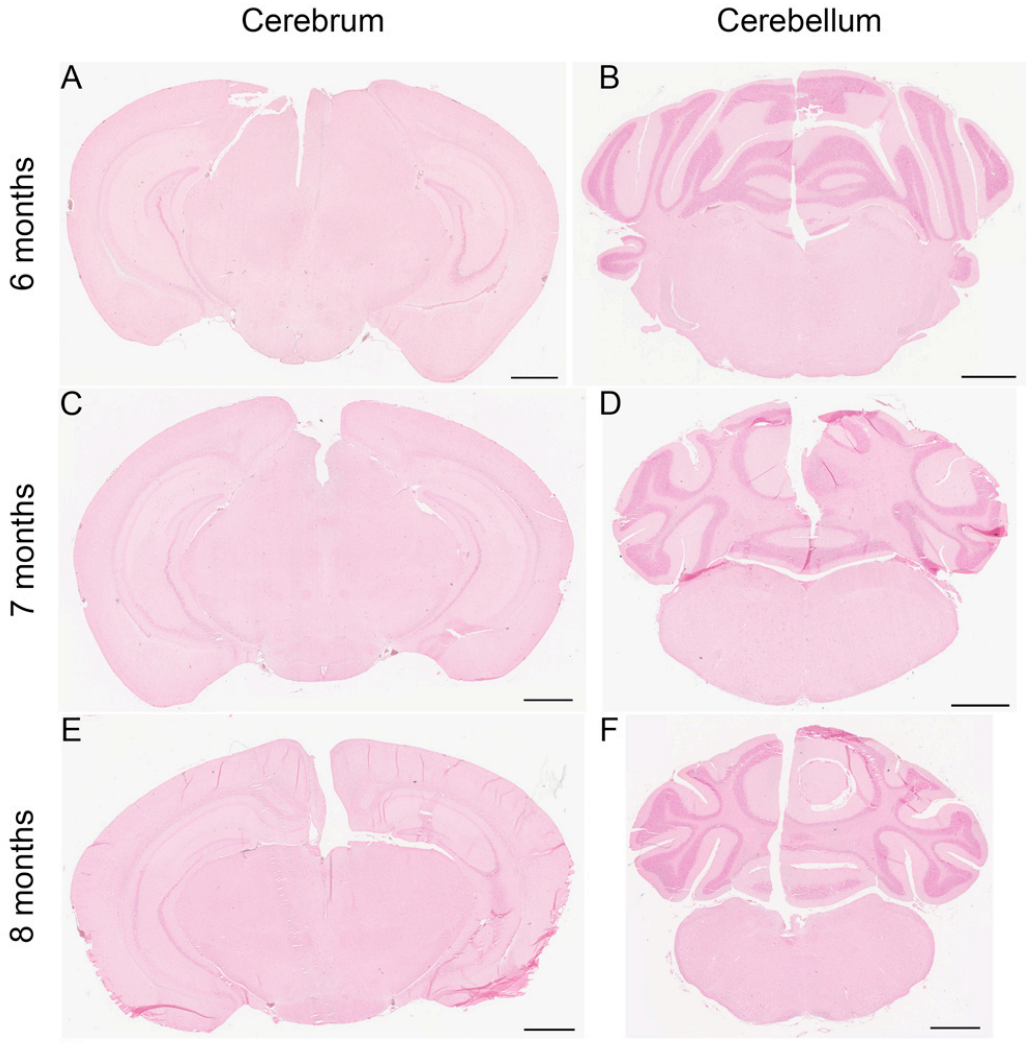

G

$Ccm2^{flox/-}$	CCM postive	CCM negative	Total
Nestin-Cre	0	6	6
PDGFb-iCreER^{T2}	16	0	16
Total	16	6	22

Fisher's exact test – $p < 0.0001$

Supplemental Figure 10. Neural-specific deletion of *Ccm2* does not result in CCMs. (**A-F**) Histology of *$Ccm2^{flox/-}$; Nestin-Cre* mouse brain at 6 months (**A-B**), 7 months (**C-D**), and 8 months (**E-F**). Staining is Prussian blue for hemosiderin with nuclear fast red counterstain. No lesions are found in these brains, and no hemosiderin is apparent. Scale bars = 1 mm. (**G**) Table comparing prevalence of CCMs in neural knockout (*Nestin-Cre*) vs. inducible endothelial knockout (*PDGFb-CreER^{T2}*).

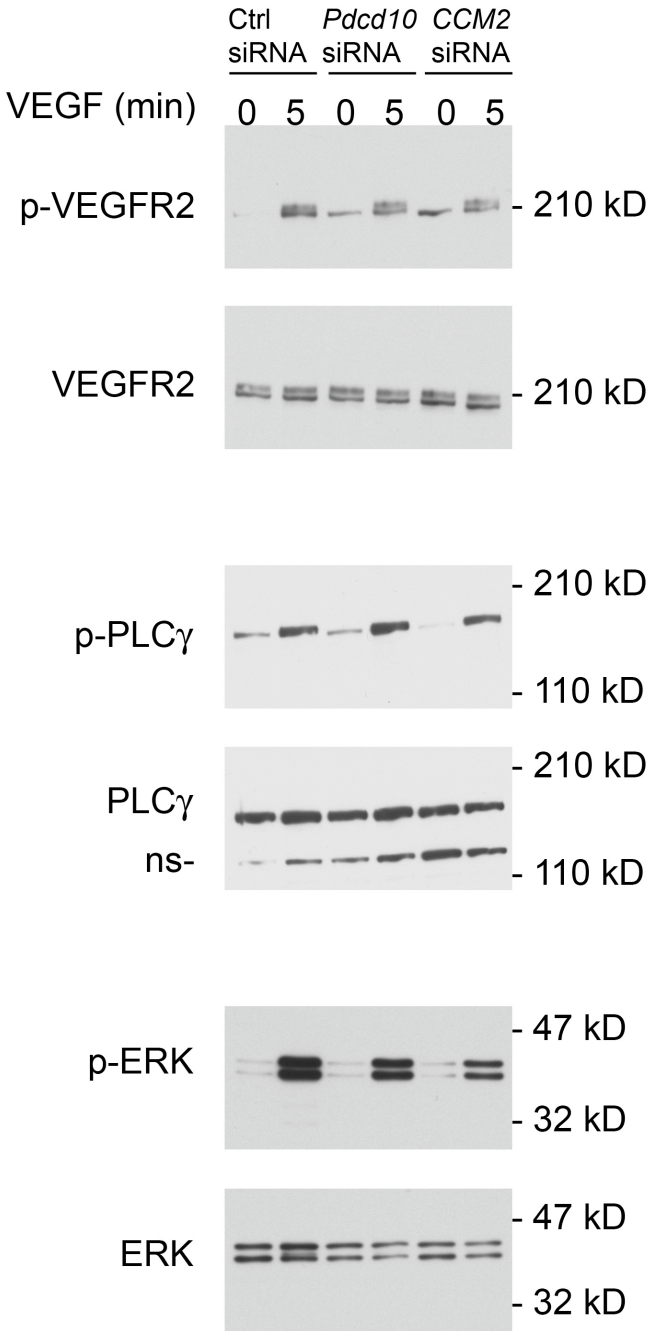

Supplemental Figure 11. Loss of PDCD10 does not affect VEGFR2-MAPK signaling. Western blot for VEGFR2, PLCγ, and ERK1/2 phosphorylation after stimulation of HMVECs with 10 ng/mL VEGF for the indicated amounts of time. ns, non-specific band.

Cross	*Pdcd10*$^{flox/flox}$ X *Pdcd10*$^{+/-}$*; Nestin-Cre*			
Genotype	*Pdcd10*$^{flox/+}$	*Pdcd10*$^{flox/-}$	*Pdcd10*$^{flox/+}$*; Nestin-Cre*	*Pdcd10*$^{flox/-}$*; Nestin-Cre*
# of progeny				
E12.5	2	7	9	8
P1	12	17	7	7

Supplemental Table 1. Table showing numbers of living offspring by genotype in matings between *Pdcd10*$^{flox/flox}$ and *Pdcd10*$^{+/-}$*; Nestin-Cre* parents.

CHAPTER 4

CONCLUDING REMARKS

The findings presented in this dissertation add two major contributions. First, I have established a reliable animal model of human CCM disease. This first step opens wide the field of opportunity for exploring the natural history and pathophysiology of the disease *in vivo*. Hypotheses related to signaling mechanisms and the cellular physiology that leads to the formation of these caverns can be directly examined in the setting of a living organism. This animal model also makes feasible preclinical testing of potential therapeutics for CCM disease, be they general anti-angiogenic therapies or more specifically targeted toward CCM pathology. Second, I have begun mapping the intricate cellular biology involved with the CCM proteins and their functional partners. My evidence suggesting that the CCM proteins are not all in a common pathway will inform clinical decisions regarding the treatment of people with familial CCM disease. The use of *Drosophila* in my studies opens the possibility of using this powerful genetic model to screen for proteins that cooperate with Pdcd10. Signaling proteins and the therapies that are targeted to them can then be validated using the mouse model of disease.

The establishment of the animal model was a major hurdle in the study of this disease. What remains, however, is to unravel the tangled skein of biochemistry to fully understand the functions of the CCM proteins, and how their loss leads to the aberrant cellular behaviors that manifest as dilated vascular caverns. A large body of work exists

addressing the biochemical signaling related to CCM, implicating a wide range of proteins, including integrins[1], small GTPases[1], MAP kinases[1], Wnt[2], Notch[3], VEGFR2[4], GCKIII kinases[5-8], and the orphan receptor Heg1[9]. Many of these proteins already present attractive targets for potential therapeutics. The many interactions implicated in CCM are hypothesized to control many aspects of cell function, including cytoskeletal dynamics[10], cell polarity[11-13], endothelial barrier function[1], and proliferation and apoptosis[5,14,15]. It now becomes a race to determine which interaction partners and which cellular functions are the most relevant to the disease phenotype, to fully fill in the gaps in our understanding of CCM pathophysiology.

REFERENCES

1. Faurobert, E. & Albiges-Rizo, C. Recent insights into cerebral cavernous malformations: a complex jigsaw puzzle under construction. *FEBS J* **277**, 1084-1096 (2010).
2. Glading, A.J. & Ginsberg, M.H. Rap1 and its effector KRIT1/CCM1 regulate beta-catenin signaling. *Dis Model Mech* **3**, 73-83 (2010).
3. Wustehube, J.*, et al.* Cerebral cavernous malformation protein CCM1 inhibits sprouting angiogenesis by activating DELTA-NOTCH signaling. *Proc Natl Acad Sci U S A* **107**, 12640-12645 (2010).
4. He, Y.*, et al.* Stabilization of VEGFR2 signaling by cerebral cavernous malformation 3 is critical for vascular development. *Sci Signal* **3**, ra26 (2010).
5. Ma, X.*, et al.* PDCD10 interacts with Ste20-related kinase MST4 to promote cell growth and transformation via modulation of the ERK pathway. *Mol Biol Cell* **18**, 1965-1978 (2007).
6. Voss, K.*, et al.* Functional analyses of human and zebrafish 18-amino acid in-frame deletion pave the way for domain mapping of the cerebral cavernous malformation 3 protein. *Hum Mutat* **30**, 1003-1011 (2009).
7. Zheng, X.*, et al.* CCM3 signaling through sterile 20-like kinases plays an essential role during zebrafish cardiovascular development and cerebral cavernous malformations. *J Clin Invest* **120**, 2795-2804 (2010).

8. Chan, A.C.*, et al.* Mutations in 2 distinct genetic pathways result in cerebral cavernous malformations in mice. *J Clin Invest* **121**, 1871-1881 (2011).

9. Kleaveland, B.*, et al.* Regulation of cardiovascular development and integrity by the heart of glass-cerebral cavernous malformation protein pathway. *Nat Med* **15**, 169-176 (2009).

10. Whitehead, K.J.*, et al.* The cerebral cavernous malformation signaling pathway promotes vascular integrity via Rho GTPases. *Nat Med* **15**, 177-184 (2009).

11. Fidalgo, M.*, et al.* CCM3/PDCD10 stabilizes GCKIII proteins to promote Golgi assembly and cell orientation. *J Cell Sci* **123**, 1274-1284 (2010).

12. Lampugnani, M.G.*, et al.* CCM1 regulates vascular-lumen organization by inducing endothelial polarity. *J Cell Sci* **123**, 1073-1080 (2010).

13. Kean, M.J.*, et al.* Structure-function analysis of core STRIPAK: a signalling complex implicated in golgi polarization. *J Biol Chem* (2011).

14. Chen, L.*, et al.* Apoptotic functions of PDCD10/CCM3, the gene mutated in cerebral cavernous malformation 3. *Stroke* **40**, 1474-1481 (2009).

15. Schleider, E.*, et al.* Evidence for anti-angiogenic and pro-survival functions of the cerebral cavernous malformation protein 3. *Neurogenetics* **12**, 83-86 (2011).